$5

QEX

INCLUDING: COMMUNICATIONS QUARTERLY

Forum for Communications Experimenters

July/August 2004
Issue No. 225

A Low-Cost, PC-Based Network Analyzer

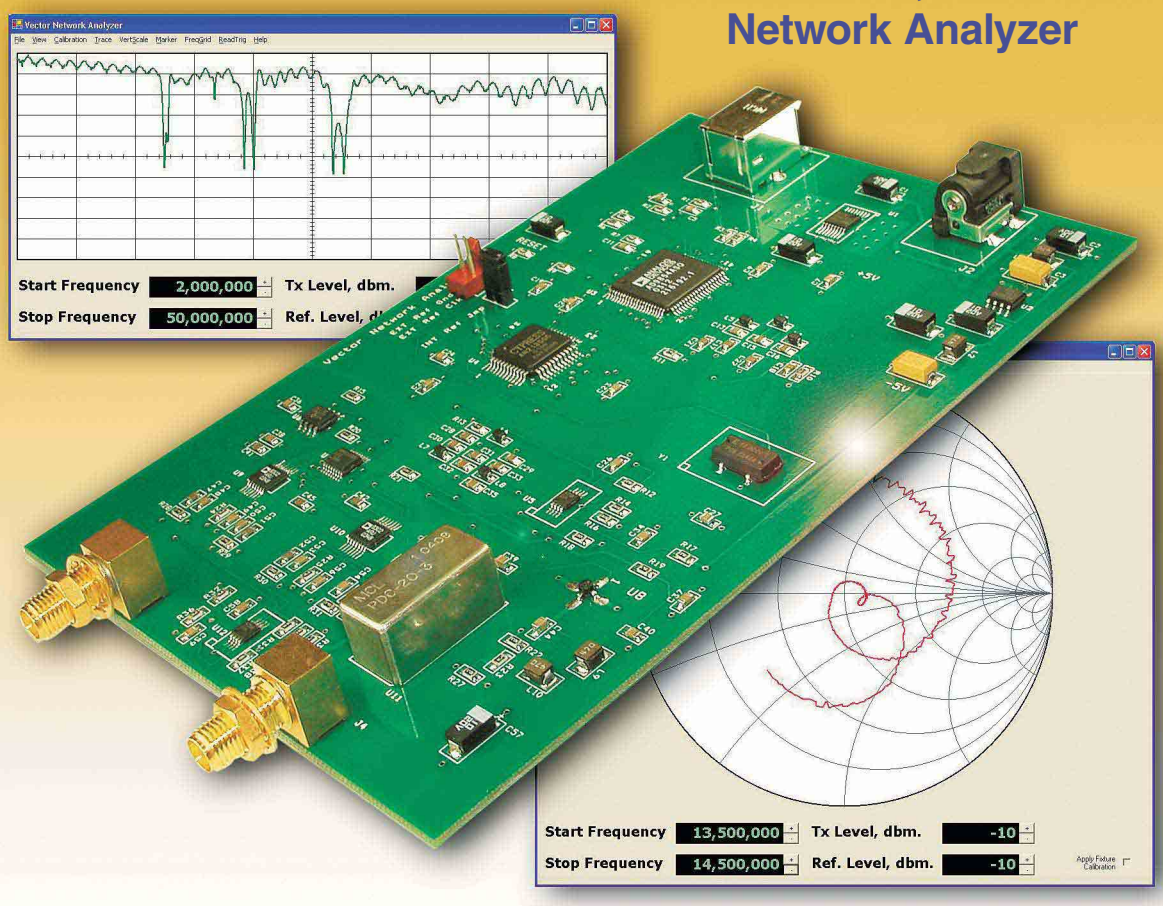

ARRL The national association for AMATEUR RADIO
225 Main Street
Newington, CT USA 06111-1494

QEX

INCLUDING: COMMUNICATIONS QUARTERLY

QEX (ISSN: 0886-8093) is published bimonthly in January, March, May, July, September, and November by the American Radio Relay League, 225 Main Street, Newington CT 06111-1494. Periodicals postage paid at Hartford, CT and at additional mailing offices.

POSTMASTER: Send address changes to: QEX, 225 Main St, Newington, CT 06111-1494 Issue No 225

Offices

225 Main St, Newington, CT 06111-1494 USA
Telephone: 860-594-0200
Telex: 650215-5052 MCI
Fax: 860-594-0259 (24 hour direct line)
e-mail: **qex@arrl.org**

Subscription rate for 6 issues:

In the US: ARRL Member $24, nonmember $36;

US by First Class Mail: ARRL member $37, nonmember $49;

Elsewhere by Surface Mail (4-8 week delivery): ARRL member $31, nonmember $43;

Canada by Airmail: ARRL member $40, nonmember $52;

Elsewhere by Airmail: ARRL member $59, nonmember $71.

Members are asked to include their membership control number or a label from their *QST* when applying.

In order to ensure prompt delivery, we ask that you periodically check the address information on your mailing label. If you find any inaccuracies, please contact the Circulation Department immediately. Thank you for your assistance.

About the Cover

Tom McDermott, N5EG and Karl Ireland describe an easy to build, professional quality vector network analyzer that makes use of your PC for processing and display.

Features

Columns

Jul/Aug 2004 *QEX* Advertising Index

THE AMERICAN RADIO RELAY LEAGUE

The American Radio Relay League, Inc, is a noncommercial association of radio amateurs, organized for the promotion of interests in Amateur Radio communication and experimentation, for the establishment of networks to provide communications in the event of disasters or other emergencies, for the advancement of radio art and of the public welfare, for the representation of the radio amateur in legislative matters, and for the maintenance of fraternalism and a high standard of conduct.

ARRL is an incorporated association without capital stock chartered under the laws of the state of Connecticut, and is an exempt organization under Section 501(c)(3) of the Internal Revenue Code of 1986. Its affairs are governed by a Board of Directors, whose voting members are elected every two years by the general membership. The officers are elected or appointed by the Directors. The League is noncommercial, and no one who could gain financially from the shaping of its affairs is eligible for membership on its Board.

"Of, by, and for the radio amateur, "ARRL numbers within its ranks the vast majority of active amateurs in the nation and has a proud history of achievement as the standard-bearer in amateur affairs.

A bona fide interest in Amateur Radio is the only essential qualification of membership; an Amateur Radio license is not a prerequisite, although full voting membership is granted only to licensed amateurs in the US.

Membership inquiries and general correspondence should be addressed to the administrative headquarters at 225 Main Street, Newington, CT 06111 USA.

Telephone: 860-594-0200
Telex: 650215-5052 MCI
MCIMAIL (electronic mail system) ID: 215-5052
FAX: 860-594-0259 (24-hour direct line)

Officers

President: JIM D. HAYNIE, W5JBP
3226 Newcastle Dr, Dallas, TX 75220-1640
Executive Vice President: DAVID SUMNER, K1ZZ

The purpose of *QEX* is to:
1) provide a medium for the exchange of ideas and information among Amateur Radio experimenters,
2) document advanced technical work in the Amateur Radio field, and
3) support efforts to advance the state of the Amateur Radio art.

All correspondence concerning *QEX* should be addressed to the American Radio Relay League, 225 Main Street, Newington, CT 06111 USA. Envelopes containing manuscripts and letters for publication in *QEX* should be marked Editor, *QEX*.

Both theoretical and practical technical articles are welcomed. Manuscripts should be submitted on IBM or Mac format 3.5-inch diskette in word-processor format, if possible. We can redraw any figures as long as their content is clear. Photos should be glossy, color or black-and-white prints of at least the size they are to appear in *QEX*. Further information for authors can be found on the Web at **www.arrl.org/qex/** or by e-mail to **qex@arrl.org**.

Any opinions expressed in *QEX* are those of the authors, not necessarily those of the Editor or the League. While we strive to ensure all material is technically correct, authors are expected to defend their own assertions. Products mentioned are included for your information only; no endorsement is implied. Readers are cautioned to verify the availability of products before sending money to vendors.

Empirical Outlook

Behind the Scenes at *QEX*

Here are a few notes about our staff and how we operate. In light of some recent changes, now seems a good time to elaborate.

Theorem: In almost any office setting, there is always one person who knows everything that goes on. Assistant Editor Lori (Maty) Weinberg, KB1EIB, is that person for us. She logs and acknowledges submissions and distributes them amongst our editorial board, which consists of our editorial staff plus ARRL Technical Advisors. She sends out post-production page proofs and handles author release forms, as well as much of our other correspondence.

My own job is to ensure the best content. That means not only determining what goes into each issue but also reviewing page proofs, conducting correspondence, assembling a letters column, writing this editorial and so on. You intrepid writers have made my job easier by largely removing worries about having enough good material to fill these pages. I do some of the copy editing before handing articles to our Managing Editor for further processing. Every now and then, I get to write an article.

Managing Editor Bob Schetgen, KU7G, is at the center of the *QEX* work storm. He assigns final formatting to text and graphics and leads articles through production to final layout. He always finds things I missed and he often has queries that eluded the rest of us. Unfortunately, Bob has had to be away from his desk for an extended period and we are lucky to have *QST* Product Review Editor Joel Hallas, W1ZR, filling in.

Production, as ably headed by Michelle Bloom, WB1ENT, is where it all comes together. Production Assistant Joe Shea does most of our layout work and Graphic Design Supervisor Sue Fagan creates our covers, among other things. The production crew work their magic on *all* ARRL publications, not just the magazines.

As of this issue, we have three Contributing Editors: Zack Lau, W1VT; Ray Mack, WD5IFS; and L.B. Cebik, W4RNL. That's right—L.B. has graciously come aboard to regularly publish his insights in *Antenna Options*. I don't need to recapitulate his expertise in antenna modeling and design. Zack and Ray will continue to write for us, but Ray is finishing a book and Zack's talents are increasingly needed in the broadband-over-power-lines (BPL) struggle. Additionally, Ray is our regular proofreader. Even as we adapt to change, the good news is that we are adding to our capacity to bring you the best in communications experimentation.

I think you will agree that all those individuals deserve hearty congratulations for their central roles in making League publications topmost in their field. Mentioned too infrequently is that ARRL's efforts—and yours— in the publishing world have augmented our collective standing in a unique way. Keep those projects going!

In This Issue

Tom McDermott, N5EG, and Karl Ireland present their 100-MHz vector network analyzer design. If you build it, this instrument will bring you capabilities that might otherwise be beyond your means.

Rob Lytle, N3FT, introduces an improvement to the so-called Jones filter. It allows the center frequency of a variable-bandwidth crystal filter to remain reasonably constant as the bandwidth is changed. Using readily available components, Markus Hansen, VE7CA, shows how to fix your HP8640B when its output pre-amplifier fails. We understand that is a fairly common situation with the generator.

Sergio Cartoceti, IK4AUY, studies a so-called H-mode mixer based on the FST3125M chip. He fully analyzes and tests his double-balanced mixer for all the usual parameters.

Ron Barker, G4JNH, returns with a follow-on to his Sep/Oct 2001 article on remote antenna impedance measurement. Ron refines his technique by making good use of the transmission-line equation.

Walt Maxwell, W2DU, comes with a rebuttal to the series of articles on transmission-line mechanics presented by Steve Best, VE9SRB. (Jan/Feb, Jul/Aug and Nov/Dec 2001). Walt points to what he perceives as errors and provides different solutions.

In *Antenna Options*, L.B. Cebik, W4RNL, kicks off a four-part series on Yagi design and optimization. In *Tech Notes*, Nickolaus Leggett, N3NL, has some words about the use of a protocol that may increase your random microwave contacts. I even have some observations about resistance and energy conversion —73, *Doug Smith, KF6DX,* **kf6dx@arrl.org.** □□

A Low-Cost 100 MHz Vector Network Analyzer with USB Interface

This article describes a low-cost vector network analyzer that operates from 200 kHz to 100 MHz, and connects to a personal computer using a USB 1.1 interface.[1]

By Tom McDermott, N5EG, and Karl Ireland

Introduction

One of the more useful pieces of test equipment for designers and experimenters is the vector network analyzer (VNA). The VNA allows measuring the forward and reverse gain and phase response of a circuit, as well as the input and output reflection properties (complex impedance). Traditionally, the VNA has used s-parameters to describe the four properties of a two-port circuit being measured. The VNA is used to measure and adjust filters, coaxial cables, amplifiers, antenna input impedance vs. frequency, and so forth. A full VNA consists of two measurement sections: one in the forward direction that measures s_{21} (forward gain and phase) and s_{11} (input reflection magnitude and phase), and a duplicate circuit in the reverse direction that measures s_{22} (output reflection magnitude and phase) and s_{12} (reverse gain and phase, usually called reverse isolation). To save cost, many instruments only provide enough hardware to measure in one direction. Then, the device under test is physically reversed and the measurements rerun. Most properly, this simplified piece of equipment is called a transmission-reflection test set; but most of the time, it is still referred to as a VNA, the same as its big brother.

One significant difference between the two instruments is that a true VNA can be more accurately calibrated through true two-port techniques, whereas the transmission-reflection test set relies on precision standards (open, short, 50 Ω) to calibrate the reflection measurement. A two-port calibration based on the TRL (Through-Reflect-Line) technique can theoretically dispense with the need for precision load standards.

Another related piece of equipment is the scalar network analyzer. The difference between the scalar analyzer and the VNA is that the scalar analyzer does not include the additional circuitry to measure the phase component of the transmission and reflec-

[1]Notes appear on page 14.

265 Daniel Dr
Plano, TX 75094
n5eg@arrl.net

2517 Lawndale
Plano, TX 75023

tion parameters of the circuit under test, while the vector analyzer measures both the magnitude and phase components. Thus the VNA is quite a bit more complicated. The vector properties are often of great interest, such as when measuring the input impedance of an antenna, or the group delay of a filter, and thus the vector analyzer is a more useful instrument for many types of measurements.

This article will describe a vector transmission-reflection type of instrument; but we'll borrow the more grandiose title VNA, since most people are more familiar with that terminology. Fig 1 is a picture of the first prototype board—before the debug/fixes! The TX and RX BNC connectors are on the left and the Universal Serial Bus (USB) and DC power connectors are on the right. The directional coupler (metal case) is next to the TX connector. Figures 2 and 3 respectively show front and rear views of the completed unit.

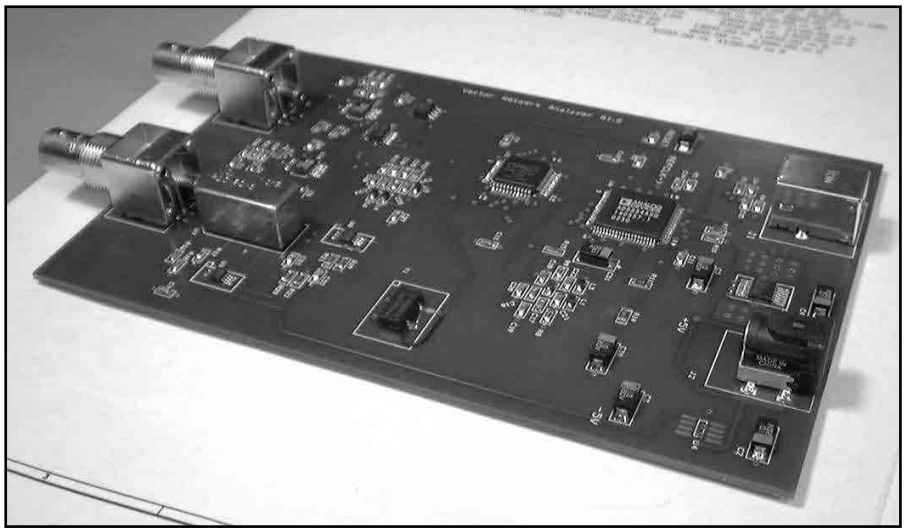

Figure 1—Photograph of the assembled prototype board. The 4-layer board is approximately 4×6 inches.

Figure 2—Photograph of the front panel of the assembled unit.

Figure 3— Photograph of the rear panel of the assembled unit.

Overview of the Instrument

Commercially available VNAs are very expensive pieces of precision equipment, costing tens of thousands of dollars. These instruments provide tremendous dynamic range (approaching 90 to 100 dB), a high degree of accuracy, and many software options for manipulating and displaying data. It's possible to sacrifice some of the dynamic range and precision to save a lot on the cost and complexity of the measurement hardware. Today's personal computers, however, provide extensive ability to manipulate and display data for virtually no additional cost—just the time and effort of creating the software. So the instrument itself is kept as simple as possible by offloading much of the work to the host computer.

Fig 4 is a block diagram of the low-cost VNA measurement device. The equipment consists of a quadrature frequency synthesizer, a reflection measurement circuit, a transmission measurement circuit, a pair of phase/magnitude RF detectors (one for transmission and one for reflection), a multi-channel analog-to-digital converter (ADC), and a specialized USB-aware microprocessor.[2] Additionally, a +3.3 V regulator and a +5 to –5 V inverter provide the digital and analog supply voltages for the board.

The need for a quadrature synthesizer takes a little explanation. The recently released Analog Devices AD8302[3] device measures the magnitude ratio and relative phase difference between two RF signals (up to 2.7 GHz). The phase response is ambiguous, however. It is symmetrical

about 0°, at which point the phase accuracy is significantly degraded. This can be seen from Fig 5, a plot of the phase and amplitude detector output responses of the device vs the input phase difference, from the AD8302 data sheet. To resolve the phase sign, the VNA instrument switches the reference input to the detector between an in-phase (I) and quadrature-phase (Q) reference signal and measures the detector output for both conditions. Software on the host computer then resolves the correct phase quadrant between the two RF detector inputs. The low-pass filters are used to reconstruct the DDS output from the digital stair-step waveform produced. The Analog Devices AD9854[4] DDS is clocked by a 24 MHz sine wave; it then internally multiplies it up to 288 MHz with an on-chip PLL. This 288 MHz internal signal clocks the DDS frequency-generation circuits and the digital-to-analog (DAC) circuits on the chip. Significant aliasing of the output signal is observed on an oscilloscope even at an output frequency of less than 100 MHz. The two low-pass filters, one on I and one on Q, remove most of these aliasing and stair-stepping artifacts and produce clean sine waves in phase quadrature.

The RF detectors are broadband and have a total dynamic range of almost 60 dB, but with the restriction that the range is ±30 dB between the reference signal and the unknown signal. The performance of these detectors sets the dynamic range of the instrument. To achieve greater dynamic range, a much more expensive tuned-receiver configuration would be required. For a reflection measurement, the practical measurement limit is about 30 dB of return loss.

Two selectors are implemented with a pair of dual-input Maxim 200-MHz video amplifiers that are programmable by the target processor. One allows selection of whether the I or Q DDS reference signal is applied to both of the RF detectors. The other selects the reflected signal or a monitor signal (used only for debugging) to be measured by the reflection RF detector.

The transmission measurement process is very simple. A BNC connector (labeled RX) and terminated in 50 ohms is connected to one of the RF detectors. This measures the amplitude and phase of the signal received on the RX connector against the internal reference signals I and Q. The reflection circuit uses a Mini-Circuits 20-dB directional coupler[5] to derive the signal reflected by the load from the other BNC connector (labeled TX). The reflected signal produced by the directional coupler is the complex reflection coefficient gamma, Γ. The magnitude and phase of this reflection signal are derived by measurements against the internal I and Q reference signals.

In operation, the host processor (the PC) sends a command to the VNA over the USB port, triggering a measurement. In the command, the host sends a single frequency word as a 64-bit integer to the target. The target processor (the microprocessor on the VNA) then programs the quadrature direct digital synthesizer (DDS) to

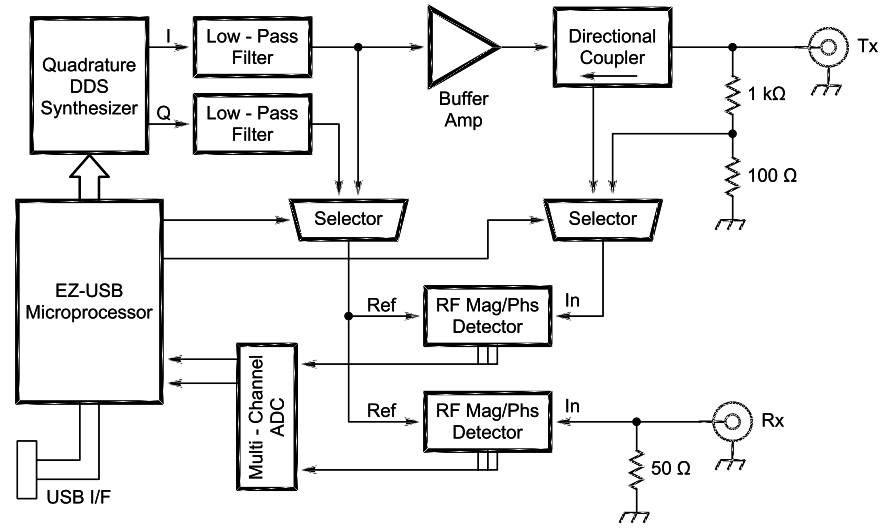

Figure 4—Block diagram of the Vector Network Analyzer.

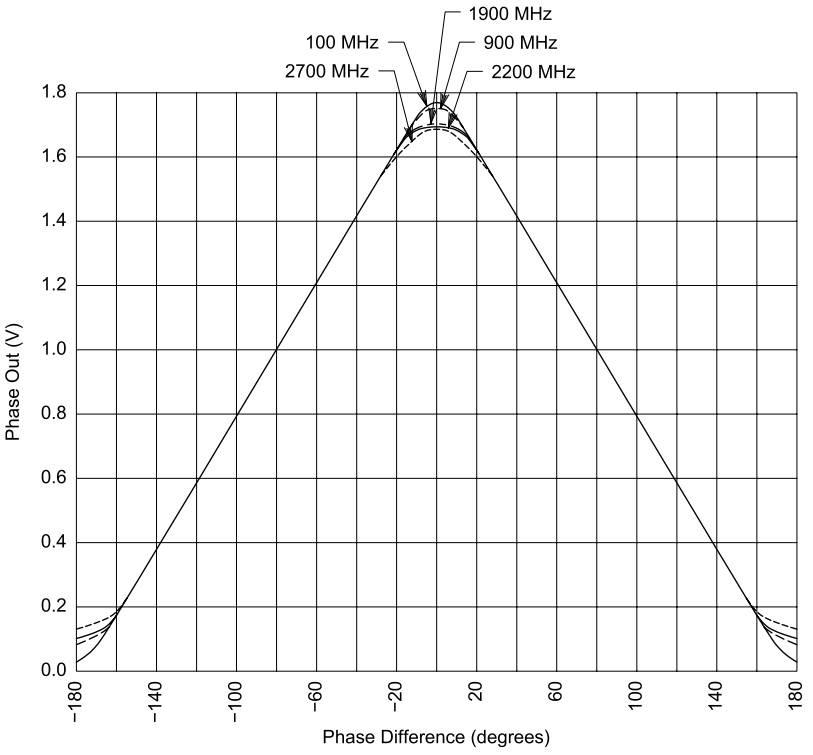

Figure 5—Analog Devices AD8302 phase output response. The response is symmetric about 0°, and thus a quadrature technique is needed to resolve the sign of the phase angle. The accuracy is poor near 0° and 180° due to detector output saturation, necessitating compensation.

that frequency. Once the frequency is programmed, the target processor makes a series of analog measurements. These measurements are made by using the input multiplexer of a multi-channel ADC chip to sequentially select and digitize the various RF detector analog output voltages. Additionally, the target processor switches between the I-reference signal and the Q-reference signal to the RF detectors and remeasures the detector's analog outputs. The target then repeats these two sets of measurements in the reflected direction. The RF detector's output a reference dc voltage, and the target processor measures these as well. In total, more than a dozen analog voltages are digitized and returned by the target processor. All of these measurements are assembled into a single 64-byte USB response packet.

Next, the host processor polls the target to see if it has the measurement ready. When it is ready, the target sends a response data packet back to the host containing the set of data samples that it has measured. The target is then ready to accept a new measurement request.

The host computer processes the measurement data set at each frequency and organizes the information into a useful display. A *Windows* application controls the USB device and provides a GUI interface that looks like a traditional VNA, displaying s-parameters in rectangular or polar (Smith chart) format, providing for calibration and error correction of the measurements, selection of the frequency sweep range, printing of the charts, and so on. The host application was written in *Microsoft Visual C++ .NET* version 2003.

The USB port is capable of supplying 100 to 500 mA (at the option of the host) to the target device. The VNA draws about 1 A, so it is powered from a +5 V dc wall-cube supply. On the VNA board, a Maxim inverter produces –5 V dc for the video selectors; a Maxim linear regulator produces +3.3 V dc for the digital parts. The voltage inverter needed to be decoupled with L-C filters to lower the noise level on the analog lines. Additionally, the video amplifiers required 10-ohm resistors and decoupling capacitors in the +5 and -5 volt lines to produce good low-level signal measurements of the return-loss signals. Power decoupling of the digital parts required just bypass capacitors. The DDS chip and the +3.3 V regulator are each heat sinked to the circuit board itself. A metalized pad on the top layer of the board is connected to the ground plane through a large number of vias. The solder mask is then opened on the top layer directly underneath each part, permitting each to be soldered directly to the circuit board itself. Without this heat sink, these two parts would overheat.

Overview of USB

Many newer computers do not include an EIA-232 serial interface. Many laptops now have only a USB interface for connection of the computer to outside devices. The USB interface supports a large variety of device types. It automatically identifies target devices, and then loads the appropriate *Windows* device driver. The driver is loaded when the USB target is plugged in, and unloaded when the target device is disconnected. USB can provide a minimum of 100 mA of supply current to the target device. In some cases it can supply more, up to 500 mA, but only 100 mA is guaranteed. This voltage is nominally +5 V, but resistive losses in the USB cable can drop it down to +4.4 V in the worst case.

When a USB device is first connected to a host and powered up, the host senses the additional connection via a 1.5 kohm resistor that the target asserts onto one USB data line. This process is called *enumeration*. Through a sequence of packets, the host learns the identity of the device type that connected, its configured capabilities, and which *Windows* device driver needs to be used to communicate with the USB target.

The target in the VNA is reprogrammable; it does not contain any non-volatile memory, just RAM. This allows the VNA target code to be changed quite painlessly. The VNA host application program downloads the executable code to the target each time it is connected and powered up—an extremely flexible arrangement. It permits different application loads to be sent to the VNA target. A minor drawback, however, is that the target then has to go through a somewhat more complex enumeration process.

The Cypress EZUSB microprocessor supports a minimum level of functionality in the processor at power-up when no code has yet been loaded to it—namely the ability to identify itself, to accept a download file, and to restart itself. After initially enumerating the target, the VNA host application software downloads the desired target code and then restarts the target. Then the newly downloaded code on the target takes control away from the Cypress-supplied default values and it *re-enumerates* itself by disconnecting then reconnecting the 1.5-k ohm resistor, this time with different capabilities identified. The new capabilities are specified by the newly downloaded and running target application. Cypress supplies a *Windows* device driver with their free development kit that is used by the VNA host application. Additionally, Cypress supplies a free C-language code framework for the target EZUSB processor that is USB 1.1, Section 9 compliant (named after the USB specification chapter). While there is a bit of a learning curve associated with it all, once understood, the framework makes developing a C-language application very easy—just the relevant USB endpoint handlers have to be coded. Everything else is done. The entire target application was developed in the evenings of about two weeks without requiring any debugger. Note that *Windows 95* does not support USB. (*Win95 OSR2.1* theoretically supports it, but what I've read claims that it is too buggy to use). *Win 98 Gold* (original edition) supports USB 1.0, and *Win 98 SE* (Second Edition) supports USB 1.1. All versions of *Windows* later than *Win98* also support USB 1.1. *WinXP* also supports USB 2.0. The 1.1 version of USB adds an interrupt *packet* type that is not used in this VNA target application.

The USB host sends packets to the target device and receives packets from the target device. The format of these packets is under software control. The USB interface is synchronous with exactly 1 ms time slots. During each slot, the host can send one control packet, one data packet, and one isochronous packet (useful for audio, for example). The target can return one data packet and one isochronous packet during the next slot. All USB target devices are polled. To retrieve a data packet, the host sends a control packet to the host requesting a response. The target then returns a data packet. Data packets can be up to 64 bytes in length, while isochronous packets can be 1023 bytes in length (1024 bytes in USB 2.0). A good text on USB is available.[6]

Software

The software consists of two independently compiled and linked software executables: the *host* software, and the *target* software. The host computer is a PC with an Intel IA32 processor (Pentium) running *Windows*. The target is a Cypress EZUSB processor (derived from the 8051) running just the target code image—no operating system or scheduler. Each

requires a different software development system.

Run-Time Software

The description of the tools below is of interest if you want the compile or change the software, which most people will not want to do. To just run the VNA software, the following binaries are needed:

- VNA host executable file,
- Microsoft .NET 1.1 Common Language Runtime (CLR) package,
- Host-compiled help file,
- VNA target (EZUSB processor) executable file,
- USB device driver file—supplied by Cypress: EZUSB.SYS,
- USB .inf file (driver information file) also supplied by Cypress. EZUSBW2K.INF.

Target Software

The target software was developed in C using the *AnchorChips* USB framework. This is available on the Cypress Web site for free in the EZUSB development download package. Literally, the framework is a couple of C module skeletons. You just need to fill in the various USB endpoint handlers and strip out anything you don't need, which isn't much. Getting this up and running on the target was really fast. After finding a hardware bug (two missing pull-up resistors), the framework came right up and ran. From that point it was a matter of adding functionality to the target through about four prototype builds. Each prototype added features over the previous build as we noted any errors in execution. These were usually quickly tracked down to the last added changes. Two tricky parts: The DDS chip comes out of reset at a slightly higher reset voltage than does the EZUSB processor, so some delay cycles were added to the USB code before it tried to initialize the DDS. The parallel interface was used on the DDS, since the chosen EZUSB device (AN2135) has an 8-bit parallel interface. Two I/O lines on the EZUSB are used for RD and WR lines to the DDS chip. Some have reported difficulty using the serial interface on the Analog Devices DDS chip, but the parallel interface was problem free. Secondly, the USB device is happier with exactly 64-byte bulk packets, so they are always sent this size. Interestingly, only one bulk-type packet is sent per frame, so sending 1-byte or 64 does not change the effective rate of packets per second because the frame rate does not change with packet size. Thus, for maximum throughput, 64 byte buffers should be used.

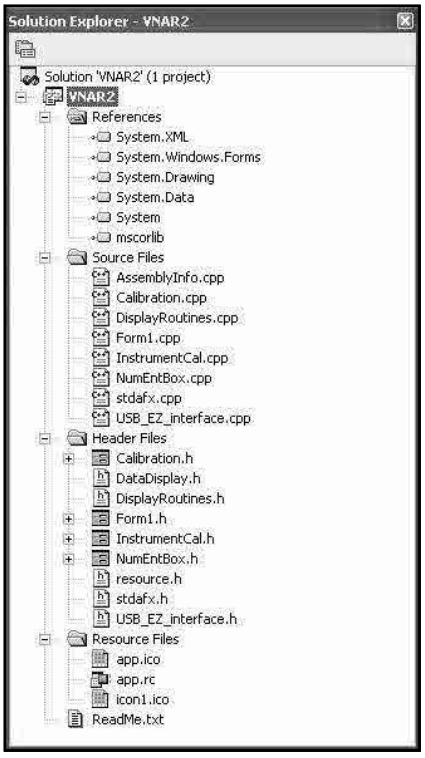

Figure 6—Host software source tree.

Host Software

The host software was written in *Microsoft C++ .NET 2003*. This is the most current version of the *Microsoft C++* compiler. The standard edition is available at a reasonable price. Microsoft used the name .NET (dot NET) to reference a lot of different products and services, which has confused people as to what it really is. The *C++ .NET* product contains a run-time library and a compiler/debugger. The common-language run-time library (CLR) provides a language-independent environment to execute the *Microsoft Intermediate Language* (IL), which is just in time compiled. It handles memory management and garbage collection (freeing up unused memory). This is pretty traditional for Basic, but novel for C and C++, which previously required the software developer to explicitly control the lifetime of objects and variables in memory. According to some, memory leaks and lifetime management constitute the largest category of programming errors in C and C++, and .NET is supposed to help minimize these types of errors. The same CLR supports Basic, C# (C-sharp) and C++, so mixing languages is possible. The 2003 edition of .NET supports a GUI designer for C++. After manually constructing several windows and dialog boxes in the 2002 edition, it's a relief to have that task partially automated. Programming in .NET is a lot different than standard C++. Reading the step-by-step tutorial book and going through the exercises is a must unless you are already familiar with .NET. Fortunately, the book and standard-edition compiler can be purchased together as a set at about the same price as just the compiler itself—if you do some shopping. The GUI designer has its own unusual way of constructing code. We chose to rewrite the initial host software prototype into a style better aligned with how that designer works. This made subsequent changes and especially additions a lot faster.

The VNA application consists of a number of software modules:

- The main program *VNAR2*, which holds the primary program control and display window
- Several dialog-box modules (calibration, numeric entry, etc.).
- Several utility modules that provide some general computations with complex numbers, and translate values into screen coordinates
- A wrapper module to encapsulate the interface to the USB device driver
- Several resource files (RESX) that hold the resources for the displayable windows

The source tree for the host program is shown in Fig 6. *Microsoft .NET C++* has an unusual approach to its filenaming convention: For the designer-generated code, the .h file holds most of the executable code, while the .cpp file contains a few headers. *Form1* is the main program, holding the top-level display and control window (Form1.h), and is also the entry point to the .NET program (Form1.cpp). For non-designer generated code, we chose to adopt the opposite convention by declaring class, module, and subroutine interfaces in .h files, putting the class methods and subroutines in the .cpp files. Old habits die hard.

Calibration contains the interface to the test-fixture calibration routines and the computations for deriving a virtual s-parameter error matrix equivalent to the fixture's influence on the measurement. *DisplayRoutines* contains code to derive screen coordinates for the display window given rectangular or polar display coordinates. In addition, it contains *FrequencyGrid, CalibrationDatSet,* and *Detector class* definitions and methods. The frequency grid allows decoupling the number of data points measured by the VNA in a single sweep from the display resolution of the screen display itself. *InstrumentCal* contains the menu interface and methods needed to perform the calibration of the individual AD8302 detectors.

The *NumEntBox* routine contains methods to allow direct entry of the start and stop frequencies or levels when a large numeric indicator is double-clicked. The EZ_USB_interface contains a wrapper for interfacing to the Cypress *EZUSB.SYS* low-level device driver.

In addition, several support data files are needed:

- The binary executable code for the target, which the host application reads and downloads to the target through the USB interface
- A calibration data set file. The application writes this file with calibration parameters after a calibration is performed. It can also be read by the application to retrieve previously saved calibration parameters. The data in the file is stored in binary format.
- Export files. The host software has an option to generate measured s_{11} and s_{21} values in a tabular format as a text output file. There are several standard file-header and polar/rectangular formats, which support several popular simulation and CAD packages. This allows measured device parameters to be directly imported to those CAD programs as an s-parameter model.
- A compiled help file was generated to provide help for the VNA; it's compatible with the Microsoft HTML help engine (which requires IE4.0 or later).

The interface to the USB driver was—and is—pretty tricky. We're not altogether satisfied with the result. The driver was written pre-.NET and it cannot be invoked directly by a .NET program. Microsoft provides a P/Invoke command that marshals data into a format compatible with direct API calls to *Windows*. The calls have to be prototyped so the compiler knows how to call them; hence, each one was done by hand. (There are about 10 calls in the driver.) The variables passed to the driver are somewhat complex, and they have to be described to the compiler as well. To describe these variables, several header files from the *Windows* Device Driver DDK need to be included. Microsoft distributed the DDK beta version free of charge, but now charges for the completed version. Worse yet, *#including* the header files breaks almost all .NET code.

The strategy was to build a .CPP and an .H file for the wrapper. The .H file describes the interface to the wrapper to the compiler and other .NET modules. The .CPP file includes the actual code, as well as the *#include* files. Then that .CPP file is compiled without the run-time library, and that .CPP file is not exposed to other .NET files, only the linker sees it; however, other modules know how to call the wrapper because of the .H descriptions which they *#include*. This worked in the 2002 edition, but broke in the 2003 edition. The 2003 edition requires that all class methods and class variables, *whether public or private*, be declared in the CPP file and be identical to those exposed in the .H file. The *#includes* needed to do this immediately to break the compilation of all the other .NET modules. A temporary solution was to bury the variable definitions inside the methods of the wrapper class as *automatic* variables. This way they are never exposed as an interface or class variable of the wrapper itself. Unfortunately, this makes the saving of driver state in a private-class variable difficult, since useful variables cannot be declared.

We ended up throwing away much of the wrapper code that made a clean wrapping of the driver, and ended up just re-acquiring driver data inside every method every time it is called. There are probably several better ways to solve this significant problem. The byproduct of our approach is that you need to have several of the header files from the DDK to compile the application, since we cannot distribute them. It is probably possible to write the driver wrapper as a .DLL in an older version of C++ and avoid many of these issues.

USB Device Driver and Initialization

USB is a plug-and-play interface in *Windows*. To associate a device driver to a device, *Windows* needs to know the ID of the USB device that is installed and which device driver to connect to it. When the VNA is plugged into a computer for the first time, the *new-hardware-detected wizard* is called by *Windows*. It causes the VNA to enumerate without any code loaded into it. The Cypress EZUSB will answer this enumeration request with the VID (Vendor ID) and PID (Product ID) code of the EZUSB processor. Then *Windows* will pop up a dialog box and ask the user to choose between supplying a disk file or letting *Windows* search for the file. In the VNA package, an .inf file (driver information file) supplied by Cypress tells windows to use the EZUSB.DRV driver file when the VID_PID device is connected. The wizard makes an entry in the registry associating the VID_PID with the device driver so that the wizard and user dialog box don't have to be displayed again. One needs to copy the EZUSB driver into the driver directory in *Windows*, which is different for different versions of *Windows*, to use it. (In *WinXP*, it's *\Windows* System32\Drivers.) Having done that the first time, *Windows* can find and load the driver anytime one plugs in that USB device.

The USB interface to *Windows* is fairly complex, and writing device drivers is not a trivial task. So the driver supplied by Cypress is used for the VNA. It's a very low-level driver, but we've had good results with it so far. It does have a few bugs. Those that are known have been avoided in the wrapper module code.

Other than the wrapper problem, very few issues were encountered in constructing and debugging the NET code. The 2003 version of the C++ .NET debugger is a lot more stable than the 2002 version.

HTML Help

A help package was generated for the VNA using the *Microsoft HTML Help Compiler 1.4*, available for free from the Microsoft Web site. There's also a good tutorial available on the Web[7] about how to use this tool to build help and context-sensitive help. Each help topic is actually an HTML page; the compiler links all the pages into a single compressed binary file using the .chm suffix along with the table of contents, index, and search tags. The tags can point within the file or across the Internet, but we decided to leave all of them within the compiled file so that an Internet connection is unneeded to use the help file — or the VNA! The computer does require *IE 4.0* or later to view the help topics since they are HTML. This type of help interface should look familiar to most *Windows* users.

Available source code can be found at **www.arrl.org/qexfiles**.

Calibration and Error Correction

All s-parameter measurements made by the VNA need to be calibrated. The actual measurement occurs on the printed circuit board itself, which is removed from the device under test (DUT). The connecting leads and components on the circuit board, connectors, interconnecting cables to the DUT and measurement imperfections of the components transform the measurement values. Additionally, the VNA does not have an absolute amplitude or phase reference, but only a relative reference. In practice, error correction and calibration are combined into a single compensation to the measurement. Different cable lengths may be needed for different measurements

and the cable length significantly affects the measurement. Thus, calibration is usually required for each different test-fixture setup. The host program has a mode to take a calibration set and store it with a descriptive file name to be recalled as needed.

Calibration involves compensating the phase delay of the instrument and the interconnecting cables. It also compensates for amplitude variation with frequency. Because the VNA is really only half a network analyzer (forward direction only), the TRL technique cannot be used. The TRL technique can avoid the need for precision standards. Instead, calibrations for s_{21} and s_{11} are derived independently using accurate RF loads—well, we hope they're accurate.

Transmission Calibration (s_{21})

The transmission calibration (s_{21}) is easier to understand. There are two interconnecting cables—one from the TX connector to the DUT, and another from the DUT to the RX connector. In the through-calibration mode, these two cables are disconnected from the DUT, and directly connected together with a *very* short connector called a "bullet." The software makes the assumption that the bullet has no length and is a perfect impedance match. That would be a poor assumption at microwave frequencies, but at 120 MHz, it's not too bad. The transmit signal is then swept across the frequency range of the instrument and the received magnitude and phase recorded for 1024 different discrete frequencies. The phase delay and amplitude received are computed and stored in a table by frequency. Obviously, longer cables would have greater phase delay and perhaps more attenuation at higher frequencies. The RX port is terminated on the circuit board with a fairly accurate 50-ohm resistive load. Similarly, the TX port is sourced from a fairly accurate 50-ohm resistive pad at the output of the TX buffer amplifier, resulting in a good source match. To apply the transmission calibration against the measured DUT data, the measurement of s_{21} of the DUT is divided by the recorded calibration value at the same frequency. Since both these data are complex numbers, this involves using complex division.

$$s_{21}^{\text{actual}} \quad \frac{s_{21}^{\text{measured}}}{\text{Cal}_{21}} \qquad \text{(Eq 1)}$$

If the measured value of s_{21} were exactly the same as the stored calibration constant, then $s_{21}{}^{\text{actual}}$ would be 1.0+*j*0, signifying that the DUT had no gain, loss, or phase shift. Since the DUT does have s_{21} imperfections, Eq 1 just derives the difference between the DUT measurement and the calibration measurement, thus removing most instrument and interconnection cable errors.

Reflection Calibration (s_{11})

The reflection calibration (s_{11}) is a bit more complex. Three calibration runs are made using different loads attached to the end of the TX cable that has been removed from the DUT: 1) with a 50-ohm load, 2) with a shorted load, and 3) with an open load. The accuracy of these calibration loads directly affects the correction accuracy of subsequent measurements. Table 1 shows the value of the reflection coefficient Γ for each load type *directly at the load itself,* assuming that they are perfect loads, which they are not. The VNA instrument measures a value for Γ that is rotated in phase and attenuated in magnitude by the interconnecting cables, PC-board traces, and components in the cable and instrument itself. The calibration computation involves de-rotating the measured value by the calibration phase delay, and adjusting the measured magnitude by subtracting the reflection calibration amplitude component. This calibration computation must be done at each frequency.

The three load components lie along the center horizontal straight line on a Smith chart, a short being at the left, 50-ohm in the center, and an open on the right. See Fig 8. The calibration measurement will indicate instead three points on a line that is rotated from the horizontal position by the amount of phase delay in the transmission cable plus the delay internal to the instrument itself. The amount of rotation is frequency-dependent.

After de-rotation to the horizontal position, the three measurements will not lie exactly on the ideal positions on the Smith chart listed in the table, but will be offset by the remaining measurement errors. Before the de-rotation, the amplitude measurement of the DUT is scaled differently on the left and righthand side of center (low and high resistive components, respectively) using the short and open cali-

Table 1
Reflection coefficient for terminated, shorted, and open loads in polar and rectangular coordinates.

Γ	*Polar Coordinates*		*Rectangular Coordinates*	
Load	*Magnitude*	*Phase*	*Real*	*Imaginary*
Short	1	±180°	–1	0
50 Ω	0	arbitrary	0	0
Open	1	0°	+1	0

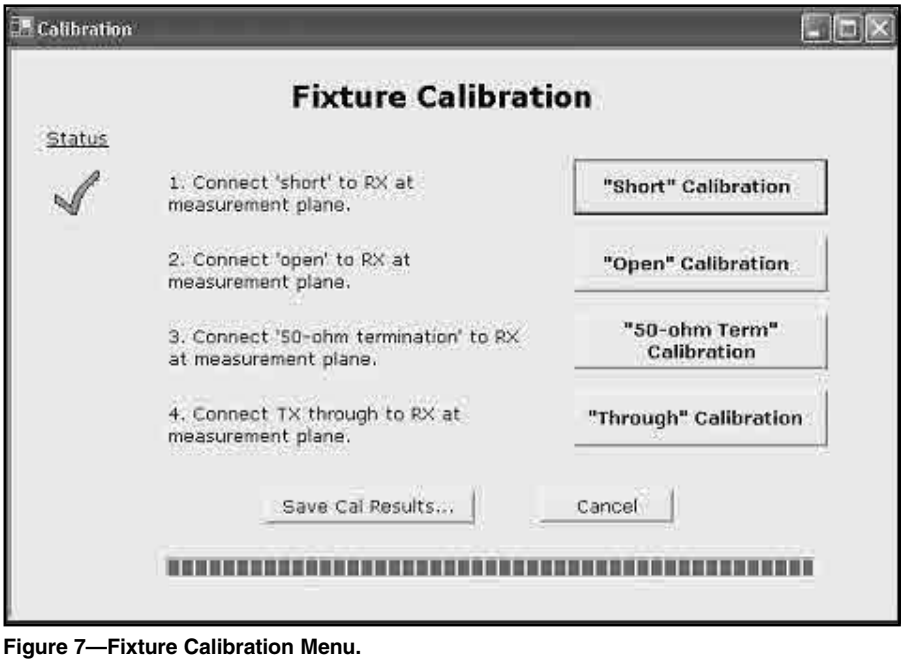

Figure 7—Fixture Calibration Menu.

bration values as full-scale (left and right, respectively), and the 50-ohm value as a zero scale constant. This is because some measurement errors are dependent on the impedance seen by the directional coupler itself. After this adjustment, the value is de-rotated by the calibration reflection phase delay value, which results in the final value for Γ. Fig 7 shows the fixture calibration menu, with the short calibration completed.

We can place reflection measurement errors into three types:

- E_d Directivity error—this error is caused by leakage in the directional coupler and impedance mismatches between the VNA and the DUT reflecting additional energy.
- E_s Source mismatch error—this error is caused by impedance mismatch between the signal source and the directional coupler. In the VNA, an attenuator pad is used between the buffer and the directional coupler to provide a reasonably good match, but it's not perfect.
- E_t Tracking errors—these are errors in the measuring circuits that provide the magnitude and phase values and include test-cable artifacts.

In his book on microwaves, Pozar describes how to analyze and derive these reflection measurement error terms for the one-port calibration.[8] The technique models the three errors as a virtual s-parameter error matrix inserted between the VNA and the DUT.

Refer to Fig 9 for s-parameter definitions. In an s-parameter matrix, the forward input voltage, a_1, reverse input voltage, a_2, forward output voltage, b_2, and reverse output voltage, b_1 are related by the s-parameters:

$$b_1 \quad a_1 s_{11} + a_2 s_{12}$$
$$b_2 \quad a_1 s_{21} + a_2 s_{22} \qquad \text{(Eq 2)}$$

Thus the voltage emerging from the network lefthand side, b_1 is the sum of the input reflection property of the network times the input voltage a_1, plus the reverse isolation of the network times the voltage supplied into the network from the right-hand side, a_2. We substitute the error terms into the s-parameters of the virtual error matrix:

s_{11} is the source directivity error, E_d.

The product $s_{21}s_{12}$ is the reflection tracking error, E_t, which we can allocate between the two terms as we like—in this case, setting s_{21} to unity, and s_{12} to E_t (see Fig 10).

s_{22} is the source matching error, E_s.

If we place the DUT that has an actual reflection s_{11}^{actual} (Γ actual) on the output of this virtual S-parameter error network, then from the input of this error network we measure s_{11}^{measured} (Γ measured). It can be shown that the actual measured value of the DUT looking through the error matrix is:

$$s_{11}^{a} \quad \frac{s_{11}^{m} - E_d}{E_s(s_{11}^{m} - E_d) + E_t} \qquad \text{(Eq 3)}$$

The derivation requires a bit of algebra and Pozar covers this in his book. We have three unknown terms and three measurements, so it is possible to solve for the three error terms. The solution to the first term is:

$$E_d \quad s_{11,\text{load}}^{m} \qquad \text{(Eq 4)}$$

This is because the reflection from a perfectly terminated load is zero. Thus a_2 of the virtual error matrix is zero, and the E_s and E_t terms fall out of the b_t voltage term (reflected signal). Similarly:

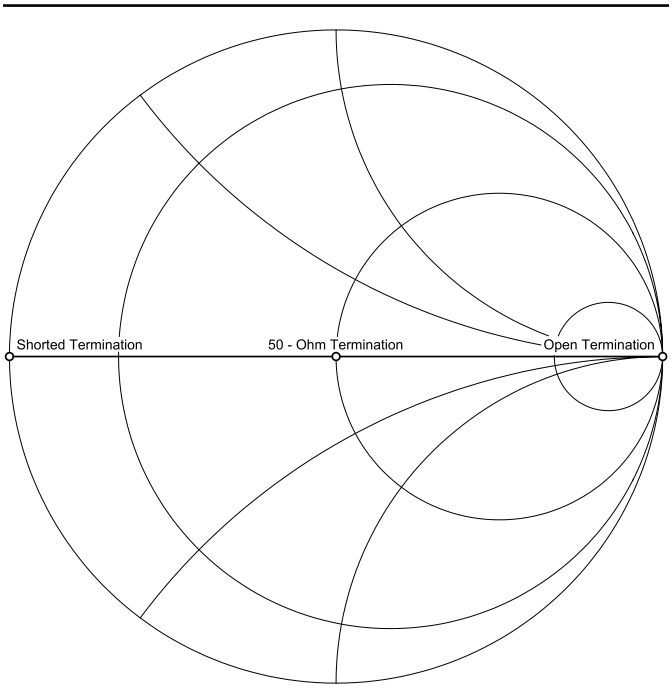

Figure 8—Smith Chart plot of ideal calibration load points after computationally removing the test cable transmission line length.

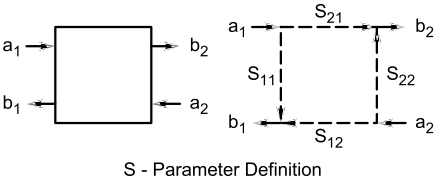

Figure 9—S-parameter definition.

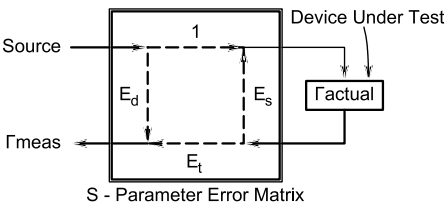

Figure 10—S-parameter error matrix.

$$E_s \quad \frac{2s_{11,\text{load}}^{m} - \left(s_{11,\text{short}}^{m} + s_{11,\text{open}}^{m}\right)}{s_{11,\text{short}}^{m} - s_{11,\text{open}}^{m}} \qquad \text{(Eq 5)}$$

and

$$E_t \quad \frac{2\left(s_{11,\text{open}}^{m} + s_{11,\text{load}}^{m}\right)\left(s_{11,\text{short}}^{m} + s_{11,\text{load}}^{m}\right)}{s_{11,\text{short}}^{m} - s_{11,\text{open}}^{m}} \qquad \text{(Eq 6)}$$

E_t includes the phase delay and attenuation of the interconnecting cable between the VNA and the device under test. Thus, different calibration files need to be collected for different cabling setups, since E_t will be different in each case.

D. Pozar's book on microwave engineering covers the

topic of VNA calibration and compensation. In the host program, the calibration routine guides the user through four test setups, and makes four measurements—short, open, load, and through. All are swept over the complete frequency range of the analyzer. It then derives the values of E_d, E_s, and E_t over frequency, and also derives the transmission calibration term discussed previously. The three reflection error terms, as well as the raw reflection calibration data, can be plotted on the polar chart to give an idea of what they look like. The calibration routine stores a table of the three derived error terms, along with the s_{21} transmission calibration value, each at 1024 frequencies, in a file on disk. The name of the file can be selected at the time the calibration file is saved.

The calibration function also allows loading a named calibration file instead of having to repeat a previous calibration run, which saves a lot of time. This makes it easier to have different calibration files for each test setup. The raw data is also saved to the file allowing rerunning the calibration and changing only one measurement type (for example "through"), and then saving the cal data set. The raw data will be overwritten by any new measurements while preserving raw data not re-collected. Then the cal file can be saved again. This updates the cal data set with only the new data type. This saved a lot of time during the debug cycle.

Fig 11 shows the measurement of a shorted cable without fixture calibration applied. Without calibration, the short describes a circle near the edge of the polar chart, illustrating that the connecting cable between the short and the VNA rotates the phase angle of the short. After the fixture calibration is applied (Fig 12), the cable phase rotation has been removed and the short shows up as point on the left side of the polar chart, with all frequencies being measured falling on the same point (0 ohms).

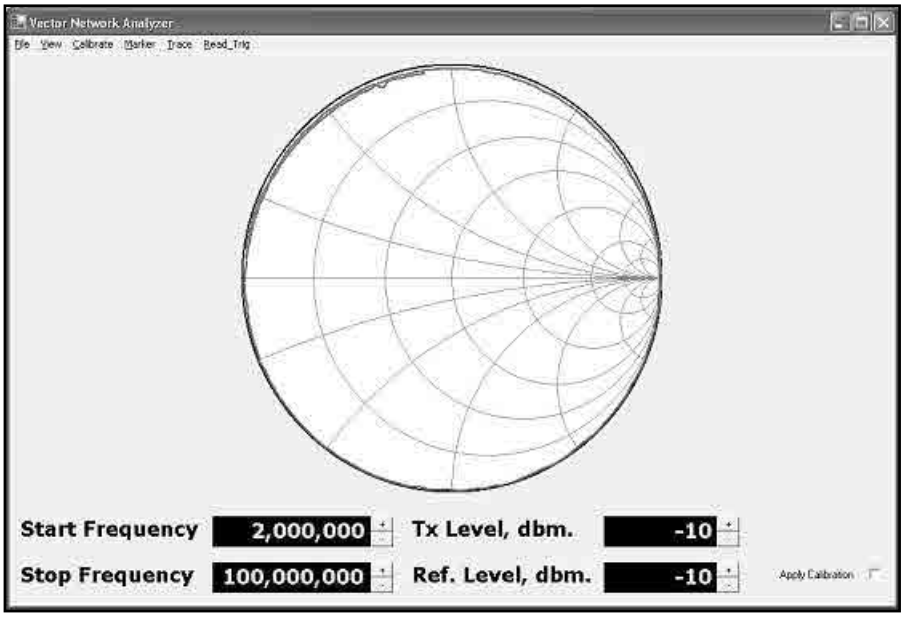

Figure 11—Shorted cable without fixture calibration.

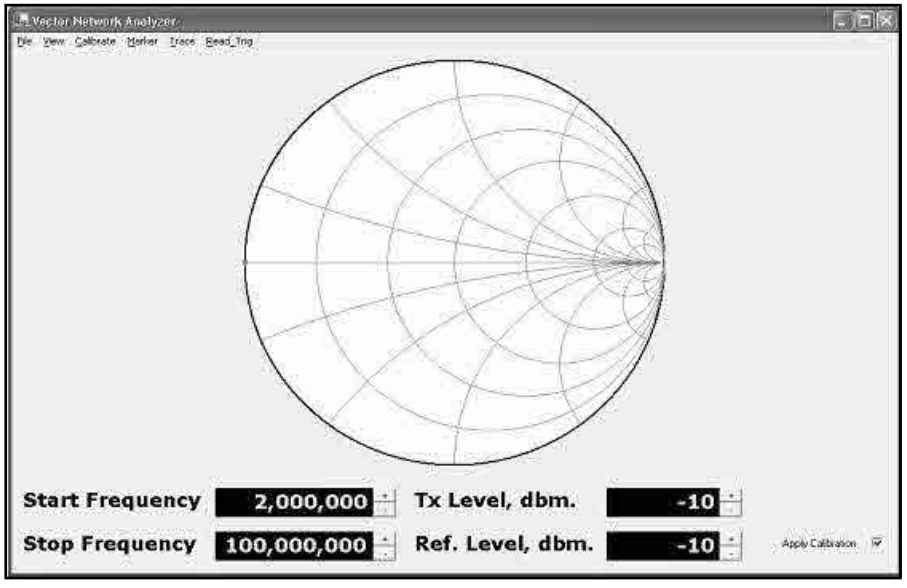

Figure 12—Shorted cable with fixture calibration applied.

Phase Measurements & Detector Calibration

At first, a simple technique was used to translate the phase detector analog measurements measured by the AD8302 from voltage to phase, in degrees, with respect to the reference signal. The arctangent of the I-measurement divided by the Q-measurement, with appropriate correction for the measurement quadrant, was utilized. Unfortunately, this simple technique suffers from a significant error because of phase-detector saturation in the AD8302. Particularly near 0 V output, the phase-detection gain drops non-linearly. The range near positive output (+1.8 V) is less saturated, but the actual positive voltage peak value varied a lot from device to device. In one case, it significantly exceeded the value of V_{ref} from the specific device being measured.

The nature of the error causes a somewhat sinusoidal error in the phase reading— the phase varies both above and below the actual value. This error was particularly significant in group-delay measurements, since the group-delay routine differentiates the phase slope at adjacent frequency sample points. Fig 11 shows the

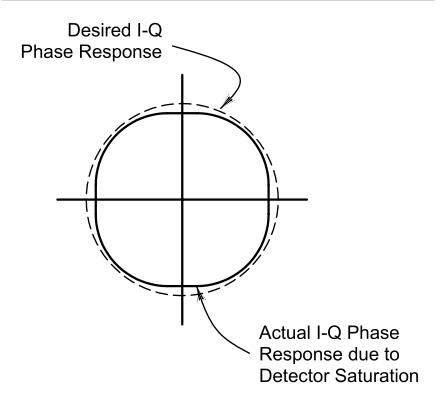

Figure 13—Error of phase reading over 360° caused by detector saturation near zero and +2.0 V.

slightly oblong shape of the phase response caused by detector saturation.

A new phase calibration routine was devised that uses a length of coaxial cable as a reference element. This calibration result is used to compensate the converted phase values. A fixed length of cable has a constant time delay, and thus has a linear phase change with frequency. The detector calibration routine measures a small fixed length of cable and compares it with the actual phase-detector measurement. The software then stores a table containing the difference, in degrees, between the measured phase and the phase calculated by linearly interpolating the cable phase. That is, it finds two points in frequency that differ in phase by 360° because of the calibration cable, then derives the phase at any frequency in between using a linear fit to the two endpoints. This phase difference is stored in a table with one-degree resolution.

A separate table is generated for the transmit and receive AD8302 phase detectors. This same calibration routine also finds the midpoint of each phase detector's output range by finding the detected output voltage— approximately +0.9 V, but slightly different from device to device—wherein the reference cable produces 0°, 180° and 360° phase differences at the same output voltage. The process converges in about three iterations. The algorithm thus fully characterizes each AD8302 by its individual performance.

This phase calibration process is done separately for the TX and RX phase detectors, since they are different physical devices and have different errors. The detector constants and correction tables are stored in a small detector calibration file in the program startup directory—the directory where the VNA program starts execution. The detector calibration does not change with the test setup; thus it only needs to be measured once, then the values are relatively permanent. The software automatically looks for and loads this detector calibration file on startup and provides a warning message to run the one-time detector calibration routine if the file cannot be found. A menu option to run the detector calibration allows the initial generation and storage of the constants in this file using a couple of short test cables. Running the detector calibration routine overwrites any existing detector cal file.

A small residual error remains after this improved calibration technique, which can be seen most easily when measuring group delay. Fig 14 shows the phase response of an approximately 3 m long cable with and without this error correction.

Fig 15 shows the transmission amplitude response, phase and group delay of a 3 m long cable. The group delay scale is 10 ns per division, thus this test cable has

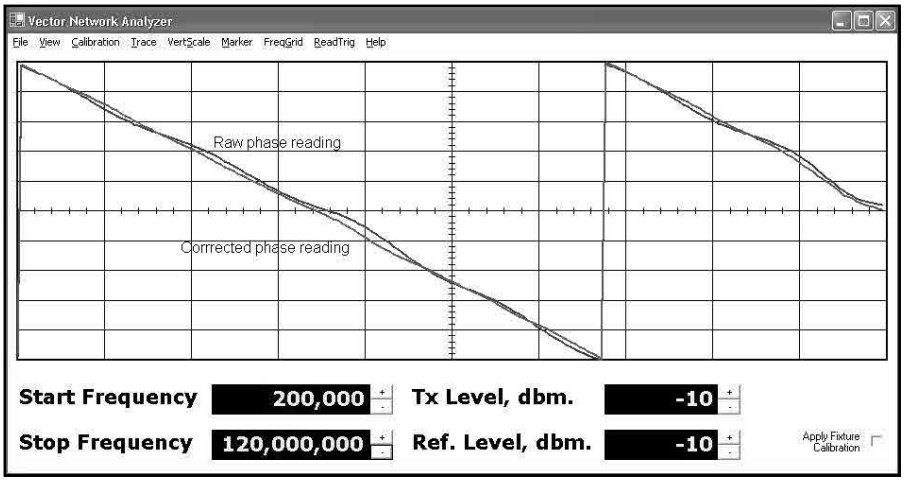

Figure 14—Phase response before and after detector calibration.

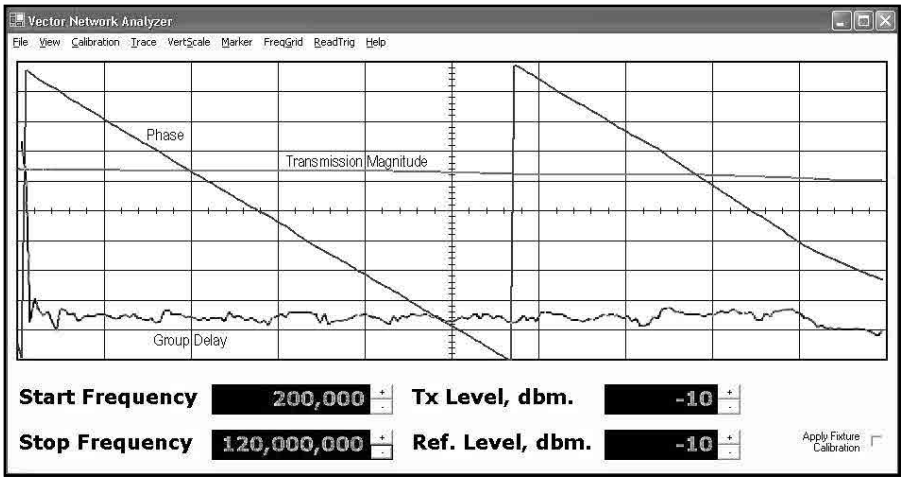

Figure 15—Transmission Magnitude, Phase and Group Delay of a 3 m test cable.

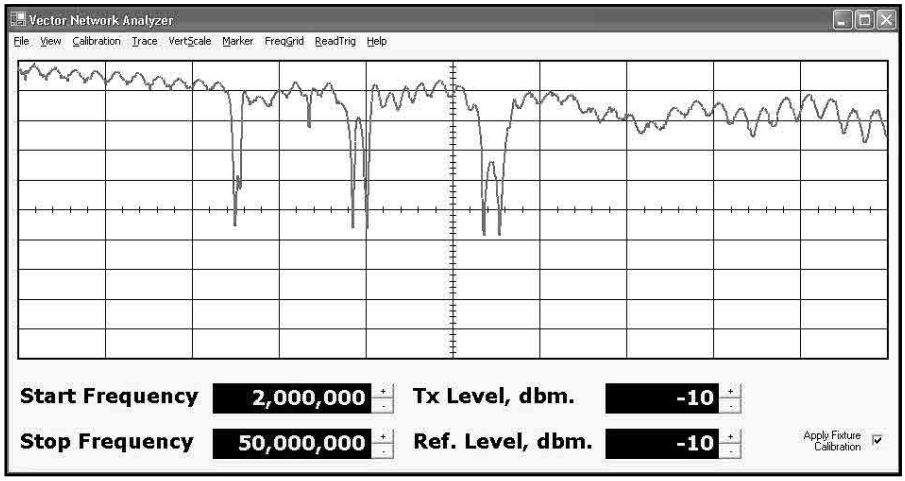

Figure 16—Return loss of KT34XA antenna through 300 feet of hardline. Vertical scale is 5 dB/div.

about 14 ns of delay. A perfect result would be a straight horizontal line for group delay. This measurement was made by differentiating the phase at each incremental frequency sample, thus it produces the noisiest measurement. When the delay differentiation is spread across several samples (called the *frequency aperture* of the group-delay measurement), the errors are significantly filtered. The result shown in the figure we consider to be quite good. Seven different detector-calibration algorithms were tried to get to this point. The drop in delay above 100 MHz is caused by reference-signal degradation, in turn caused by the DDS's reconstruction low-pass filter cutoff limitation described earlier.

Software Source Code

VNA source files for both the target processor and the host processor have been made available in open format on the Web for amateur and non-commercial use. It's hoped that readers will add useful and interesting functionality to the VNA and make any changes similarly available for amateur and non-commercial use.

Software Tool Sources

The development software can be purchased inexpensively. The target is written in C and 8051 assembly. Cypress provides a limited-capability free copy of the Keil compiler in its development package. Another compiler package, Reads-51, which is free for non-commercial use can be downloaded from the Web,[9] but the target software has not been ported to that package yet. The host software is written in C++. The Microsoft compiler can be purchased as part of the Microsoft C++ .NET 2003 Step-by-Step Deluxe Learning Edition, which contains both the excellent Step-by-Step book and the C++ standard-edition compiler, bundled together.[10] The set can be found at local bookstores, or at a discount from several Web-based bookstores. We found it commercially available on the Web for less than $80. The *HTML Help compiler v1.4* is free from the Microsoft Web site, and a good tutorial is available by Char James-Tanny, as was mentioned earlier. The installer was generated using the Jordan Russell INNO installer program, which is free for any use (commercial or not) and is very simple to use.[11]

Applications

There are a large number of applications for a VNA. We'll examine a couple of them here.

Antenna Return Loss (SWR)

One of the most common measurements made is the standing wave ratio of an antenna. A low SWR means that the antenna input impedance is close to that of the measuring reference impedance. *Return loss* is the common term for an equivalent measurement, that being the ratio of the reflected voltage to the incident voltage, usually expressed in dB. To convert from return loss to SWR, the following formulas are used (S = SWR, ρ= reflection coefficient, RL = return loss in dB):

$$\rho = 10^{-\left(\frac{RL}{20}\right)} \qquad \text{(Eq 7)}$$

$$S = \frac{1+\rho}{1-\rho} \qquad \text{(Eq 8)}$$

So, for example, a return loss of 20 dB is a reflection coefficient of 0.1, and an SWR of 1.22. A return loss of 10 dB is a reflection coefficient of 0.316, and an SWR of 1.92.

The following measurements show the magnitude of the return loss versus frequency for a KT34XA antenna at the end of 300 feet of hard-line cable. The resonance points are clearly visible. The phase part of the impedance is that at the ham-shack end of the cable, not at the antenna. Fig 16 shows the return loss at 5 dB/div of the antenna swept from 1 MHz to 50 MHz. The 20-m, 15-m and 10-m

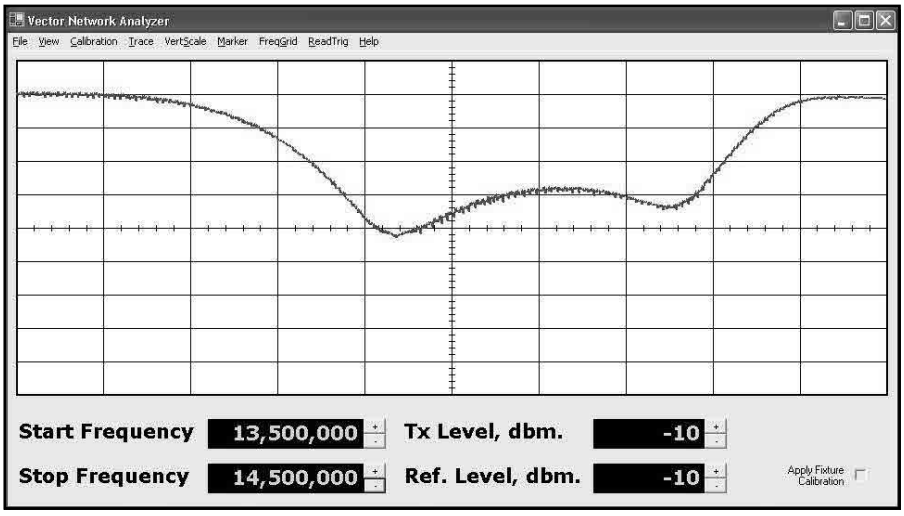

Figure 17—Return loss of Fig 16 from 13.5 MHz to 14.5 MHz. 26 dB return loss (best case at 13.94 MHz) is an SWR of 1.105 (at the ham-shack end of the feed line).Vertical scale is 5 dB/div.

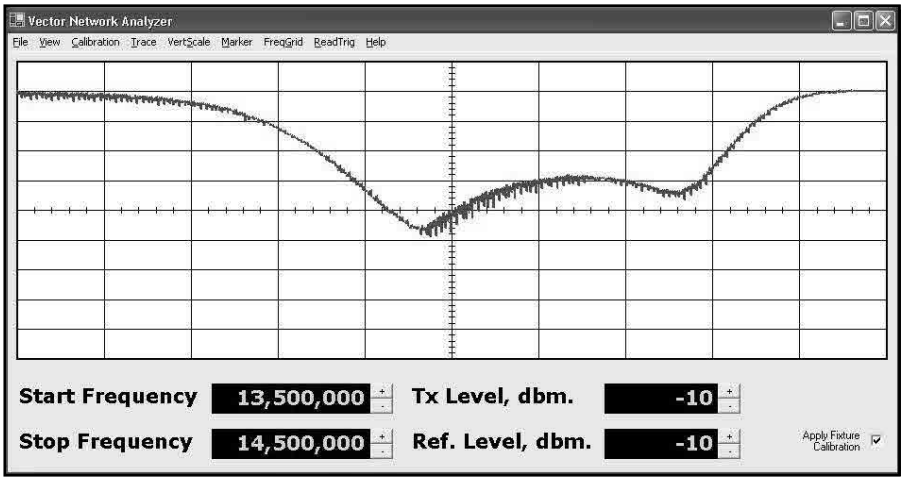

Figure 18—Return loss of Fig 17 with fixture calibration applied (the fixture is the instrument itself and one m of cable). Note the best-case return loss is now 28 dB at a frequency of 13.96 MHz (an SWR of 1.083). Vertical scale is 5 dB/div.

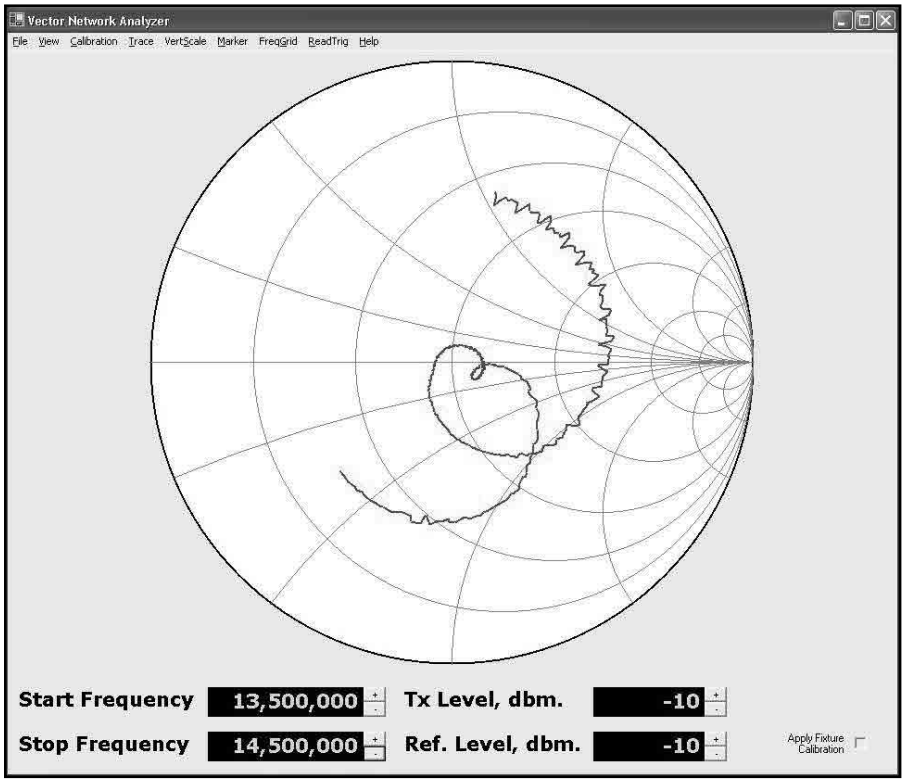

Figure 19—Return loss of Fig 18 on a polar scale.

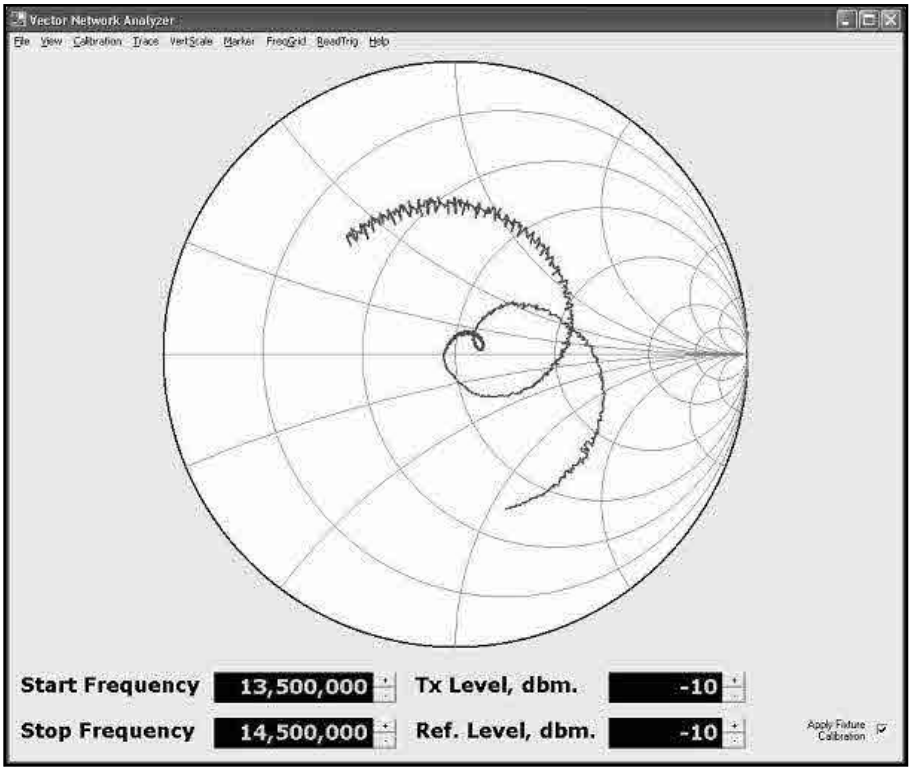

Figure 20—Return loss of Fig 19 with calibration applied. Note the significant amount of phase rotation that is removed with instrument calibration and just 1 meter of cable correction.

band resonances are easily seen. Fig 17 shows a closeup of the return loss from 13.5 to 14.5 MHz; Fig 18 shows the same reading after the instrument has been calibrated with a 1-m length of cable. This short cable is used to connect to the analyzer to the hard-line cable and thus represents the load that would be seen by a transmitter connected to the cable. Note that the apparent return loss is improved at some frequencies because imperfections in the instrument and directional coupler have been subtracted out of the measurement. Fig 19 shows this same closeup on a polar plot. Fig 20 is the same polar plot but with fixture calibration enabled. Note the rotation of the polar plot.

The instrument limitation for return loss measurements is about 30 dB, and this degrades by a few dB at frequencies above about 50 MHz. The apparent return loss of the antenna looks better than it really is at higher frequencies because of the increasing loss of the 300 feet of hard line with frequency.

Notes

[1]Universal Serial Bus Specification, Revision 1.1, Compaq, Intel, Microsoft, NEC, September 23, 1998, available at **www.usb.org/developers/docs/**.

[2]AN2135 Microprocessor Data sheet and Cypress EZUSB Development kit are available from Cypress Semiconductor, Inc., **www.cypress.com**, look under **USB Full-Speed Peripherals**.

[3]Analog Devices, Inc, AD8302 data sheet, Rev A., **www.analog.com**.

[4]Analog Devices, Inc., AD9854 DDS data sheet, Rev B, **www.analog.com**

[5]Minicircuits Inc., directional coupler PDC-20-3, datasheet available at **www.minicircuits.com/dg03-192.pdf**.

[6] J. Axelson, *USB Complete*, 2nd edition, Lakeview Research, ISBN 096508195-8, **www.lvr.com**.

[7]C. James-Tanny, *Creating HTML Help with Microsoft's HHW*, 2003, JTF Associates, Inc,**www.mvps.org/htmlhelpcenter/htmlhelp/hhtutorials.html**.

[8]D. Pozar, *Microwave Engineering,* Addison Wesley, 1998, ISBN 0-471-17096-8.

[9]Rigel Corporation Inc, Reads-51 package, PO Box 90040, Gainesville, FL 32607, **www.rigelcorp.com**.

[10]J. Templeman, A. Olsen, *Microsoft Visual C++ .NET Step by Step, Version 2003*, Microsoft Press, ISBN 0-7356-1907-7 is just the book; ISBN 0-7356-1908-5 is the Deluxe Learning Edition that includes the C++ standard edition compiler package.

[11]Jordan Russell's software, INNO installer program, **www.jrsoftware.org/isinfo.php**. □□

Crystal Filters with Variable Bandwidth and Constant Center Frequency

The author presents a new approach to variable-bandwidth crystal filters allowing the center frequency to remain constant while bandwidth is changed.

By Robert Lytle, N3FT

This new filter was inspired by the Ten-Tec Jones filter (Lee Jones, WB4JTR, US patent #5051711). The Jones filter achieves variable bandwidth but with a shift in the center frequency of the filter. Depending on the application, this may be good or bad.

For a simple receiver, the Jones filter could be used to advantage by setting the frequency shift so that the wide and narrow bandwidths are on either side of the BFO frequency. The narrow side would be for CW and the wide side for SSB[1]. Fig 1 shows the Jones filter. As can be seen from the figure, the shunt varactors are

[1]Notes appear on page 17.

22525 SW Baseline
Hillsboro, OR 97123
rob@pythonemproject.com

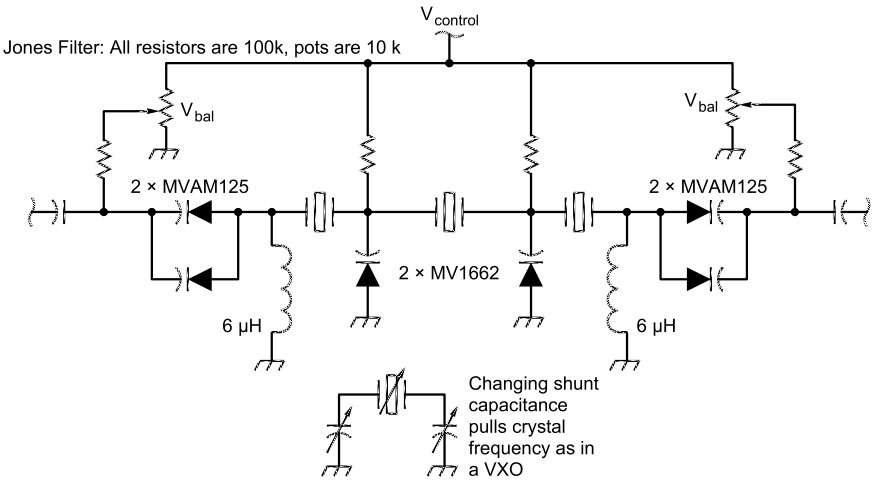

Figure 1—A typical Jones filter with voltage-controlled matching networks, plus a simple diagram illustrating the capacitive pulling effect on a crystal.

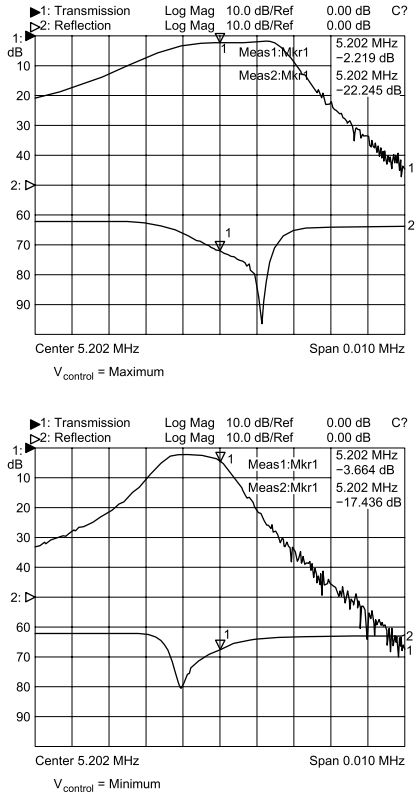

Figure 2—The measured insertion loss vs. frequency (vs. Vcontrol) of a three-crystal Jones filter. Top—maximum bandwidth, bottom—mimimum bandwidth.

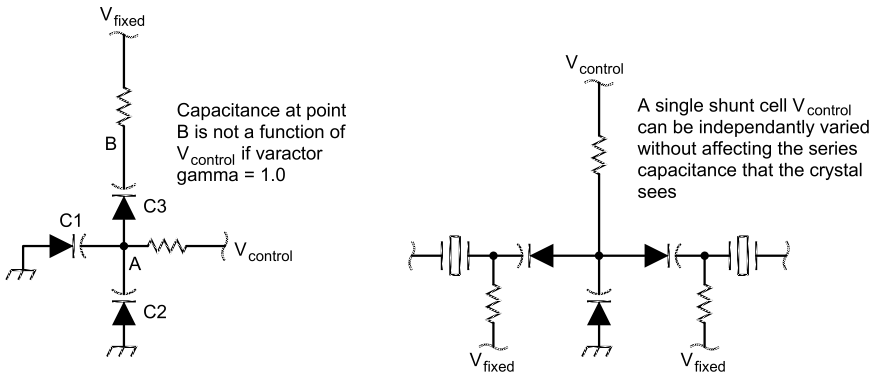

Figure 3—Diagrams to illustrate the independence of Vcontrol on the series capacitance presented to a crystal.

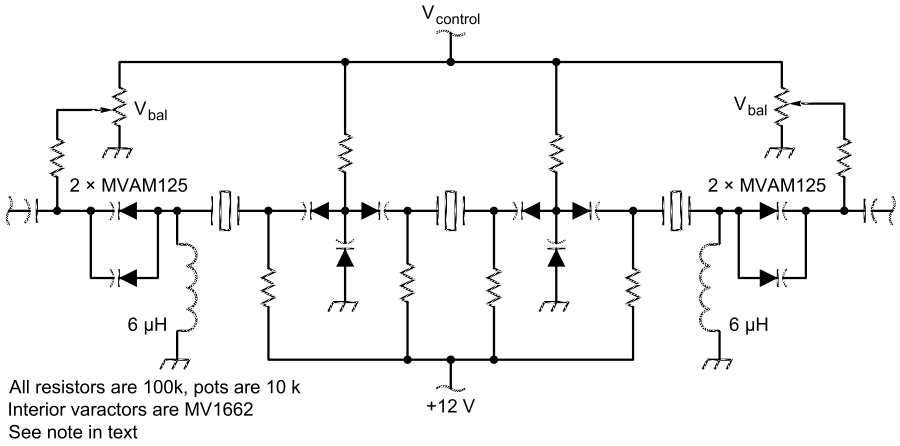

Figure 4—The schematic diagram of the new filter. Notice the voltage-controlled matching networks. These were borrowed from the Jones filter and work very well.

pulling the frequency of the crystals, much as in a VXO. Fig 2 shows the response of a Jones filter at minimum and maximum usable bandwidth. Refer to Fig 6 for the test setup. Notice the shift in center frequency. For applications needing a fixed center frequency (eg, spectrum analyzers and more sophisticated receivers), the frequency shift of the Jones filter may not be a good match for the application.

The key to developing the new filter was the realization that certain varactors had novel properties when connected in series. To get to this understanding, we need to discuss the C vs. V_r curves for varactors. For any varactor one can express the capacitance vs. reverse bias by the equation:

$$C = \frac{C_o}{(V_r + V_\varphi)^\gamma} \qquad (1)$$

Gamma (γ) is a function of the doping profile of the diode. V_ϕ is the turn-on voltage of the diode. C_o is a constant depending on the diode geometry.

It is particularly interesting if the gamma of two series-connected diodes is close to 1.0. In that case, one can show algebraically that the capacitance of two series connected varactors is no longer dependent on the voltage on the middle node. Referring to Fig 3, simply substitute the varactor equation into the equation for series-connected capacitors, adding Cshunt to the second capacitor (i.e. C3 in series with C1+C2). C1 is the shunt cap, which normally would shift the filter center frequency. Now only the voltage at point B sets the capacitance at B. The equation is:

$$C_{fixed} = \frac{C_o}{(V_r + 2V_\varphi)} \qquad (2)$$

Where V_r=V_{fixed}. The Vcontrol terms cancel out.

What this means is that by using varactors with a gamma of nearly 1.0, a network can be constructed which allows for the bandwidth adjustment of a filter without upsetting the center frequency of the filter. Many varactors have been found to have gammas close to 1.0 over at least part of their ranges. For example, the MVAM125, MMBV109L and MMBV609L may be usable. Some of these are smaller-value SMT types, so they would have to be paralleled. The varactors chosen for this project are particularly good in this regard. Although the retailer (Hosfelt[2]) is marking them as matched triplets of MV1662s, the diodes are much too hyperabrupt to be of that type. Hyperabrupt refers to the diode doping profile. Abrupt junctions tend to have a smaller ratio of maximum to minimum capacitance whereas the hyperabrupt diodes have a large ratio.

Fig 4 shows the entire test filter. The potentiometers on each end are adjusted for flattest passband response. Each 6 µH inductor is simply four turns on a BN61-202 balun core. A smaller core will work just as well with a few more turns added. The crystals used in this project are all 5.200 MHz, taken from carrier filters on a surplus ATT FDM unit. The filter cans were opened and the crystals

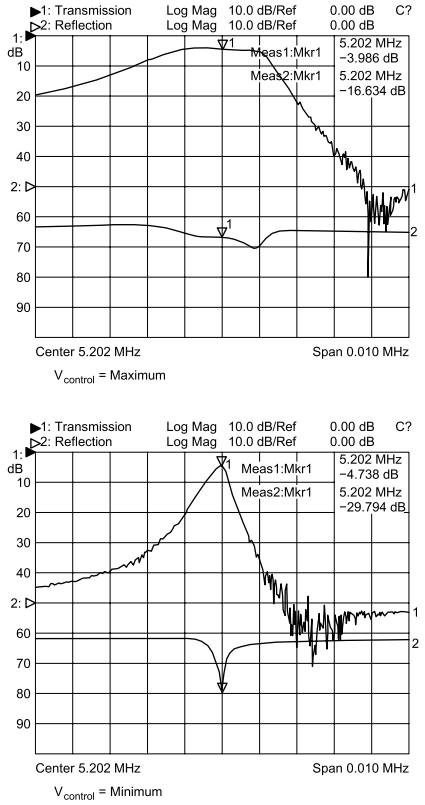

Figure 5—The measured insertion loss of the new filter as a function of Vcontrol. Top—maximum bandwidth, bottom—mimimum bandwidth.

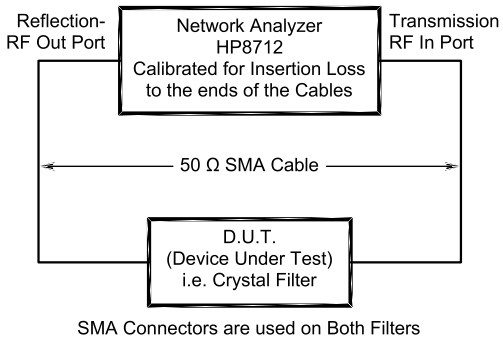

Figure 6—The test setup used to measure the insertion loss of the filters.

extracted. Crystals for other frequencies can be used, with varactors of an appropriate C_o .

Fig 5 shows the passband response of the new filter at minimum and maximum usable bandwidth. See Fig 6 for the test setup. Notice that the center frequency remains fairly constant. The second trace on each plot is the filter input return loss (add 10 dB).

In conclusion, a new type of variable bandwidth crystal filter has been developed that maintains a constant center frequency and may have uses in test equipment and radio receivers.

Notes

[1]Conversation with W7ZOI.

[2]Hosfelt Electronics, 2700 Sunset Blvd, Steubenville, OH 43952, 800-524-6464, p/n MV1662/S. At last count they had over 5000 of these left. There are three diodes per package.

Rob Lytle was originally licensed as a ham as WN3YXB at the age of 12. At the age of 16 he became an Extra Class ham with call sign N3FT. A few years later, he graduated with a BSEE from the University of California at Berkeley. Most recently he had been employed as an Applications Engineer at TriQuint Semiconductor in Hillsboro, OR. Rob still enjoys the hobby with emphasis on construction projects, antenna projects, and working 6 and 160-m. ☐☐

Help for Amplifier Failure in the HP8640B

If you own an HP8640B signal generator and the output power has become intermittent or it has quit working altogether, then this article may be just what you need.

By Markus Hansen, VE7CA

[Editor's note: This is one man's tale of what he did to fix his generator. Neither ARRL nor the author assumes liability for any damage caused by performing the modifications he describes.]

Last year, I was very fortunate to acquire a used and working Hewlett-Packard HP8640B signal generator. It is a test instrument that I had dreamt of owning for years. The HP8640 series generators were a premier signal generator when they were first introduced sometime in the early 1970s. The generator produces a very low noise RF output from 500 kHz to 512 MHz. The HP8640B incorporates a built-in 550-MHz frequency counter and a phase-lock synchronizer. Most versions have a 10 dB step attenuator with a range from +20 dBm to –145 dBm. In addition, the output signal can be amplitude or frequency modulated. For the serious RF experimenter, this is a wonderful tool to have sitting on the workbench.

Recently, my generator began to display odd behavior. Though it would produce output when it was turned on, every once in a while the output would drop to zero and then shortly after, return to full power. Over a period of several weeks, this behavior became more frequent until one day when I turned it on it didn't produce any output at all. Turning it on and off several times would sometimes help to restore output power but eventually it quit altogether.

Upon inquiry, I was informed by a couple of fellow hams who had been employed by RF engineering companies where HP8640 generators were used that this is a common problem with this series of HP generators. I was told that the problem often is a result of the failure of either the pre-amp or final-amp hybrids. I was also informed that these particular hybrid amplifiers are no longer available.

Using my scope, it didn't take me long to discover that there was RF at the input to the pre-amp hybrid and no RF at its output. Upon examination of the HP8640B circuit diagram,[1] I determined that the input and

674 St Ives Crescent
North Vancouver, BC V7N 2X3
Canada
ve7ca@rac.ca

[1]Notes appear on page 22.

output terminations are looking into 50 ohms. Wes Hayward, W7ZOI, had at one time suggested that maybe one of the three-terminal monolithic power amplifiers similar to the MAV-11 would be a suitable substitute. I decided that I had nothing to lose by trying.

Locating the Problem

The first thing to do is to determine why the generator is not working. On the back is a large heat sink and extending from the heat sink is a BNC connector marked "Aux. Output." Connect a scope or a RF power meter to the BNC connector and turn the generator on. If there is no output at this point the problem is either the hybrid pre-amp, the supply voltage for the pre-amp or any of the circuits preceding the pre-amp. If there is no RF at the BNC outlet, turn the generator upside down and remove the bottom cover. Turn the generator so the back is facing you and remove the cover from the AM/AGC Amplifier Assembly that is located in the lower right hand corner. This assembly is divided into two sections: the A26A3 Modulator Assembly is on the left side (which contains the pre-amp hybrid), and the A26A1 Power Amplifier and AGC Detector Assembly are on the right side.

In each section you will see what looks like a large power transistor in a case style similar to a TO-3 or TO-8 transistor. The hybrid amplifiers are contained under the caps of these units. On the printed circuit board (PCB) in the left section, locate the end of the 50-ohm coax line with the center connector terminating in a circuit pad. See Fig 1.

Turn the frequency range switch of the generator to its lowest range and turn the generator on. With a scope, determine if there is any RF at the end of the 50-ohm coax. If there is, and it is a square wave measuring 550 mV p-p, then you have confirmed that everything before the pre-amp is working and the problem is either the pre-amp or the power supply. The only way to really find out if it is one or the other is to remove the pre-amp hybrid by removing the two screws holding it in place. Once the pre-amp is removed, check the supply voltage to see if it's +44.6 V. The +44.6 V input is clearly marked on the PCB. If there is no voltage present or it is the wrong value, then proceed to fix the power supply problem. The reason that you have to remove the pre-amp to check the voltage is that the pre-amp may have an internal short, which was the case with my pre-amp. The power supply has a crowbar shutdown feature, so that if the output is shorted, the voltage goes to zero to avoid damage to the power supply.

Changing the Supply Voltage to Accommodate the MAV-11

The MAV-11 requires 5.5 V while the hybrid amplifiers both run on 44.6 V. The 44.6 V line enters the AM/ Amplifier Assembly box that contains both amplifiers via a multiple-pin connector and then along a PCB trace in the center of the box. There is no spare pin on the connector so a feedthrough capacitor has to be added to bring in a voltage line for the MAV-11.

With the back of the generator towards you, take off the top cover. The AM/AGC Amplifier Assembly is now located in the bottom left corner. Re-

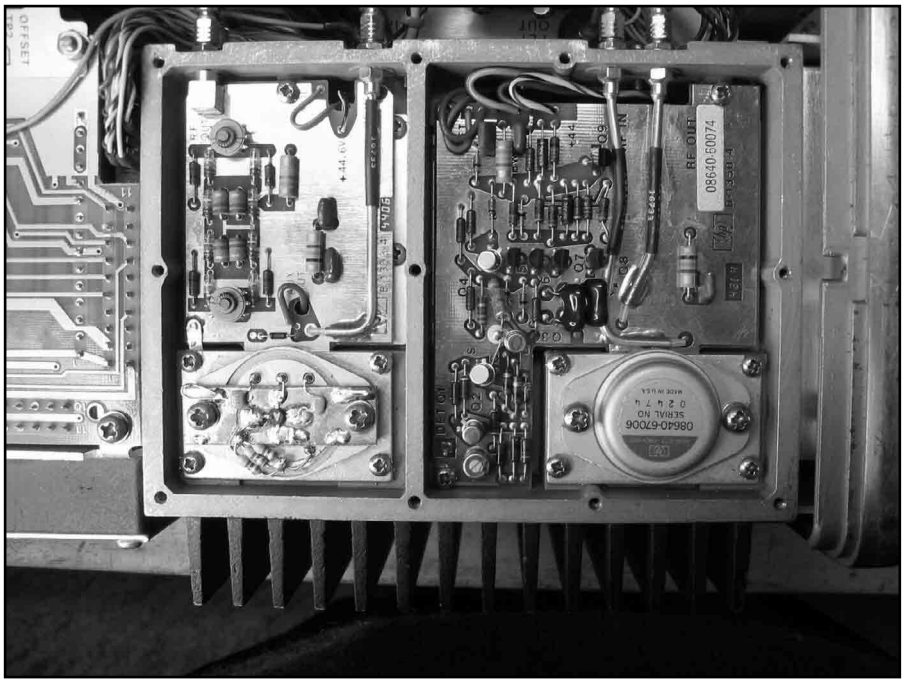

Fig 1—A26A3 Modulator assembly. Note coax terminates on a circuit pad.

Fig 2—Detail of added feedthrough insulator.

move the AM/Amplifier Assembly from the generator by following the instructions on the amplifier lid. Once removed, turn it so that the side opposite the heat sink is facing up. There you will find a removable rectangular aluminum plate. After you remove the screws and the plate, you will see a row of feedthrough capacitors in the cavity below. From one end, there are two wires that go from feedthrough capacitors to the section that contains the hybrid pre-amp. The second wire (white with black and red bands on mine) from the end is connected between the feedthrough capacitor +44.6 V input line and a pad on the pre-amp PCB that is marked 44.6 V. Unsolder this wire from the feedthrough capacitor. Make a mark on the aluminum plate in the middle between the two end feedthrough capacitors. Drill a hole to fit a feedthrough capacitor. I used a good quality 0.001 µF feedthrough capacitor that I had purchased from Down East Microwave. One end is threaded so that when it is screwed into the aluminum plate the result is a very secure RF connection. Connect the wire that was soldered to the +44.6 V feedthrough insulator to the new feedthrough capacitor using heat shrink tubing to cover the solder connection. Connect a 12'' length of insulated wire to the outside of the new feedthrough insulator and again pass a short length of shrink tubing over the connection. See Fig 2. Now reassemble the AM/Amplifier Assembly and insert it back into the generator.

The other end of the wire just attached to the outside of the new feedthrough insulator is now soldered to a hole at the end of a trace that leads to C4 that is on the power supply rectifier assembly circuit board. See Fig 3.

I chose this point as the voltage is approximately +15 V, leaving sufficient room to drop the voltage to 5.5 V for the MAV-11 while limiting the current to 60 mA. Also this particular winding has the largest current capability of all the transformer windings. C4 is 8200 µF and large enough that I was not able to detect any ripple on my scope.

Substituting a MAV-11 for the Hybrid Pre-Amp

I had some Mini-Circuits MAV-11 amps on hand so I decided to try one as a substitute for the pre-amp hybrid. You may want to choose another model such as the MAV-11SM or ERA-1SM. [4]

Begin by removing the cap from the existing pre-amp hybrid module. I inserted the module in a vise and by using a metal punch I was able to get under the seal of the cap and pry it up

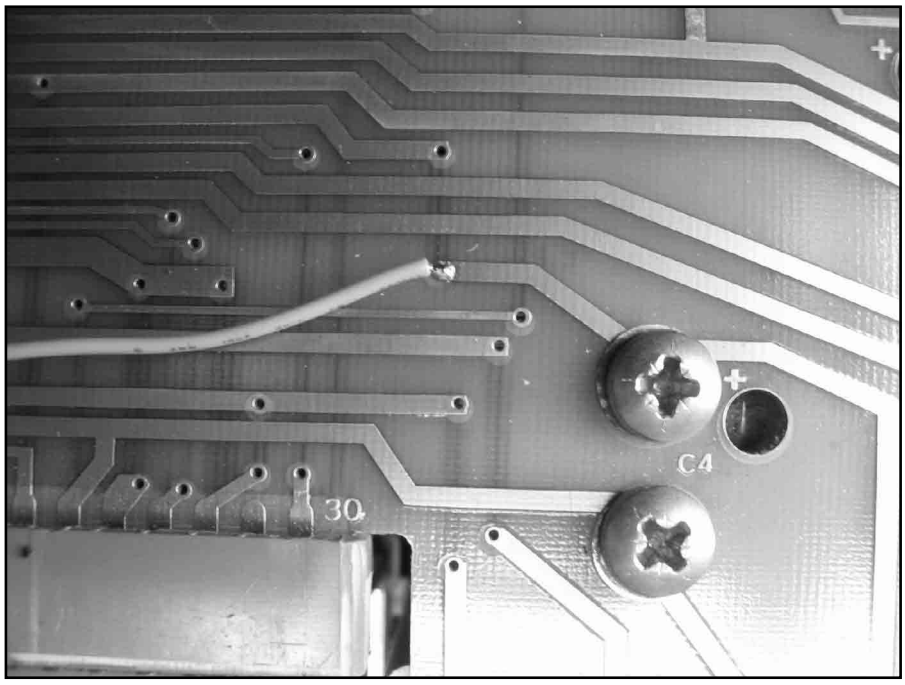

Fig 3—Detail of inner end of wire from feedthrough insulator to C4.

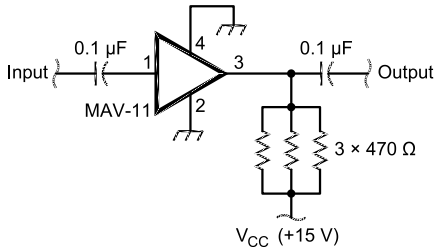

Fig 4—Circuit of replacement for pre-amp hybrid.

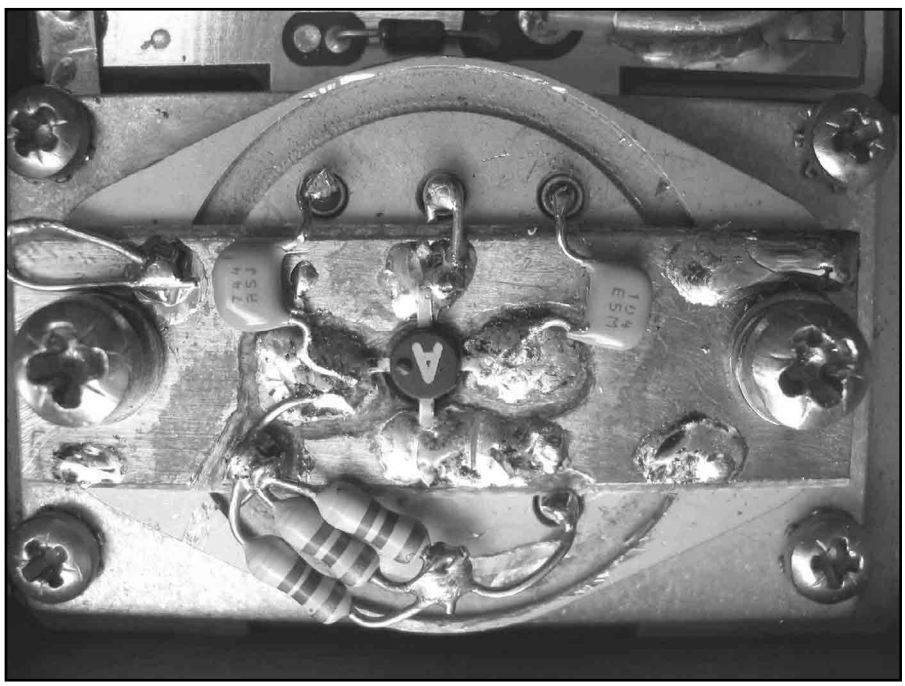

Fig 5—MAV-11 preamp as installed.

and off. I removed the hybrid from the base by tapping the edge with a small screwdriver. I decided to use the original base for the hybrid because it has the connecting posts that connect through to the PCB below and it has room on top for a MAV-11 and associated parts. I cut a small piece of PCB to fit between the connecting posts and extended it over the mounting holes of the base. If you use a MAV-11 then drill a hole in the center of the PCB large enough so that the MAV-11 drops into place and the four leads lie atop the PCB. I used a Dremel tool to cut isolation pads for the input and output pins of the MAV-11.

Facing the back of the generator and looking at the base that holds the hybrid pre-amp, the connecting posts farthest from the back of the generator from left to right are: output, ground and input. The connecting posts closest to the back are the left post (not used) and the right post (voltage supply input). Connect a 0.1-µF monolithic or surface-mount capacitor from the base input post to the input pin of the MAV-11. Between the voltage supply input post on the base and the output pin of the MAV-11, connect three 470 Ω ¼ W resistors in parallel. The three parallel resistors should measure about 157 Ω and serve to drop the supply voltage from 15 V to approximately 5.5 V and limit the current to about 60 mA. From the output pin of the MAV-11, connect another 0.1 µF monolithic or surface mount capacitor to the output post of the base.

Fig 4 is a schematic diagram of the MAV-11 circuit. Fig 5 is a photo of the MAV-11 circuit as installed.

Before putting the AM/AGC Amplifier Assembly cover back on, make sure that the new components do not touch the lid of the cover. I cut a small single-sided PCB to cover the MAV-11 and new components and soldered the copper side of the PCB to the screen that is sandwiched between the cover and the assembly box.

It took me several hours to perform the above changes. I strongly recommend that you do not hurry when making them. You don't want to make a mistake that may cause other problems that are not fixable because of the scarcity of some of the HP original parts.

Results

When I completed the substitution and turned on the generator, with the attenuator set to 0 dBm, the generator output meter read 0 dBm and my RF power meter[2] connected to the output connector also registered 0 dBm. This was with the frequency set to 7.0 MHz. I was one very happy person. According to the built-in analog meter and my RF power meter, the output power is within ±0.2 dB across the generator's full operating frequency range at a power setting of +10 dBm. (I had previously calibrated the RF power meter using the signal generator as the source and confirmed the calibration using another HP8640A that a friend owns.) I have the avionics version of the HP8640B and the max power output is rated at +16 dBm though it is not rated to be flat at that power level.

The AM and FM features of the generator were not affected by the substitution. To determine if the phase-noise performance of the generator had been

Fig 6—Spectrum analyzer showing genrator output at 7.0 MHz and +10 dBm.

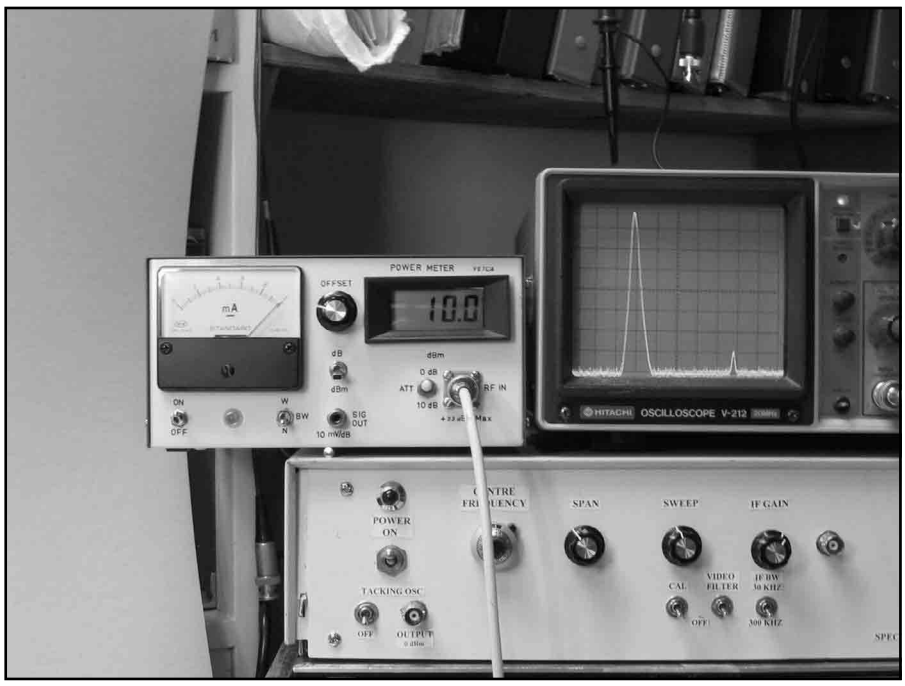

Fig 7—Power meter confirms 10 dBm level.

affected by the substitution, I remeasured the two-tone dynamic range of my homebrew receiver using the HP8640B and a crystal oscillator. I was able to reproduce the same results that I had measured previously (99 dB IP3 dynamic range at 2 kHz spacing at 14 MHz). Fig 6 shows the generator connected to my power meter and spectrum analyzer with the generator output power set to +10 dBm while operating at 7 MHz. The second harmonic is in excess of 60 dB below the carrier level. All is well!

Obviously, there are other reasons why a HP8640 series signal generator may fail. However, it became clear after discussions with fellow hams who had years of experience working with this particular series of generators that the hybrid pre-amp is prone to failure. I hope this article will help those who experience a similar problem.

There is also a similar amplifier used for the output amplifier, which may have different gain and output power capabilities. Similar methods might be successful to repair that amplifier as well.

I found one supplier of used parts and modules for the HP8640 series generators.[3] However, they did not have any hybrid amplifiers for sale. I have not been able to confirm this, but I was told that the last year the HP hybrids were being produced they sold for over $200 US. I paid $2.65 for the MAV-11's when I purchased them a couple of years ago. Now that is progress!

If anyone has solved HP8640 series generator problems relating to original HP parts no longer being available, please send details to my e-mail address at **ve7ca@rac.ca**. I would be pleased to post the information on my Web site, **www.qsl.net/ve7ca**.

Notes

[1]EA5AGV is offering a compilation of 251 Hewlett-Packard, Tektronix and some from other brands of technical manuals on a CD-ROM. Check **www.jvgavila.com/manuals.htm** for details. In addition see **www.jvgavila.com/hp8640b.htm** for Jose's solution for his HP8640 that had a broken range selector gear.

[2]Power Meter based on W7ZOI/W7PUA design (June 2001 *QST*) with digital readout addition by K3NHI (May/June 2002 *QEX*). My Spectrum Analyzer is also based on a design by W7ZOI/W7PUA, see *QST*, August and September 1998.

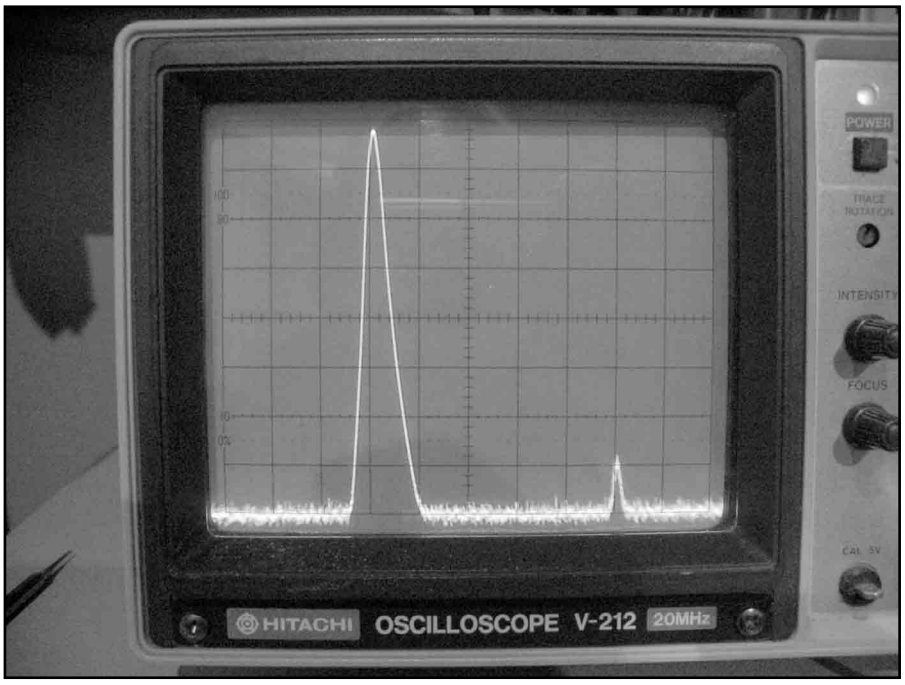

Fig 8—Second harmonic below -60 dBc.

[3]For used HP8640s or new and used parts see: Sphere Research Corporation at **www.sphere.bc.ca/test**.

[4]I recently found another manufacturer of three-terminal feedback amplifiers that produce higher output power than the MAV-11. The amp is an AG604-86 that produces 19.5 dBm output power with an output IP3 of +34 dBm. Spec sheets are available on the company Web site, **www.wj.com** The AG604-86 may be suitable for replacement of the HP8640 output amplifier.

Markus Hansen, VE7CA, has been licensed as an Amateur Radio operator since 1959. His interests lie mainly in building his own antennas and equipment. You will find him chasing DX on CW and also looking for new grids on 6 m. He has published several antenna articles in the ARRL Antenna Compendium series as well as an article describing his Portable Tri-Band Yagi in the November 2001 issue of QST. *He can be reached at* **ve7ca@rac.ca**. □□

A Doubly Balanced "H-mode" Mixer for HF

Here's the latest on high-level switching mixers.

By Sergio Cartoceti, IK4AUY

RF Mixer Parameters: *IIP3*, *G*, Port Isolation

If you have a home-built receiver or transceiver for the amateur bands—or even manufactured equipment—that has proven weak in the front end, this article is for you. You could consider adding a band-pass filter at the input, which is desirable[1] for second-order IMD protection; but it will not necessary help the third-order IMD, measured as third-order intercept point or *IP3*. That is the figure of merit you would want as high as possible to avoid *in-band* third-order IMD problems. You could also plan to replace diodes having poor second- and third-order behavior with better PIN diodes at the input/output switching points in the front end, increase the current through them or use relays. Yet there are also RF mixers at each conversion.[2] Input *IP3* or *IIP3*, can be seen as a cumulative figure, involving all stages in a receiver; or measured in a single stage, such as for a mixer device alone.[3]

You would desire a receiver cumulative noise figure (*NF*) as low as practically possible. Observing the values we could get for these two parameters in an active device like a preamplifier, with a gain *G*, we think about them as tradeoffs because it is difficult to maintain low *NF* and high *IIP3* together. We need to measure the impact on a receiver's noise-floor performance.

Wes Hayward, W7ZOI, describes a figure of merit for receivers named *Receiver Factor* or *RF = IIP3 – NF*. The most important equation in a receiver that relates noise floor to *NF* is:

$$Noise\ Floor\,(\text{in dBm}) \quad -174 + 10\log(BW) + NF \qquad \text{(Eq 1)}$$

where

BW = bandwidth, in hertz.

NF= noise figure, in decibels.

Noise floor has been alternately called "MDS (minimum discernable signal), the input signal of a generator that will cause the output power to increase by 3 dB...."[4] as per

[1]Notes appear on page 32.

Via di Corticella 241
I-40128 Bologna, Italy
ik4auy@arrl.net

ARRL Laboratory test procedures.

So we try our best to achieve good values in every stage as required for desired system performance. Wonderful software tools for system evaluation are available, such as in *Experimental Methods in RF Design* (ARRL) or in Agilent software *APPCAD*—this one is freely down-loadable from the Web.[5]

When we evaluate a mixer, we may measure third-order IMD at the output and gain (a passive mixer has a loss, so it is a negative value for *G*) and then we calculate *IIP3*:

$$OIP3 = P_{out} + \frac{IMD3}{2} \qquad \text{(Eq 2)}$$

where

P_{out} = power in each of two tones in decibels relative to a milliwatt,

IMD3 = decibels relative to the power in each tone.

Calculate *IIP3* using:

$$IIP3 = OIP3 - G \qquad \text{(Eq 3)}$$

where *IIP3* and *OIP3* are in decibels referenced to a milliwatt, *G* is in decibels (minus sign for loss).

Another important parameter is *port isolation* referred to the IF port. We need to measure LO-to-IF and RF-to-IF isolation in decibels. More isolation is better. Don't forget isolation at the LO-RF port.

High-Level H-mode Mixers in the Literature

The ARRL Handbook (2004, p 15.29) has a good concise definition of this H-mode term used in an RF-mixer context. Before you call for a paternity test on this mixer, I had better relay some of the *Handbook* text here briefly:

"Colin Horrabin, G3SBI, continued experimenting with variations of Jacob Mahkinson's original high-performance mixer circuit. This led to the development of a new mixer configuration called an H mode mixer. This name comes from the signal path through the circuit. See [*Handbook*] Fig 15.45A. Horrabin is a professional scientist/engineer at the Science and Engineering Research Council's Darebury Laboratory, which has supported his investigative work on the H-mode switched-FET mixer, and consequently holds intellectual title to the new mixer. This does not prevent readers from taking the development further or using the information presented here."

"This is still the action of a switching mixer, but now the source terminal of each FET switch is grounded, so that the RF signal switched by the FET cannot modulate the gate voltage. In this configuration the transformers are important...."

See also *Experimental Methods in RF Design*, p 5.15. The four-FET mixer differed from earlier circuits since Ed Oxner, KB6QJ, of Siliconix in the 1970s used FETs as series switches, while Horrabin uses the FETs as grounded switches. This is still a commutating mixer, but transformer action now generates the needed signals, and it appears with one more transformer.

It has also been proved in passive diode-ring mixers[6] that a diplexer at the IF or the other ports is beneficial, because it provides the correct termination impedance over a broad frequency range. It has been employed as well, at the IF port, in the CDG2000 project, a recent work by G3SBI and company. CDG2000 is an advanced transceiver project with a first mixer built around a Fairchild FST3125M IC[7] as an H-mode mixer.[8] This quad-FET bus switch IC is part of a family of bus switches now also manufactured by Philips as CBT3125, by TI as SN74CBT3125, by ON Semiconductor as 74FST3125, Pericom as PI5C3125 and perhaps others. The suffix may differ by package, but the small SOIC is better for this RF application.

The device has TTL/CMOS-compatible control inputs. The CDG2000 authors presented also a very low-noise LO synthesizer needed to reach high

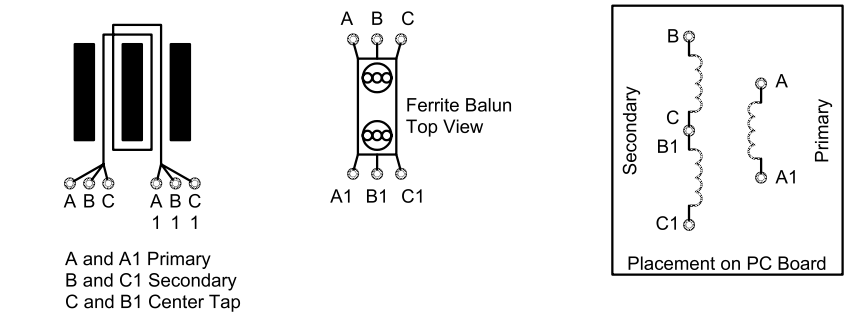

Fig 1—Ferrite binocular transformer winding details. First, label the ends of three pieces of #29 AWG enameled copper wire as shown, then twist them together. Wind four turns (see above, but four turns) of the twisted wire into an ferrite binocular-balun core (Amidon #BN-43-2402). On the finished transformer, ends A and A1 are the primary winding; ends B and C1 form the secondary, which has a center tap at B1 and C.

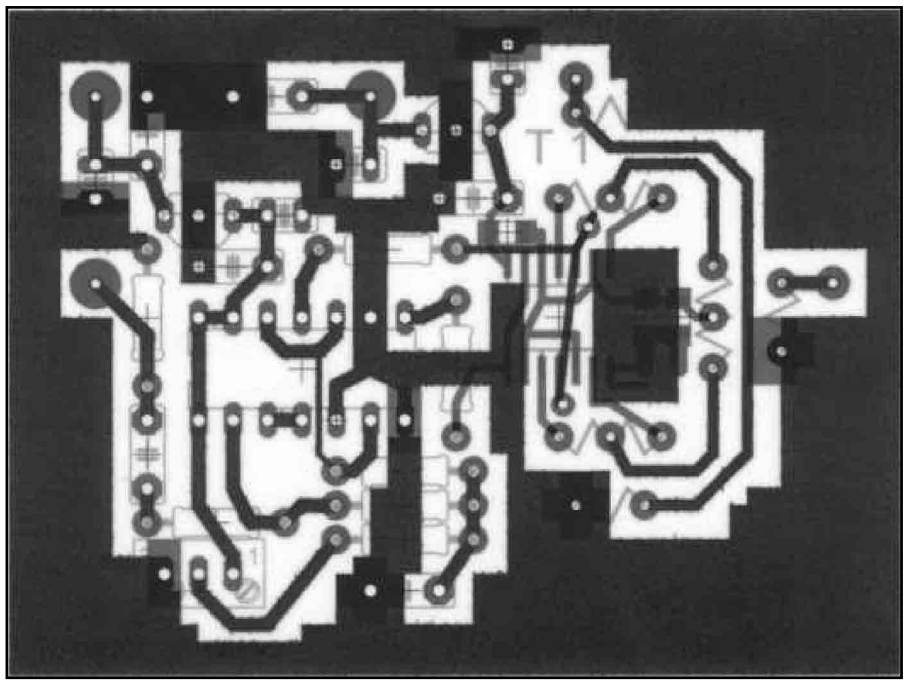

Fig 2—An enlarged x-ray view of the H-mode mixer board (no scale). Parts are shown in light gray.

dynamic range. I have fabricated a PC board around that basic version, with three transformers, but without a division by two of the LO frequency, just for simplicity and fundamental LO frequency availability. It is surely a fine way to get LO signals of the right phases and duty cycles for the "I" and "Q" outputs without any adjustment.

The original circuit was presented in *Radcom*, the RSGB monthly magazine, in Pat Walker, G3VA's column "Technical Topics" a few years ago by G3SBI.[9] I7SWX/F5VGU, Giancarlo Moda[10] is known to be the person who suggested to the triad of G3SBI, W7AAZ and W4ZCB to try an FST3125M IC for the H-mode mixer configuration to simplify the circuit with a lower cost IC, yet with reasonably good performance, with *IIP3* in the area of +40 dBm. (I remember some previously published schematics with an integrated quad D-MOSFET package with fast switching, see ARRL *Handbooks* of recent years.) Lately, Giancarlo published in *Radcom* a version with two transformers only, homemade around ferrite binocular beads, as a way to simplify tests for optimizing different frequency ranges. He used a process of rewinding them to find useful combinations of ferrite mix and number of turns, because he wanted to try this mixer for IFs as high as 70 MHz as a possible use in up-conversion commercial transceivers.

Giancarlo has already reported a positive experience in replacing the third mixer (a single-MOSFET type) with an early H-mode version with a 74HC4066 IC for 9 MHz to 455 kHz IFs, inside an old IC-751 transceiver. He wished to also replace the first mixer with a FST3125M, a faster and better-performance IC, time permitting.

Hannes Coetzee, ZS6BZP, previously mentioned a 74HC4066 IC as an analog-switch mixer in *RF Design* (June 1995, this is not an H-mode type). For four harmonically related bands (7 to 28 MHz), he achieved a direct-conversion to audio baseband receiver, with a fine audio chain, as seen in *Electronics World*, reprinted in *Communications Quarterly* (Oct 1998). Lately, I found on PA3CKR's Web site a brief evaluation report of the same early basic schematic, with three different types of transformer.[11]

As entertainment in his retirement, I recently convinced my father Romano, I4FAF, a fast Amateur Radio homebuilder, to help me try both versions in practice. One with three transformers, and the I7SWX version, with two transformers.

I also discovered that JA9TTT, Mr Kato, had performed tests on both versions. He posted the spectrum-analyzer photos of his two-tone IMD tests on his personal Web site at **ja9ttt.homedns.org/**)

My father and I made a personal choice and selected the version with three transformers, mainly because we have previously employed home-

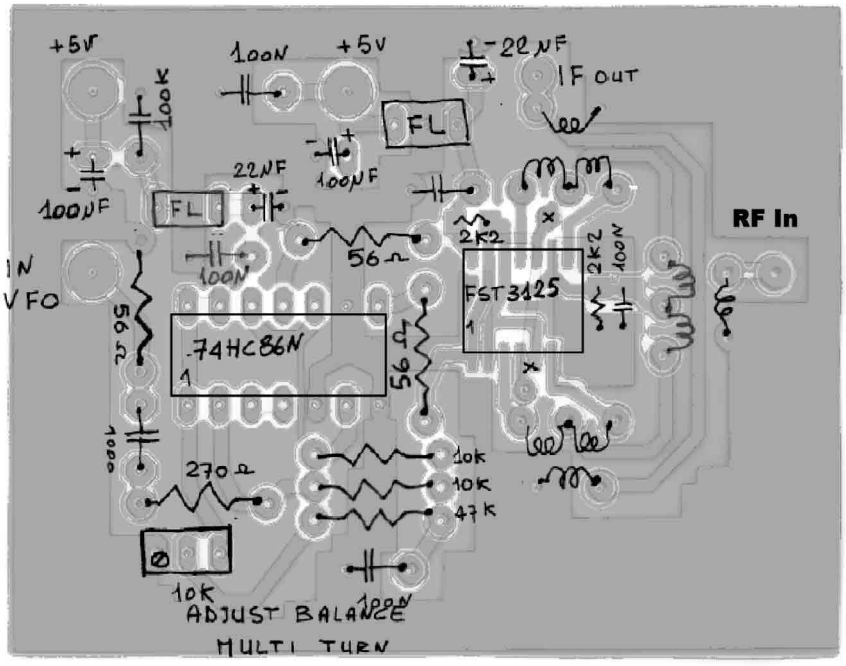

Fig 3—H-mode mixer PC board component values and placement (no scale).

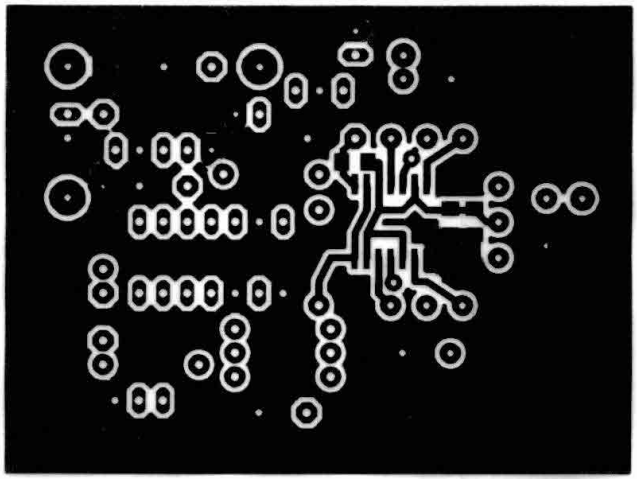

Fig 4—H-mode mixer PC board component-side etching pattern. The finished board should be 65×50 mm.

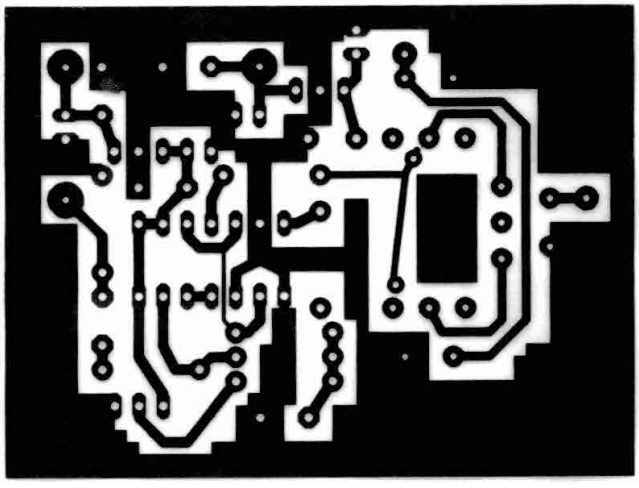

Fig 5—H-mode mixer PC board mirrored solder-side etching pattern. The finished board should be 65×50 mm.

made ferrite binocular-bead transformers and it seemed to us easier to wind them. (The version with two transformers has one with a five-filar winding.) Maybe the three transformers yield slightly better port isolation and higher *IIP3* values. Carefully review our performance data in Tables 1 through 4 below.

Some years ago in *QST*, we saw Ulrich Rohde's, KA2WEU, schematic[12] of a high-performance switch-mode mixer based on four D-MOS switching FETs as discrete components. Later, he showed us one circuit built around an SD5000 IC in *QEX* (Jan/Feb, 2003, pp 21-31).

Recently, ICOM announced, for their 40th anniversary of activity, a +40-dBm *IP3* transceiver. I must admit, however, that its price could be a valid cause for conjugal separation! Band conditions are variable; how well you do on the air depends also on the type of antenna you use and your location, so you don't always need such a bulletproof front end. Nonetheless, you can now enjoy an H-mode mixer with high *IP3* on a small budget. We are glad to share with you our experiences. We give you our PC board artwork and transformer details in Figs 1 through 5. We have had many requests, and readers showed much interest in it after my letter to the editor, published in *QEX,* Sept/Oct 2003.

Balance and Isolation Adjustment without a Spectrum Analyzer

Use one RF signal generator inside the 7 MHz band at –20 dBm level, 50 Ω output at the RF port. Use another RF generator at the LO port and connect your receiver with a 50 Ω coaxial cable to the mixer's IF port. An attenuator between mixer and receiver will mitigate mismatch effects caused by receivers that do not have perfect 50-Ω input impedances. Attenuation of 3-10 dB is enough; see *Handbook* tables for resistor values to build one. Tune the receiver to the 7 MHz signal and adjust the balance trimmer for minimum S-meter reading. This is a simple procedure for those without a spectrum analyzer, but our port-isolation data were all taken with an 80 dB-range spectrum analyzer.

Warning! Avoid leaving the input to the LO squarer open or with the input signal generator connected but switched off while dc is applied to the board. The squarer IC will show some signs of oscillation in such floating states and it gets warm. When a signal is applied to it, there is no problem. Giancarlo said he changed the squarer circuits to avoid self oscillations, but we did not experience that problem with the LO applied and running. Use a 74HC86 for maximum LO frequencies around 45-50 MHz; or better yet the 74AC86, which is about three times faster.

Performance Data

We performed a first test with the squarer logic signals inverted with respect to our schematic (see Fig 6), for balance evaluation with the slower HC logic squarer (see Table 1). We per-

Table 1
Test Data for H-MODE Mixer with FST3125M, Three-Transformer Version

Values shown for our evaluation PC board configuration, our transformers data, squarer 74HC86 pin 8 (complementary output) wired with 56 Ω resistor to pins 4 and 10 of FST3125M and pin 11 (Q output) wired with 56 Ω resistor to pin 1 and 13 of FST3125M). Decibel measurement accuracy around 1 dB.

RF (MHz)	*LO (MHz)*	*IF (MHz)*	*RF-IF (dB)*	*LO-IF* (dB)*	*LO-RF* (dB)*	*Gain (dB)*
28.5	37.5	9	38 (†21)	34 (†38)	27	–5.5
21	30	9	26 (†26)	33 (†32)	32	–5
14	23	9	37 (†26)	40 (†40)	34	–5
7	16	9	33	41	38	–5
3.7	12.7	9	36 (†36)	45 (†45)	41	–5
1.8	10.8	9	38 (†38)	46 (†46)	41	–5

Notes
RF in was 0 dBm, squarer used was 74HC86 (slower than 74AC86).
LO in was 0 dBm at squarer input.
*I cannot measure squarer output in dBm, so isolation is in decibels, LO to IF, is an attenuation seen on spectrum analyzer IF port of LO frequency referred to 0 dBm level (= RF in.) to give an idea of its level at IF port. We noticed a 10 dB improvement in LO-RF isolation if the two LO signals, Q and complementary, from the 74HC86 are routed in the opposite way to the FST3125M IC with a cross connection of both 56 Ω output resistors (as jumpers so pin 8 is routed to FST3125M pins 1 and 13 and pin 11 is routed to FST3125M pins 4-10 as shown in the main schematic).
RF to IF in dB, band optimized with adjust balance and
† measured values with adjust balance optimized for 7 MHz RF in. I think it is a good practical choice.

Table 2
Test Data for H-MODE Mixer with FST3125M, Three-Transformer Version

Values shown for our *SMD PC board* configuration, our transformer data, with *SMD* squarer *74AC86* pin 8 (complementary output) wired through 56 Ω resistor to pins 4 and 10 of FST3125M and pin 11 (Q output) wired through a 56 Ω resistor to pins 1 and 13 of FST3125M. Decibel measurement accuracy around 1 dB.

RF (MHz)	*LO (MHz)*	*IF (MHz)*	*RF-IF (dB)*	*LO-IF* (dB)*	*LO-RF* (dB)*	*Gain (dB)*
28.5	37.5	9	44 (†36)	37 (†37)	38	–5.5
21	30	9	39 (†39)	48 (†47)	39	–5
14	23	9	49 (†47)	43 (†43)	44	–5
7	16	9	48	47	45	–5
3.7	12.7	9	66 (†47)	45 (†45)	46	–5
1.8	10.8	9	66 (†37)	46 (†46)	48	–5

Notes
Balance seams slightly better with the SMD PC board, so is average port isolation.
RF in was 0 dBm, squarer used was 74AC86 in a small SOIC package (about three times faster). LO in was 0 dBm at squarer input
* I cannot measure squarer output in dBm, so isolation in dB, LO to IF, is an attenuation seen on spectrum analyzer IF port of LO frequency referred to 0 dBm level (= RF in) to give an idea of its level at IF port. RF to IF in decibels, band optimized with adjust balance and
† measured values with adjust balance optimized for 7 MHz RF in. I think it is a good practical choice.

formed a second test with squarer logic signals inverted with respect to our schematic for balance evaluation with the faster AC' small SOIC squarer (see Table 2). Finally, we performed a third test (with logic signals as shown in the main schematic) for balance evaluation and with the faster AC small SOIC squarer. That proved to be the better combination (see Table 3). Two-tone third-order IMD data for our H-mode Mixer with the FST3125 and three transformers are found in Table 4.

Figs 7 and 8 show data taken by JA9TTT, Mr. Kato, that are available on his Web site[13] as photos from an Advantest TR4171 Spectrum Analyzer with his two-tone test setup. We have carefully—and with a lot of patience—calculated the corresponding *IIP3* values from the data. My Spectrum Analyzer system with around 80 dB of SFDR is not enough for the >90 dB of SFDR.

Tests of the two-transformer version have been performed around three homemade Amidon binocular-bead transformers of the same size but of different permeabilities. See Table 5 for BN43-2402; Table 6 for BN61-2402 and Table 7 for BN73-2402.[14] It is important to read the note pertaining to these tables. It is clear that BN43-2402 is the winner here and we were very pleased to agree with those data, since we already selected BN43-2402 in our personal tests. We informed I7SWX about these JA9TTT data because he had the same problem, no such high SFDR instruments test-set available in his early development of the two-transformer H-mode mixer version. Someone guessed that a mixer with only two transformers could contribute less to IMD than one with three; but by these data, it is not proved. The three-transformer version is still slightly better.

Table 3
Test Data for H-MODE Mixer with FST3125M, Three-Transformer Version

Values shown for our SMD PC board configuration, our transformers data, with SMD squarer 74AC86 pin 8 (complementary output) wired through a 56 Ω resistor to pins 1 and 13 of FST3125M and pin 11 (Q output) wired through a 56 Ω resistor to pins 4 and 10 of FST3125M. Decibel measurement accuracy around 1 dB.

RF (MHz)	*LO (MHz)*	*IF (MHz)*	*RF-IF (dB)*	*LO-IF* (dB)*	*LO-RF* (dB)*	*Gain (dB)*
28.5	37.5	9	64 (†38)	48 (†48)	44 (†45)	–5
21	30	9	80 (†49)	42 (†42)	52 (†54)	–5
14	23	9	60 (†50)	44 (†45)	52 (†55)	–5
7	16	9	70	50	58 (†58)	–5
3.7	12.7	9	66 (†38)	53 (†53)	62 (†62)	–5
1.8	10.8	9	72 (†38)	55 (†54)	64 (†63)	–5

Notes
Balance is better with the SMD PC board and fast AC squarer and so is average port isolation.
RF in was 0 dBm, squarer used was 74AC86 small SOIC package (about 3 times faster).
LO in was 0 dBm at squarer input .
I cannot measure squarer output in dBm, so isolation in dB, LO to IF, is an attenuation seen on spectrum analyser IF port of LO frequency referred to 0 dBm level (= RF in.) to give an idea of its level at IF port. RF to IF in dB, band optimized with adjust balance and
†measured values with adjust balance optimized for 7 MHz RF in. I think it is a good practical choice.

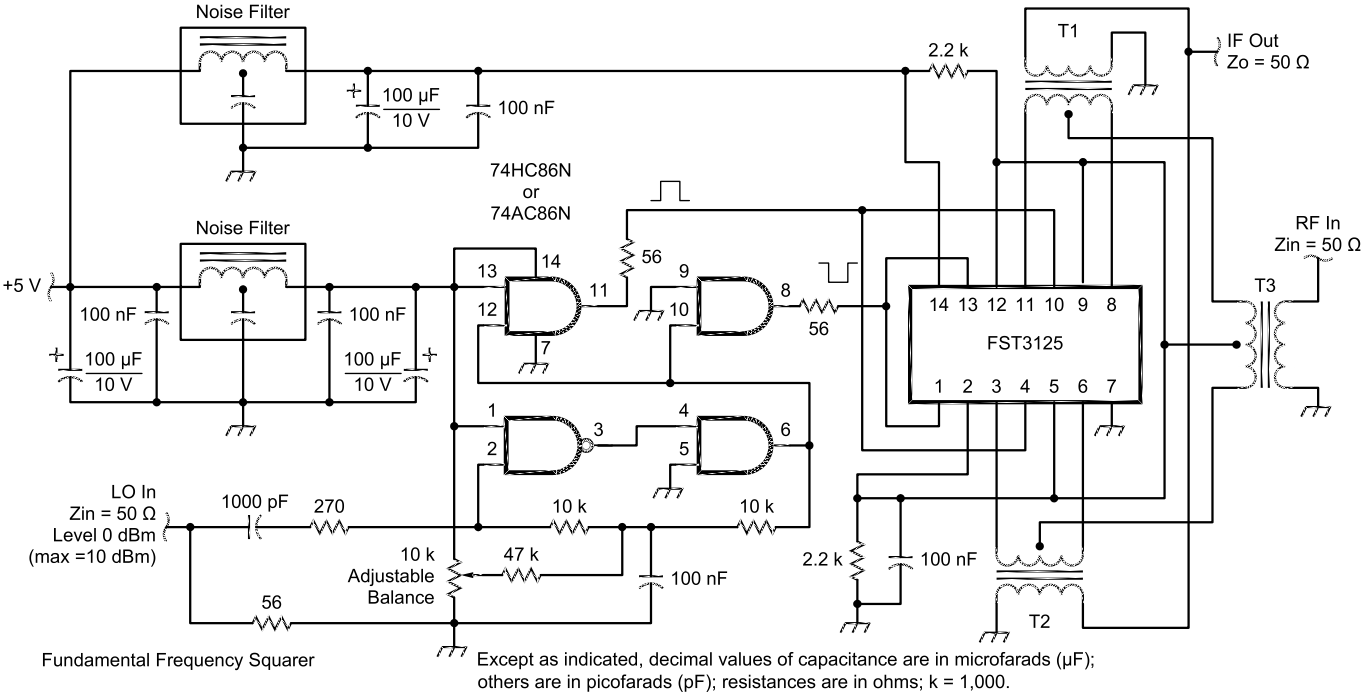

Fig 6—Schematic of the IK4AUY-I4FAF three-transformer H-mode mixer.

Table 4
Two-tone Third Order IMD Tests: Figure of Merit *IIP3*

H-mode mixer with FST3125 IC and three transformers.

Author	*Frequency (MHz)*	*IMD (dB)*	*OIP3 (dBm)*	*IIP3 (dBm)*	*G (dB)*
CDG2000 by	RF in 30, LO 39, IF 9			37 @ 14	–4 @ 30
G3SBI & Co*	RF in 2, LO 11, IF 9			40 @ 3.5	–5.5 @ 2
PA3CKR**†	he tested three types of transform see his Web site for details.			+41 to 44	–6
JA9TTT†	RF in 7.43, 7.44, 2x0 dBm IF 17 MHz (LO 10 MHz)	94 dB down	+41	+47	–5.9
JA9TTT†	RF in 7.43, 7.44, 2x0 dBm IF 9 MHz	85 dB down	+36.6	+42.5	–5.9
JA9TTT†	RF in same as above IF 2 MHz	63 dB down worst 30 dB	+24.5	+31.5	–7
JA9TTT†	RF in as above IF 455 kHz	40 dB down (ferrite limit)	+8.5	+20	–11.5
JA9TTT†	as above IF 27 MHz	85 dB down	+36.7	+42.5	–5.8

Notes

*FST3125 power supply at 7 V. The LO runs at twice the required frequency and is divided by two with a 74AC74. I suggest you read the series in *Radcom* (RSGB) from June to December, 2002. It describes a very good receiver design and low-noise synthesizer. Performance numbers are on page 19, July, 2002, with complaints for a (relatively) slightly lower *IIP3* due to transformers. G3OGQ told me he and G3SBI tested 15 different types of transformers and the best results where with Mini Circuits TT4-1A, yielding about 5 dB better *IP3* than hand wired transformers (BN202-43). Also see *Experimental Methods in RF Design* (Newington, Connecticut: ARRL, 2003) for a logic circuit for blanking.

PA3CKR Web site **www.qsl.net/pa3ckr/

†JA9TTT Web site and IK4AUY-I4FAF **www.qsl.net/ik4auy/** evaluating board are of the same basic configuration, with a fundamental-frequency squarer and a 74HC86, usable with LOs up to 45/50 MHz or better (almost three times faster) 74AC86 SOIC.

More Experiments with FST3125M: A Sample-and-Hold-Type SSB-CW Detector

By now, we are already receiving very well on the 20-m band. With a laboratory signal generator LO, we also got good readability and clean reception of 3CØV (Annóbon Island) on 7.049 MHz with a dipole antenna. Now, our prototype receiver system is as follows:

- An analog, air-variable capacitor 5 MHz VFO;
- A 9-MHz IF with diplexer and INRAD SSB-CW quartz band-pass filters;
- A Bill Carver, W7AAZ-designed 120-dB-range AGC/IF amplifier unit;[15]
- Followed by an experimental sample-and-hold switch-mode SSB-CW product detector, taking signals from 9 MHz to audio.

We used an FST3126M fast switch with a lower on resistance. The typical value is 4 Ω. We compared this sample-and-hold detector with one built around a 74HC4066 in a circuit originally presented by Rohde for a lower IF of 1.44 MHz.[16] The 74HC4066 is a pin-for-pin replacement for the CD4066, but it requires PC board modifications, since the '4066 is not a pin-for-pin replacement for the FST3125M (the switching logic is also different).

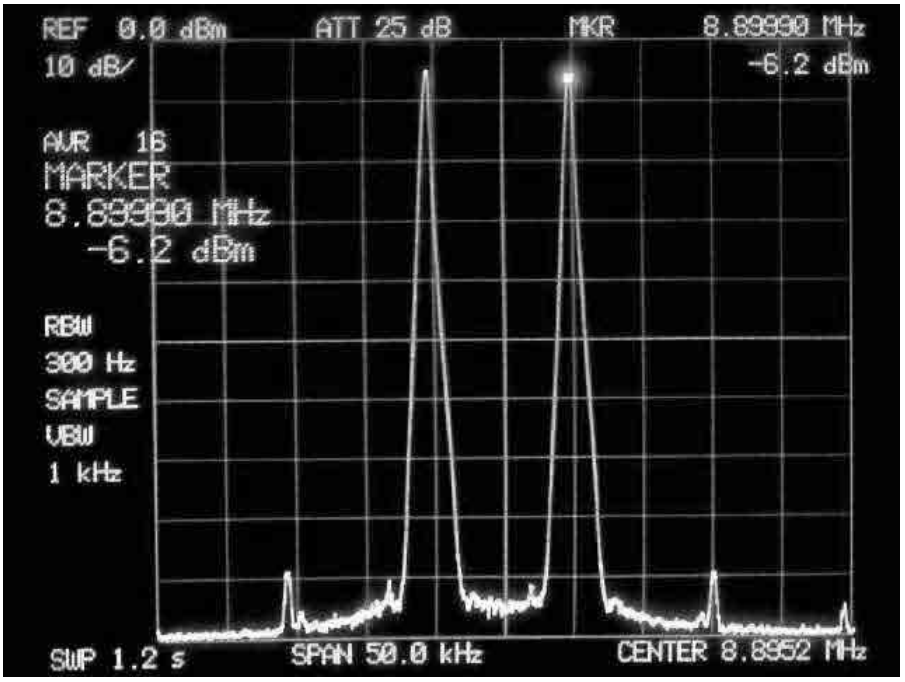

Fig 7—Two-tone IMD of an H-mode mixer with mix 43 transformers using two transformers (I7SWX type) at 9 MHz. (Takahiro Kato, JA9TTT, 2T_43_9M.jpeg at ja9ttt.homedns.org/hamf/myexp/2T-H-mode-DBM.html)

The original sample-and-hold schematic adapted for an FST3126M is fine. We got clear, crisp audio. This IC is equivalent to FST3125M and it has direct switching logic as in the CD4066 or 74HC4066, so a logical 1 connects

Table 5—Two Transformer Version

Design based on G. Moda, I7SWX, article in *Radcom* (RSGB, TechTopics, April 2003, pp 82-83). Data tested by JA9TTT, Mr. Kato, from his Web site: two-tone third-order IMD, *IIP3* and Gain. Some data not given there were carefully calculated by the author from Kato's original Spectrum Analyzer photos (Advantest TR4171 with at least 90 dB SFDR two-tone and spectrum analyzer system). Both transformers wound on Amidon BN43-2402 binocular cores. (See Note 14.)

Author	*Frequency (MHz)*	*IMD (dB)*	*OIP3 (dBm)*	*IIP3 (dBm)*	*G (dB)*
JA9TTT	RF in 7.43, 7.44, 2x0 dBm IF 17 MHz (LO 10 MHz)	88 dB down	+38.7	+44	–5.3
JA9TTT	RF in 7.43, 7.44, 2x0 dBm) IF 9 MHz (LO 16.4)	82 dB down	+35	+41.2	–6.2
JA9TTT	RF in same as above IF 2 MHz worst	63 dB down 30 dB	+24.5	+31.5	–7
JA9TTT	RF in as above IF 455 kHz	41 dB down (ferrite limit)	+14	+20.9	–6.9
JA9TTT	as above IF 27 MHz	78 dB down	+34	+39	–5.3

Port-isolation data (JA9TTT): RF to IF around 27 dB (with RF in at 0 dBm), LO to IF around 50 dB (LO = 10 MHz).

Table 6—Two Transfornmer Version

Data test by JA9TTT, Mr. Kato, from his Web site: two-tone third-order IMD, *IIP3* and Gain. Some data not given there were carefully calculated by myself from Kato's original Spectrum Analyzer photos (Advantest TR4171 as above). Both transformers on Amidon BN61-2402. (See Note 14.)

JA9TTT	RF in 7.43, 7.44, 2x0dBm IF 17 MHz (LO 10 MHz)	75.8 dB down	+33	+37.9	–4.9
JA9TTT	RF in 7.43, 7.44, 2x0dBm IF 9 MHz (LO 16.4)	75 dB down	+32	+37.5	–5.5
JA9TTT	RF in same as above IF 2 MHz	76.8 dB down	+33	+38.4	–5.4
JA9TTT	RF in as above IF 455 kHz	47.8 dB down (ferrite limit)	+18	+23.9	–5.9
JA9TTT	as above IF 27 MHz	64.2 dB down	+27	+32.1	–5.1

Port-isolation data (JA9TTT): RF to IF around 23 dB (with RF in at 0 dBm), LO to IF around 48 dB (LO = 10 MHz).

Table 7—Two Transfornmer Version

Data test by JA9TTT, Mr. Kato, from his Web site: two-tone third-order IMD, *IIP3* and Gain. Some data not given there were carefully calculated by the author from Kato's original Spectrum Analyzer photos (Advantest TR4171 as above). Both transformers on Amidon BN73-2402. (See Note 14.)

Author	*Frequency (MHz)*	*IMD (dB)*	*OIP3 (dBm)*	*IIP3 (dBm)*	*G (dB)*
JA9TTT	RF in 7.43, 7.44, 2x0 dBm IF 17 MHz (LO 10 MHz)	47 dB down	+17	+23.5	–6.5
JA9TTT	RF in 7.43, 7.44, 2x0dBm IF 9 MHz (LO 16.4)	47.2 dB down	+18	+23.6	–5.6
JA9TTT	RF in same as above IF 2 MHz	48.6 dB down	+19	+24.3	–5.3
JA9TTT	RF in as above IF 455 kHz	48.6 dB down	+19	+24.3	–5.3
JA9TTT	as above IF 27 MHz	45.8 dB down	+16	+22.9	–6.9

Port-isolation data (by JA9TTT): RF to IF around 29 dB (with RF in at 0 dBm), LO to IF around 47 dB (LO = 10 MHz)

Table 8
Expected Accessory and Modification Impacts on a Receiver

Device	*IP2*	*IIP3*	*MDS*	*SFDR*	*XM*	*lo PNDR*	*comments*
Passive Passband Filter between Antenna/Receiver	++	++(=IL)	–(Inserton Loss)	=/depnds Δf two tones	+	=	desirable ††
Atten. On	+	++(=atten.)	–– (=atten.)	=	++	=	††
Preamp On	–	––	+, depends	-, depends	–	=	in some cases
Preamp Off	+	++	––	=	++	=	††
Internal Mods in "Black Boxes"	+	++ ie mixer mod	+	++ ie mixer mod	+	+	>more difficult

Notes
+ expected improvement , - expected worsening, = no or minimal variation.
††With an RF attenuator on you shift the receiver dynamic range starting point upward. There's a similar effect with the preamplifier turned off (called also IPO). This is a step to try. With preamp on, you shift receiver dynamic range starting point downward. Use carefully, in some band/antenna-system circumstances it is probable that SFDR could be even deteriorated if preamp is limited in *IIP3*, *NF*, in presence of strong in-band signals. See also D. Smith, KF6DX, "More On Receiver Dynamic Range" in **www.doug-smith.net/moredynamics.htm**.

port A to port B (see Note 7). We also modified the audio output stage because we found that in our implementation, the original low-pass filter circuit showed more gain than needed in our application. It was originally built around a TL074, a quad amplifier IC that proved much too noisy. So, we replaced that audio portion with a dual-stage, dual-supply circuit that uses a Motorola MC33078P IC as audio buffer and low-pass filter, with a low amount of voltage gain (around 5), directly driving a trusted TDA2003 IC audio power amplifier for 4-8 Ω headphones or speakers. We used the same 74AC86 squarer for I and Q signals at the LO/BFO.

With a spectrum analyzer or receiver at the IF port, we could adjust the balance trimmer for a minimum value of the closer even LO/BFO harmonics. The BFO-IF isolation was a nice 36 dB, or about 10 dB of improvement over a 74HC4066 version; but the '4066 seemed less critical in its original circuit. This type of switching product detector showed an audio output level of around one-third the input level. So for a 1100 mV(P-P) 9-MHz IF signal in, output was around 450 mV(P-P) with no visible distortion on the sinusoids. Together with our audio buffer and LPF, the output level is 6 dB down at 4 kHz—fine for broad-range SSB audio. Of course, the beginning of our receiver chain is our front-end unit, as presented in Mar/Apr 2003 *QEX* (pp 45-56).

We wanted to test this prototype receiver during the 2003 CQWW DX SSB contest. That's why IR4B, my contest call, showed up as only a part-time entry into this year's competition.

Table 9
Component List

ICs
FST3125 M (Fairchild), 14 lead SOIC small package
74HC86 or 74AC86, 14 lead plastic dual in line package

Resistors (normal carbon film ¼ W, 5%)
56 Ω, 2
270 Ω, 1
2200 Ω, small chip, 2
10 kΩ, 2
47 kΩ, 1
10 kΩ, multiturn trimpot PC board variable resistor, vertical

Capacitors
1000 pF, small ceramic, 1
100 *NF*, small chip, 1 (it is the one in parallel with a 2200 Ω chip resistor)
100 *NF*, small ceramic multilayer for ac decoupling, 4
100 µF, 25 V electrolytic, 3

Noise filter, small integrated LCL, three-lead package, 2
T1,T2,T3—BN-43-2402 (OD 0.280, height 0.240 inches) Amidon, 3. See ferrite Binoculars winding details in Fig 4.

Comparing the prototype with two other receivers—a fully analog receiver and a Kenwood TS570DG—We were pleased with the on-air experience on 10-160 m with a lot of strong signals around. Audio quality was very good and pleasing to the ear.

We tested it with a Marconi signal generator for noise floor at around –127 dBm in a 2.4 kHz bandwidth with no preamplifier/BPF ahead of the first H-mode mixer (–5 dB loss). Because it was not assembled yet, there was no further amplification after the 9 MHz IF SSB-CW crystal filters (–3.5 dB loss for SSB filter and –7 dB for CW) before the W7AAZ IF-AGC amplifier unit was used. The IF amplifier is capable of a lot of gain. Its noise floor is 0.03 µV = –137 dBm and it has an AGC range of 120 dB, starting at –128 dBm, so it must be very well shielded. By comparison, the CDG2000 has one post amplifier to compensate for roofing-filter losses.

Be careful about the BFO because in this single-IF-conversion architecture, its frequency is effectively very close to the IF. The BFO must be well shielded in a separate metal box. Reduce its level inside the box to the 0 dBm needed for the product detec-

tor and use double-shielded or 100%-shielded 50-Ω coax cable for RF connections. We usually prefer more gain distribution, and we also got good results with an all-MOSFET IF AGC/amplifier unit with W7ZOI's filter tailending technique; but we find quite attractive—and much more flexible—a receiver architecture with a good mix of high-quality analog and digital/DSP circuits. We're pleased with the result.

For weak-signal performance, you still need a quiet IF-gain distribution, a well-behaved AGC with the proper threshold and time-constant selection under different conditions[17] and proper phase delay in the sharp bandpass filters. A high-quality product detector and noiseless audio stages alleviate listening fatigue. All those critical issues work together with an LO having the lowest possible phase noise.

Epilogue

We have observed consistent results in three units built, but the transformers must be identical. Here's an odd thing: If the I and Q LO signals from the 74HC86 are routed in opposite directions to the FST3125M with cross-connection of both 56 Ω output resistors (as jumpers, so pin 8 is routed to FST3125M pins 1 and 13, and pin 11 is routed to FST3125M pins 4 and 10), you achieve even better LO-RF isolation—by about 10 dB.

Design bonuses include that only a 5 V dc low-current supply is required, fundamental LO frequency input is around 0 dBm and you get very high *IIP3* with acceptable port isolation and reasonable parts expense.

The practical goal of this article are to share with you my own experiences and those of other authors with H-mode mixers built around a bus-switch IC, to provide an evaluation PC board and some data. The original three-transformer version yielded slightly better *IIP3* results and port isolation than the two-transformer version. Port isolation is frequency-dependent with balance adjustment. We obtained better than average isolation values with a smaller, all-SMD PC board together with ac logic. Please visit my Web site at **www.qsl.net/ik4auy/**.

The two-transformer version is close in performance and could be used for replacement in some older commercial radios if a smaller PC board were designed where space is at a premium.

Acknowledgments

As amateurs, we like very much to be updated on the latest technology, novelties and improvements for our homebuilt radios. We like to try to improve some old designs as Giancarlo Moda, I7SWX, told us in his articles in *Radio Rivista* (ARI) and *Radcom* magazines. We wish to thank Giancarlo for a good job of advancing his tests for higher IFs in upconversion receivers. A special thanks to G3SBI, W7AAZ, W4ZCB and G3OGQ and company for

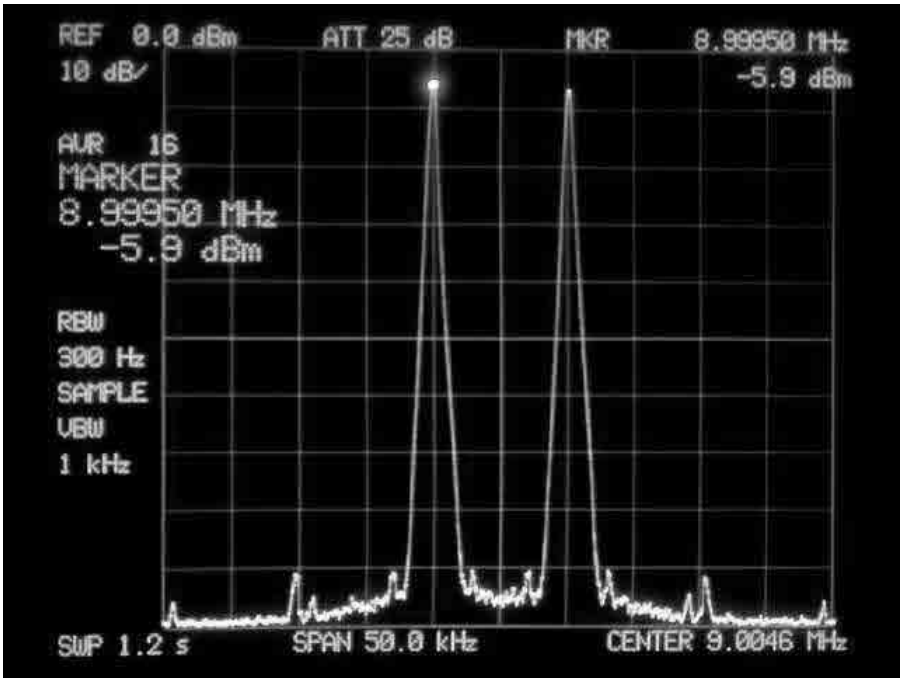

Fig 8—Two-tone IMD of an H-mode mixer with mix-43 transformers using three transformers (G3SBI/W7AAZ type) at 9 MHz. (Takahiro Kato, JA9TTT, (H_DBM_9_0.jpeg) at ja9ttt.homedns.org/hamf/myexp/H-mode-Mixer.html)

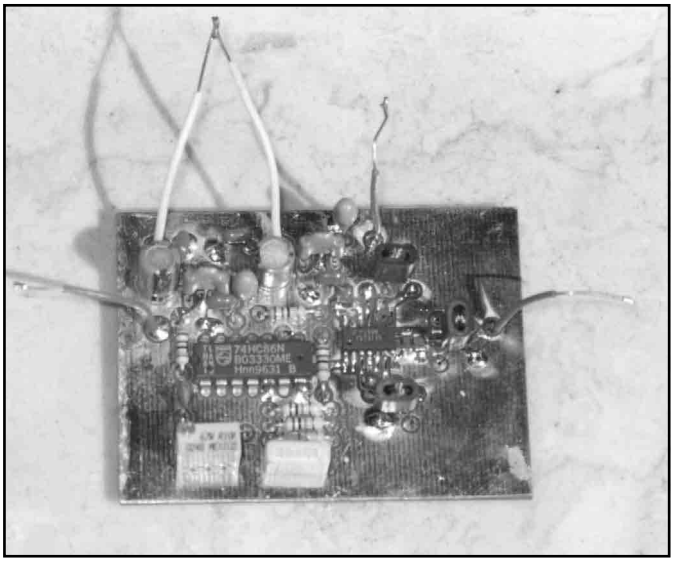

(A)

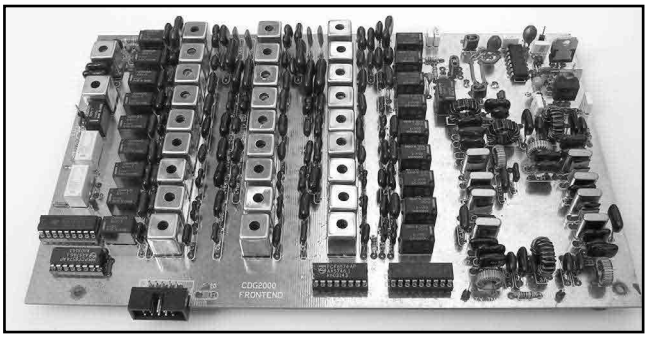

(B)

Fig 9—(A) The IK4AUY and I4FAF mixer evaluation board. (B) The CDG2000 front-end board incorporating the mixer. The mixer's three transformers are visible at the upper-right corner. The front end has relay switching for T/R and attenuators, a 9 MHz notch filter, 9 HF passband filters (Butterworth shape) with dc "wetted" relay contacts, H-mode mixer here built by us with our homebrew three binocular transformers, a 74AC74 LO divide-by-two squarer, diplexer and special double roofing filter with input and output hybrid couplers with SSB bandwidth, a computer control interface.

their terrific work in developing an advanced Amateur Radio project, the CDG2000; and to G3XJP for a fine "PIC a Star: a software transmitter and receiver." Also, many thanks to my father Romano, I4FAF, patient builder of our evaluation board (Fig 9A) and front-end board for the CDG2000 (Fig 9B).

Notes

[1]S. Cartoceti, IK4AUY, "A High-Level Accessory Front-End for the HF Amateur Bands," *QEX*, March/April 2003, pp 45-56. Feedback in "Letters to the Editor" for one errata and performance data in *QEX*, May/June 2003, p 63.

[2]U. Rohde, KA2WEU/DJ2LR, "Key Components of Modern Receiver Design: A Second Look," *QST*, Dec 1994, pp 38-44. Also Part 1 in *QST*, May 2003, pp 29-32; Part 2, June 1994, pp 27-31.

[3]U. Rohde, KA2WEU, "Theory of Intermodulation and Reciprocal Mixing," Part 2, *QEX*, Jan/Feb 2003, pp 21-31. A good look at measuring *IP3* in mixers, and there is a schematic of an high performance switching type mixer around SD5000 IC reporting *IP3* in the range of 36 to 42 dBm. U. Rohde, DJ2LR, "Communications receivers for the year 2000," *Ham Radio* (now on CD ROM from ARRL), Nov 1981, pp 12-29. Page 5 presented a two-FET passive high-level mixer. Doug DeMaw, W1FB (SK), and AD0W, "Modern Receiver Mixers for High Dynamic Range," *QST* Jan 1981, pp 19-23. For a nice look at the performance of some more traditional active and passive diode mixers, also see "*IP3* Discussion" by John Torpe of AOR UK (LTD) **www.aoruk.com/comments.htm**.

[4]W. Hayward, W7ZOI; R. Cambell, KK7B; and R. Larkin, W7PUA, *Experimental Methods in RF Design* (Newington: Connecticut: ARRL 2003), pp 5.15, 6.9-6.11, 6.27-6.53. L. Asbrink, SM5BSZ, "*Linrad*: New Possibilities for the Communications Experimenters," Part 4, *QEX* Sept/Oct 2003, pp 29-31.

[5]Agilent Web site for *APPCAD* software, V 2.51, **ftp.agilent.com/pub/semiconductor/morpheus/docs/setup251.exe** or for version 3.02 in **www.hp.woodshot.com/**.

[6]J. Stephensen, "Reducing IMD in High-Level Mixers," *QEX*, May/June 2001, pp 45-50. It's also in *Experimental Methods in RF Design* companion CD.

[7]FST3125M Fairchild data sheet at **www.fairchildsemi.com/pf/FS/FST3125.html** (with logic 0=port A connected to B, logic 1=open or high impedence). FST3126M data sheet at **www.fairchildsemi.com/pf/FS/FST3126.html** is pin-to-pin compatible with FST3125M, but switching logic is logic 0=port A is open or high impedence to port B, logic 1=port A connected to B, this is same logic as CD4066 or 74HC4066.

[8]CDG2000 by G3SBI, G3OGQ, G8KBB in *Radcom* (RSGB) June-Dec 2002 and also in Warrington Amateur Radio Club Web site at **www.warc.org.uk/**.

[9]The first announcement about an H-mode mixer seems to be in *Radcom,* Technical Topics (TT), Oct 1993, pp 55-56 by Colin Horrabin, G3SBI and in TT of July, Aug, Sept 1998. Also *Radio Communication Handbook*, RSGB, sixth ed., pp 6.48-6.53.

[10]Giancarlo Moda, I7SWX/F5VGU, "I7SWX Two-Transformer H-mode Mixer," *Radcom* magazine (RSGB), in TT, April 2003, pp 82-83; "Modifiche al ricevitore dell'IC 751 per migliorarne l' *IP3*. "An H-mode mixer application, In *Radio Rivista,* ARI magazine, April 2002, p 21; "Nuovi Mixer ad elevata dinamica," *Radio Rivista*, March 1999, p 29; "Il Mixer digitale," *Radio Rivista*, July 1997, p 28; I7SWX's switched-ring mixer with FST3125 in *Radcom*, TT, Sept 2003, pp 70-71. For a late application following I7SWX's earlier experiences in a complete front-end and transceiver project, see Peter Rhodes, G3XJP, "Pic a Star: a software Transmitter and Receiver," *Radcom*, Nov 2003, pp 84-85.

[11]PA3CKR Web site **www.qsl.net/pa3ckr/hlmixer/index.html**.

[12]U. Rohde, KA2WEU/DJ2LR, "Recent Advances in Shortwave Receiver Design," *QST*, Nov 1992, p 51.

[13]**ja9ttt.homedns.org/hamf/myexp/H-mode-Mixer.html**.

[14]Notes for Tables 5, 6 and 7: Test data by JA9TTT about I7SWX two-transformer version but with the squarer circuit (74HC86 or 74AC86) used in our three-transformer version. One transformer is a four pentafilar (4×5) winding, wire diameter is 0.16 mm (#34 AWG). Be careful to correctly wind ferrite binoculars. Giancarlo Moda has detailed his experience with the FST3125M H-mode mixer in his article (April, 2003, *Radcom*), but he could not give performance data due to lack of suitable laboratory grade instrumentation (to measure such high *IIP3* or low third-order IMD levels). He presented a no-adjustment fundamental-frequency squarer. Avoid leaving the LO input to the squarer open or with a signal generator connected but off, with dc applied to the board. This can generate random frequencies, and the circuit can get warm. When a signal is applied to it, there is no problem. Giancarlo said he changed the squarer circuit to avoid self oscillation, but we didn't experience that problem with an LO signal applied to it (use 74HC86 for maximum LO, around 45/50 MHz—or better a 74AC86 IC about three times faster).

[15]W. Carver, K6OLG (now W7AAZ), "A High-Performance AGC/IF Subsystem," *QST*, May 1996, pp 39-44 (also in *Experimental Methods in RF Design,* ARRL book companion CD).

[16]U. Rohde, KA2WEU, "Recent Advances in Shortwave Receiver Design," *QST*, Nov 1992, p 53.

[17]D. Smith, KF6DX, "Digital Automatic Gain Control for Radio Transceivers" in **www.doug-smith.net/digitalagc.htm**. Look also at the very fine L. Asbrink, SM5BSZ, technical site **antennspecialisten.se/~sm5bsz/index.htm** for weak-signal reception and receiver tests. For a nice 110 dB dynamic range from 0.05 to 60 MHz Vector Network Analyzer with passband gain and group delay display by N2PK: **users.adelphia.net/~n2pk/index.html**.

***IK4AUY, Sergio**: Amateur Radio license at 16, active since 1980 as his father I4FAF's second operator. He got his own call at 18. He is now 39, and still enjoys DX and Contests. Sergio holds a degree in economics and commerce from Bologna University and works in a local bank as credit analyst. He started young and read a lot of good amateur related books and magazines in his spare time.*

He holds S79AU from the Seychelles Islands and Amateur Extra US license AC7PC (my Italian address only is good for mail), 5BDXCC Challenge and is on the DXCC Honor Roll as well. In some contests he uses special call IR4B, and he is one of Marconi Memorial Station (IY4FGM) official operators from his summer home where he started, young, his first wireless radio experiments, now mausoleum and museum, in Pontecchio Marconi (Bologna). Sergio and other IY4FGM operators work in the organizational team of the annual Italian HF DX Convention at the end of September.

***I4FAF, Romano,** is an old timer in Amateur Radio; his age is 70. He started young at 18 by repairing radios in the Navy. He has been an ARRL member since 1980. He is on the DXCC Honor Roll. I4FAF mainly enjoys homebrewing since retirement, having built HF transceivers, power amplifiers and test equipment.*

Both Romano and Sergio are members of ARI, the Italian national association, and the ARRL. They have published five technical articles in Radio Rivista *since 2000. They have a Web site at **www.qsl.net/ik4auy/**.* □□

Improved Remote Antenna Impedance Measurement

With the spreadsheet described here, you can measure the impedance of your antenna from the shack without prior knowledge of anything about the feeder based on two impedance measurements using known resistive terminations.

By Ron Barker G4JNH, VK3INH, ex VK2INH

Background

In a previous *QEX* article, I described a spreadsheet compiled in *MS Excel* for the remote measurement of antenna impedance without the need to know the physical length of the transmission line.[1] That method was based on the Smith chart equations and was a two stage process. In the first stage, the transmission line was disconnected from the antenna and terminated with a resistive load of known value. Readings of resistance and reactance were taken at the near end at the frequency of interest and entered into the spreadsheet to reveal the effective electrical length or Smith chart length of the line. In the second stage, the antenna was reconnected to the transmission line, readings of resistance and reactance taken again at the near end at the same frequency and entered into the spreadsheet to reveal the antenna impedance. The spreadsheet took into account the transmission line loss but made no provision for its measurement. Thus the loss had to be measured separately or assumed to be as specified. This is exactly the same process used with paper Smith charts, the advantage of the spreadsheet being that the tedious and time-consuming business of plotting and measuring on the chart with its attendant risk of error is eliminated.

In that article, I referred to the 17th edition of *The ARRL Antenna Book*, which lists several sources of error in using the Smith chart for remote antenna impedance measurement and pointed out that the spreadsheet took account of all except that relating to the characteristic impedance of the transmission line.[2] The resistive component of the characteristic impedance of coaxial cable can be slightly differ-

[1]Notes appear on page 42.

171 Leicester Rd
New Packington, Ashby De La Zouch
Leics LE6 1TR
UK
ron.g4jnh@talk21.com

ent than that specified and there is also a small reactive component. I reported the results obtained on a length of UR67 (UK equivalent of RG-213) in which the effective electrical length had been measured using terminations of 20 ohms and 120 ohms, which gave a small but not insignificant difference of 0.006 λ. These values were then used to measure the impedance of a known load and the results obtained were within what I considered acceptable for most if not all amateur needs. When the results were averaged they were remarkably close to the known values and I made the following observation: "It is tempting to surmise that if the differences between the two derived values of Smith chart line length were due to a difference between the specified and actual characteristic impedance of the cable or due to the effect of the coaxial fittings the attendant errors would be in opposite directions when one termination was lower than the characteristic impedance of the line and the other higher and that by averaging them the errors would cancel. There is scope for a lot more experimentation here."

Introduction

Since completing the previous article, I have conducted more impedance measurements on different feeders using both 20-ohm and 120-ohm terminations and found that in some instances the difference in derived Smith chart line length could be significantly greater than the value of 0.006 λ reported above. In some cases, the difference was sufficient to lead to what I considered to be unacceptable discrepancies in the values of remote impedance measurements. These observations and the earlier unsuccessful attempts to determine line loss from the known impedances at both ends, which I mentioned in the previous article, lead me to conclude that there was a need to use measured rather than specified values for Z_0 and to be able to handle Z_0 values with a reactive component. I wasn't making much progress until I read Dr Steven Best's excellent article in the Jan 2001 issue of *QEX*.[3] When I saw the transmission line equation as presented in his Eq 20, I realized that it was in a form that could be manipulated without the need to understand the mysteries of exponential and hyperbolic functions to provide a method for revealing complex Z_0, loss and electrical length from two impedance measurements with known terminations. Here it is:

$$Z_{IN} \quad Z_0\left(\frac{\frac{Z_A}{Z_0}+\tanh(\gamma L)}{1+\frac{Z_A\tanh(\gamma L)}{Z_0}}\right) \qquad \text{(Eq 1)}$$

where:

Z_{IN} = impedance at input end of line.
Z_A = impedance at antenna.
Z_0 = line characteristic impedance.
L = line length in meters.
γ = line propagation factor, ($\alpha + j\beta$).

and:

α = line loss in nepers per meter.
β = polar electrical length of line in radians per meter.

For a given transmission line at a given frequency, the hyperbolic function in the equation is a constant, albeit a complex number; and for reasons which will become clear later, for our purposes that is all we need to know about it. Indeed, all of the components of the equation are complex numbers and we shall take advantage of the complex algebra facility in *MS Excel* to handle the calculations.

The first part of this article explains the manipulation of the above equation to enable a transmission line's complex impedance, effective electrical length and loss to be derived from just two impedance measurements at the near end at the same frequency using two known terminations. A further manipulation of the equation gives the antenna impedance at the same frequency based on one further impedance measurement at the near end with the antenna connected. All of the impedance equations are derivations of Dr Best's Eq 20 with no recourse to the Smith chart equations on which the previous article was based. Next follows a description of the compilation of the spreadsheet with some practical observations on impedance measurement methods.

In the final section of the article, impedance measurements are presented for a dummy antenna of known impedance at the remote end of a carefully measured 37.0 m length of RG-213 at frequencies from 1.0 to 15.0 MHz. These measurements are used to compare the new spreadsheet with the original and with what would be expected from the measured length using the published values of characteristic impedance, loss and velocity factor in the transmission line equation.

Measurement of Transmission Line Characteristic Impedance

The method used for the measurement of the transmission line characteristic impedance is based on the fact that the value of tanh(γL) for a given length of transmission line at a specific frequency is a constant as, of course, is the characteristic impedance. By taking two impedance readings at the same frequency at the near end of the line with different known terminations at the remote end, we get two results that can be entered into Eq 1. This gives us a pair of simultaneous equations with two unknowns, Z_0 and tanh(γL), which can be solved for both. In the interest of minimizing the effects of experimental error, the two known terminations should be as different as possible consistent with giving readings within the range of the impedance bridge. My preferred values are 20 and 120 ohms.

The first stage in this procedure is to transpose Eq 1 to isolate tanh(γL) on one side as follows:

$$Z_{IN} \quad Z_0\left(\frac{\frac{Z_A}{Z_0}+\tanh(\gamma L)}{1+\frac{Z_A\tanh(\gamma L)}{Z_0}}\right)$$

therefore:

$$Z_{IN}\left(1+Z_A\frac{\tanh(\gamma L)}{Z_0}\right) \quad Z_0\left(\frac{Z_A}{Z_0}+\tanh(\gamma L)\right)$$

$$Z_{IN}+Z_{IN}Z_A\frac{\tanh(\gamma L)}{Z_0} \quad Z_a+Z_0\tanh(\gamma L)$$

$$Z_{IN}Z_A\frac{\tanh(\gamma L)}{Z_0}-Z_0\tanh(\gamma L) \quad Z_A-Z_{IN}$$

$$\tanh(\gamma L)\left(\frac{Z_{IN}Z_A}{Z_0}-Z_0\right)= Z_A-Z_{IN}$$

$$\tanh(\gamma L) \quad \left(\frac{Z_A-Z_{IN}}{\frac{Z_{IN}Z_A}{Z_0}-Z_0}\right) \qquad \text{(Eq 2)}$$

We now need to be able to distinguish between the two sets of readings so we need separate identities that are:

R_L = remote resistance termination lower than Z_0.

Z_L = measured input impedance with low resistance termination.

R_H = remote resistance termination higher than Z_0.

Z_H = measured input impedance with high resistance termination.

We then get:

$$\tanh(\gamma L) \left(\frac{R_L - Z_L}{R_L Z_L - Z_0}\right) \left(\frac{R_H - Z_H}{R_H Z_H - Z_0}\right)$$

therefore:

$$(R_L - Z_L)\left(\frac{R_H - Z_H}{Z_0} - Z_0\right) = (R_H - Z_H)\left(\frac{R_L - Z_L}{Z_0} - Z_0\right)$$

$$\frac{R_L R_H Z_H}{Z_0} - R_L Z_0 - \frac{Z_L R_H Z_H}{Z_0} + Z_L Z_0$$
$$\frac{R_H R_L Z_L}{Z_0} - R_H Z_0 - \frac{Z_H R_L Z_L}{Z_0} + Z_H Z_0$$

$$R_L R_H Z_H - R_L Z_0^2 - Z_L R_H Z_H + Z_L Z_0^2$$
$$R_H R_L Z_L - R_H Z_0^2 - Z_H R_L Z_L - Z_H Z_0^2$$

$$-R_L Z_0^2 + Z_L Z_0^2 + R_H Z_0^2 - Z_H Z_0^2$$
$$R_H R_L Z_L - Z_H R_L Z_L - R_L R_H Z_H + Z_L R_H Z_H$$

$$Z_0^2(-R_L + Z_L + R_H - Z_H) =$$
$$R_H R_L Z_L - Z_H R_L Z_L - R_L R_H Z_H + Z_L R_H Z_H$$

$$Z_0^2 \quad \frac{R_H R_L Z_L - Z_H R_L Z_L - R_L R_H Z_H + Z_L R_H Z_H}{-R_L + Z_L + R_H - Z_H}$$

$$Z_0 \quad \sqrt{\frac{R_H R_L Z_L - Z_H R_L Z_L - R_L R_H Z_H + Z_L R_H Z_H}{-R_L + Z_L + R_H - Z_H}} \qquad \text{(Eq 3)}$$

Only the positive root is valid. Having established a method to derive Z_0 we can now turn our attention to line loss and effective electrical length.

Calculation of Transmission Line Loss and Effective Electrical Length

For the purpose of determining the impedance of the antenna, the only transmission line parameter we need to know other than Z_0 is $\tanh(\gamma L)$ which we will derive from Eq 2 using the input impedance measurements from either of the remote terminations. It is not necessary to know the line loss and effective electrical length that go to make up $\tanh(\gamma L)$, but I would expect most experimenters would want to know them, if for no other reason than for comparison with what would be expected. Since we are going to have to determine the value of $\tanh(\gamma L)$ to derive antenna impedance, it might appear most obvious to get at the values for line loss and effective electrical length by extracting them from it. This can be done but because $\tanh(\gamma L)$ is a complex number, the only way I could find to extract its component values involved the use of a quadratic equation which will of course give two solutions with the attendant problem of establishing a rule to select the correct root in every situation. This problem can be avoided by the use of an alternative approach based on the reflection coefficient equation that was Eq 2 in Dr Best's *QEX* article:

$$\rho \quad \frac{\frac{Z}{Z_0} - 1}{\frac{Z}{Z_0} + 1} \quad \frac{Z - Z_0}{Z - Z_0} \qquad \text{(Eq 4)}$$

where:

ρ = complex reflection coefficient.

Z = complex impedance at point of reference.

Z_0 = complex characteristic impedance of line.

This equation gives the reflection coefficient in *rectangular* form as a complex number with a value within the limits of $\pm 1 \pm j$. For our purpose, we need it in *polar* form to give us its magnitude and angle. The relationship between the rectangular and polar forms is illustrated by the *Argand* diagram shown in Fig 1. The horizontal axis of the diagram represents the real component of the complex number and the vertical axis the imaginary component. The numerical values for the example shown are $0.75+j0.5$, the real component represented by the line OA and the imaginary component by the line AB. The line OB is known as the *modulus* or *absolute* of the complex number and in this application it represents the *magnitude* of the reflection coefficient with a value in the range 0.0 to 1.0. The angle AOB is known as the *argument* of the complex number and in this application it represents the *angle* of the reflection coefficient which has a value in the range $-\pi$ to $+\pi$ radians (-180° to +180°). Excel has the facility to provide both the absolute and the argument of a complex number. Intriguingly, the Smith chart is a reflection coefficient Argand diagram with modified coordinates. For more on this, refer to Appendix 1.

Matched transmission line loss in dB is 10·log of the ratio of the magnitudes of reflection coefficient at the near and remote ends of the line. Although the magnitude of reflection coefficient is a function of voltage (or current but not power), the difference in the values at the opposite ends of the line is a result of loss in both the forward and reflected waves, hence the use of 10 for the dB multiplier rather than the usual 20 when dealing with voltage ratios. The values of magnitude of reflection coefficient at

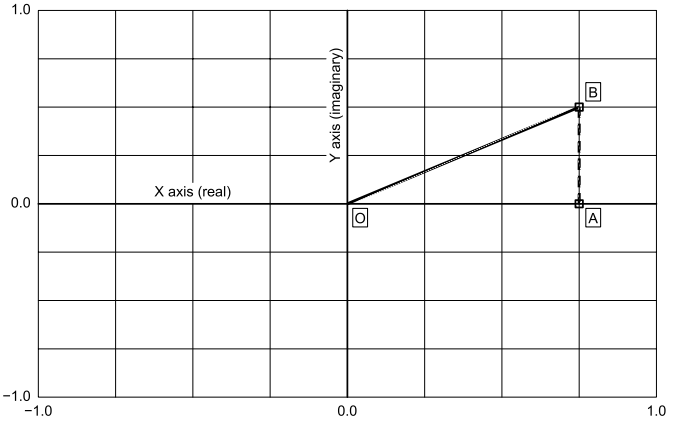

Figure 1—Argand Diagram showing the relationship between the rectangular and polar forms of reflection coefficient.

	A	B	C	D	E	F	G	H	I	J	K	L
1												
2		FEEDER PARAMETERS AND REMOTE ANTENNA IMPEDANCE MEASUREMENT										
3												
4		1. Terminate the feeder with a resistive load of 1/3 to										
5		1/2 of the specified Zo and measure R+/-jX at the					Enter value of load resistance.			20.0	ohms	
6		near end at the frequency of interest.					Enter measured impedance.*			72.0-43.7j	ohms	
7												
8		2. Change the termination to a resistive load of 2 to 3										
9		times the specified feeder Zo and measure R+/-jX					Enter value of load resistance.			120.0	ohms	
10		at the near end at the same chosen frequency.					Enter measured impedance.*			26.8+13.2j	ohms	
11												
12		3. Connect the antenna and measure R+/-jX at the										
13		near end at the same chosen frequency.					Enter measured impedance.*			39.6+28.0j	ohms	
14												
15		For this spreadsheet to operate the					Feeder complex impedance			50.2-1.1j	ohms	
16		Analysis Toolpak must be enabled by					Matched feeder loss			0.68	dB	
17		clicking on tools and then on Add-Ins.					Feeder effective length			0.308	λ	
18		Then tick the Analysis Toolpak box in										
19		the Add-Ins list and click OK.					Antenna impedance			69.7-46.8j	ohms	
20							True SWR at antenna			2.25		
21		* Impedances must be entered as R+/-Xj.					True SWR at transmitter			1.99		
22		Excel does not recognise impedances					SWR at tx. ref. to 50 ohms			1.93		
23		entered as R+/-jX.					Feeder loss at actual SWR is			0.87	dB	
24											compiled by g4jnh	

Figure 2—User screen 1 with basic instructions and one results column.

	M	N	O	P	Q	R	S	T	U	V	W	X
1												
2		Antenna details.		Dummy load - 100 ohm resistor in parallel with 150 pF capacitor in a PL259 plug.								
3		Feeder details.		37.0 metres RG213 mil. spec. accurately measured.								
4												
5	Enter frequency			1.000	3.000	5.000	7.000	9.000	11.000	13.000	15.000	MHz
6	Enter value of load resistance.			20.0	20.0	20.0	20.0	20.0	20.0	20.0	20.0	ohms
7	Enter measured impedance.			78.9+48.6j	26.1+16.2j	25.3-16.7j	72.0-43.7j	66.4+43.0j	26.7+13.0j	28.0-21.4j	83.3-39.9j	ohms
8												
9	Enter value of load resistance.			120.0	120.0	120.0	120.0	120.0	120.0	120.0	120.0	ohms
10	Enter measured impedance.			25.7-18.6j	70.0-45.9j	68.3+39.5j	26.8+13.2j	28.6-17.1j	78.7-35.2j	59.7+35.9j	25.7+6.7j	ohms
11												
12	Enter impedance measured											
13	with antenna connected.			28.9-15.6j	53.6-35.8j	93.9+13.3j	39.6+28.0j	24.6+2.4j	32.9-28.8j	109.7-33.2j	46.8+43.6j	ohms
14												
15	Feeder complex impedance			51.4-2.4j	49.8-2j	50.1-1.4j	50.2-1.1j	50.7	51.5-0.8j	51.3-2j	49.9-2.7j	ohms
16	Matched feeder loss			0.22	0.43	0.58	0.68	0.72	0.90	0.79	0.80	dB
17	Feeder effective length			0.188	0.064	0.435	0.308	0.181	0.052	0.419	0.288	λ
18												
19	Antenna resistance			102.8	93.5	82.6	69.7	58.4	46.6	38.9	29.2	ohms
20	Antenna reactance			-7.0	-26.0	-40.4	-46.8	-48.5	-52.1	-50.7	-48.3	ohms
21	True SWR at antenna			2.00	2.03	2.15	2.25	2.39	2.72	2.86	3.27	
22	True SWR at transmitter			1.93	1.89	1.94	1.99	2.07	2.21	2.34	2.58	
23	SWR at tx. ref. to 50 ohms			1.97	1.98	1.93	1.93	2.04	2.23	2.44	2.40	
24	Feeder loss at actual SWR			0.27	0.53	0.73	0.87	0.97	1.28	1.17	1.30	dB

Figure 3—User screen 2 with provision for eight columns of results identified by frequency.

both ends of the line with the antenna connected are used to determine the line loss at the actual SWR. The derivation of the equation used for this was described in the earlier article (see Note 1).

Because the angle of reflection coefficient is the result of the forward and reflected voltage vectors rotating in opposite directions it changes by 2π radians or 360° for each half λ of line. Therefore, the effective electrical length of the line expressed as an angle is equal to half of the difference between the angles of reflection coefficient at the two ends of the line. So the effective electrical length is derived by subtracting the angle of reflection coefficient at the near end from that at the remote end and dividing by 2. If the value of the reflection coefficient at the near end is higher than that at the remote end, the result will be negative which just means that the line is shorter than a whole number of electrical half λ by that amount. I prefer line length to be expressed as a positive number and the spreadsheet utilizes the Excel logic function to add π radians (½ λ) to the result when it would otherwise be negative. Finally, the angle in radians is divided by 2π to convert it into λ.

Measurement of Antenna Impedance

To derive the impedance of the antenna from measurements made at the transmitter end of the transmission line, Eq 1 has to be transposed to isolate Z_A on one side as follows:

$$Z_{IN} \quad Z_0\left(\frac{\frac{Z_A}{Z_0}+\tanh(\gamma L)}{1+\frac{Z_A\tanh(\gamma L)}{Z_0}}\right) = \qquad \textit{Eq 1}$$

$$\frac{Z_{IN}}{Z_0} \quad \left(\frac{\frac{Z_A}{Z_0}+\tanh(\gamma L)}{1+\frac{Z_A\tanh(\gamma L)}{Z_0}}\right) =$$

$$\frac{Z_{IN}}{Z_0}\left(1+\frac{Z_A\tanh(\gamma L)}{Z_0}\right) = \frac{Z_A}{Z_0}+\tanh(\gamma L)$$

$$\frac{Z_{IN}}{Z_0}+\frac{Z_{IN}Z_A\tanh(\gamma L)}{{Z_0}^2} \quad \frac{Z_A}{Z_0}+\tanh(\gamma L)$$

$$Z_{IN}+\frac{Z_{IN}Z_A\tanh(\gamma L)}{Z_0} \quad Z_A+Z_0\tanh(\gamma L)$$

$$\frac{Z_{IN}Z_A\tanh(\gamma L)}{Z_0}-Z_A \quad Z_0\tanh(\gamma L)-Z_{IN}$$

$$Z_A\left(\frac{Z_{IN}\tanh(\gamma L)}{Z_0}-1\right) = Z_0\tanh(\gamma L)-Z_{IN}$$

$$Z_A \quad \frac{Z_0\tanh(\gamma L)-Z_{IN}}{\frac{Z_{IN}\tanh(\gamma L)}{Z_0}-1} \qquad \text{(Eq 5)}$$

That completes the math on which the spreadsheet is based and we can now turn our attention to its compilation.

The Spreadsheet

The spreadsheet is compiled in *MS Excel,* and for *Excel* to handle the complex algebra calculations it is necessary for the engineering functions facility to be enabled. To check, select a cell and enter =(COMPLEX(0,1)). If the engineering functions are enabled you will see the single letter i displayed in the cell when the enter key is pressed but if they are not you will see #VALUE! For details of how to enable the engineering functions facility, refer to Appendix 2.1.

The layout of the spreadsheet is based on that used in the earlier article and comprises two user screens that occupy the first 24 rows of columns A to X. Most of the processing takes place between rows 26 and 41 but some of the cells in the user screens are also active. Screen 1, which is shown in Fig 2, provides for only one set of results but includes brief instructions on the use of the spreadsheet. In cells J6, J10 and J13 the impedance values are entered as complex impedances rather than as resistance and reactance in separate cells. This has the advantage of economizing on screen space, but it is important to note that the values must be entered in the form R±X*j*. *Excel* will not recognize impedances entered as R±*j*X. The known terminations do not have to be purely resistive as cells J5 and J9 will also accept complex impedances. Screen 2, which is shown in Fig 3, provides for 8 columns of results but may

[1]Notes appear on page 41.

	A	B	C	D	E	F	G	H	I	J	K
26	EQUATION 3 - NUMERATOR									359124-158636j	
27	FEEDER COMPLEX CHARACTERISTIC IMPEDANCE							50.163043410683-1.06549026305713j			ohms
28											
29	ANGLE OF REFLECTION COEFFICIENT AT LOW RESISTANCE TERMINATION									3.1215	radians
30	ANGLE OF REFLECTION COEFFICIENT AT TX. WITH LOW RESTISTANCE TERMINATION									-0.7462	radians
31	FEEDER EFFECTIVE ELECTRICAL LENGTH - POLAR									1.9338	radians
32											
33	MAGNITUDE OF REFLECTION COEFFICIENT AT LOW RESISTANCE TERMINATION									0.4301	
34	MAGNITUDE OF REFLECTION COEFFICIENT AT TX. WITH LOW RESISTANCE TERMINATION									0.3682	
35											
36	TANH (GAMMA - L)							0.590700233929659-2.51178351985523j			
37	COMPLEX ANTENNA IMPEDANCE							69.6688881564534-46.8320745826687j			ohms
38											
39	MAGNITUDE OF REFLECTION COEFFICIENT AT ANTENNA									0.3855	
40	MAGNITUDE OF REFLECTION COEFFICIENT AT TX. WITH ANTENNA CONNECTED									0.3300	
41	DITTO BUT REFERENCED TO 50 OHMS									0.3182	

Figure 4—The working lines for screen 1 with values.

be extended as required by the use of the drag handle. This screen includes provision for entering frequency for column identification and for the graphical display of results against frequency. To facilitate graphing the resistive and reactive components of the antenna impedances are presented in separate cells in this screen. The results shown in Fig 3 will be discussed later in the article.

Rows 26 to 41, in which most of the action takes place, are shown in Fig 4 with values and their description. All of the formulas including those for the active cells in the user screen are shown in Fig 5. If you have not previously used the complex algebra facility in *Excel*, you will find some of the protocol in Fig 5 unfamiliar. For more on this, refer to Appendix 2.2. If the result of a calculation is an imaginary or a complex number, the normal *Excel* procedure for controlling the number of decimal places displayed is inoperative. All of the figures it has worked out up to a maximum of 15 significant figures are displayed, hence the very long numbers in three of the cells in Fig 4. To obtain control of the number of decimal places displayed, it is necessary to separate the real and imaginary components, round them and then recombine them into a complex number as in cells J15 and J19. The calculation of Eq 3 is divided between two cells, J26 and J27, to enable the formulas to be more readily accommodated on the printed page.

I would suggest that before entering the formulas, the values shown in cells J5, J6, J9, J10 and J13 in Fig 2 be entered. Then enter the formulas starting with cell J26 through to J41. The appearance of the values shown in Fig 4 as the formulas are entered will confirm that they have been entered correctly. Finally, enter the formulas in cells J15 to J17 and J19 to J23.

Alternative Software

The only spreadsheet software in my computer is *MS Excel 97* but my good friend and computing enthusiast, Morrison, VK3BCY, has several alternative spreadsheet systems installed and has very kindly tested this spreadsheet in each of them. He found that it works correctly with some open source software—in particular, Open Office (**www.openoffice.org**), available for both Windows and Linux operating systems, and also Gnumeric (**www.gnumeric.org**), only available for Linux.

Using the Spreadsheet

To make use of this spreadsheet, it is necessary to be able to make quite accurate measurements of resistance and reactance. I use a homebrew impedance (as distinct from admittance) bridge that has been very painstakingly calibrated to provide an accuracy of ± 2 ohms or better for any combination from 0 to 150 ohms resistance and – 60 to + 60 ohms reactance at frequencies up to about 15 MHz. I would consider that to be a minimum standard of accuracy for serious work with this spreadsheet. *The ARRL Antenna Book* 17th edition provides details of the design, construction and calibration of a suitable impedance bridge.[4] An alternative approach is the admittance or parallel bridge, as it is sometimes called, which is generally accepted as being easier to calibrate than an impedance bridge and I would recommend to anyone contemplating constructing a bridge to study two excellent articles by Wilfred N. Caron, one of which reports some interesting findings on two commercially available bridges.[5, 6]

In recent years, there has appeared on the amateur market a range of instruments known as antenna analysers. I

	J
15	=COMPLEX(ROUND(IMREAL(J27),1),ROUND(IMAGINARY(J27),1),"j")
16	=10*LOG10(J33/J34)
17	=J31/2/PI()
18	
19	=COMPLEX(ROUND(IMREAL(J37),1),ROUND(IMAGINARY(J37),1),"j")
20	=(1+J39)/(1-J39)
21	=(1+J40)/(1-J40)
22	=(1+J41)/(1-J41)
23	=10*LOG10((1/J40-J40)/(1/J39-J39))
24	
26	=IMSUM(IMPRODUCT(J5,J6,J9),IMPRODUCT(-1,J5,J6,J10),IMPRODUCT(-1,J5,J9,J10),IMPRODUCT(J6,J9,J10))
27	=IMSQRT(IMDIV(J26,(IMSUB(IMSUM(J6,J9),IMSUM(J5,J10)))))
28	
29	=IMARGUMENT(IMDIV(IMSUB(J5,J27),(IMSUM(J5,J27))))
30	=IMARGUMENT(IMDIV(IMSUB(J6,J27),(IMSUM(J6,J27))))
31	=IF(J30>J29,(J29-J30)/2+PI(),(J29-J30)/2)
32	
33	=IMABS(IMDIV(IMSUB(J5,J27),(IMSUM(J5,J27))))
34	=IMABS(IMDIV(IMSUB(J6,J27),(IMSUM(J6,J27))))
35	
36	=IMDIV(IMSUB(J5,J6),IMSUB(IMDIV(IMPRODUCT(J6,J5),J27),J27))
37	=IMDIV(IMSUB(IMPRODUCT(J27,J36),J13),IMSUB(IMDIV(IMPRODUCT(J13,J36),J27),1))
38	
39	=IMABS(IMDIV(IMSUB(J37,J27),IMSUM(J37,J27)))
40	=IMABS(IMDIV(IMSUB(J13,J27),IMSUM(J13,J27)))
41	=IMABS(IMDIV(IMSUB(J13,50),IMSUM(J13,50)))

Figure 5—Active cells for screen 1 with formulas.

have no personal experience of any of these and I have seen only one rigorous review, that by Ian White, G3SEK, on the MFJ 269.[7] The accuracy he reported was impressive but the unit is not able to determine the sign of the reactance. The manual explains that this can usually be determined by noting what happens when you make a small change in frequency. However, as I pointed out in note 7 of the previous article, when measurements are being made at the end of a transmission line, this is not an acceptable method (see Note 1). This assertion was called into question following the previous article so it is opportune to explain the reason in more detail here.

In the normal way of things, the reactance of an inductor increases with increasing frequency and the reactance of a capacitor decreases with increasing frequency. This may or may not be true when the reactance occurs as a result of the interaction of forward and reflected waves on a transmission line. For a given length of line, increasing the frequency of an applied signal is equivalent to increasing its electrical length, which in turn is equivalent to going round the Smith chart in a clockwise direction. A line that is ½ λ long at a particular frequency would be a full λ long at twice that frequency, which is equivalent to one full circle of the Smith chart. To demonstrate what happens to the reactance seen at the input of the line, let us take the example of a half λ of 50-ohm line terminated in a 20-ohm load when the frequency is progressively increased until the line is 1.0 λ long. Ignoring line loss, the impedance values would be as is listed in Table 1.

Note that between 0.500 and 0.700 λ, the reactance is inductive and is increasing with increasing frequency, which means that it is following the normal rules. But between 0.700 and 0.750 λ it decreases with increasing frequency despite still being inductive. Between 0.750 and 0.800 λ, the reactance is capacitive and is increasing with increasing frequency, again the opposite of what would be expected. Beyond 0.800 and up to 1.000 λ, the reactance falls with increasing frequency and thus follows the normal rule. Examination of a Smith chart shows that the point at which the change from following the normal rule to being the opposite of the normal rule varies with SWR and in some parts of the chart the change of reactance with line length—and thus of frequency—is almost flat. It must be concluded, therefore, that when making impedance measurements at the end of a transmission line, the change of reactance with frequency should not be used to determine the sign of the reactance.

Table 1
Demonstration that the change in reactance as frequency is changed does not always obey the normal rules when measured on a transmission line.

Line length (λ)	*Resistance (ohms)*	*Reactance (ohms)*
0.500	20.0	0.0
0.550	21.7	13.4
0.600	28.2	28.1
0.650	44.4	44.4
0.700	83.3	51.4
0.725	110.8	35.9
0.750	125.0	0.0
0.775	110.8	–35.9
0.800	83.3	–51.4
0.850	44.4	–44.4
0.900	28.2	–28.1
0.950	21.7	–13.4
1.000	20.0	0.0

Evaluation of the Spreadsheet in Use

The evaluation described here is just one of several, all of which gave similar results. For the purpose of this evaluation, I chose a very carefully measured a 37.0-m length of new and unused mil. spec. RG-213 terminated at both ends with PL-259 plugs. The cable carries the identification M -17/74 RG213 MIL–C–17F RG213U 50 W" but no manu-facturer's name. The terminations for the evaluation were 20- and 120-ohm resistors and a dummy antenna comprising a 100-ohm resistor in parallel with a 150 pF, capacitor all incorporated into PL-259 plugs. The resistors were 1% tolerance, 0.6 W, metal film and the capacitor was a 1% tolerance polystyrene type. A double male adapter was used to connect the terminations to the line.

Tests were conducted at frequency intervals of 2.0 MHz from 1.0 to 15.0 MHz and the results are shown in Fig 3. The results were also processed using the spreadsheet described in the previous article and by using the measured length of the cable and AC6LA's excellent *Transmission Line Details* (TLD) software which can be downloaded free of charge from the net.[8] The published values of all of the relevant line parameters for all the grades of line likely to be of interest to radio amateurs (and many more) are incorporated into this software which makes it a very useful source of information in addition to its main function of performing the transmission-line equation calculations. TLD includes values for RG-213 from two manufacturers: Belden's 8267 and Wireman's CQ110, which are not exactly the same. The Belden 8267 values were used in this evaluation. All of the results are summarized in Table 4, which also includes calculated values of the dummy antenna impedance and impedance measurements with the dummy antenna connected directly to the bridge terminals.

The feeder effective electrical lengths shown in Fig 3 were used to determine the velocity factor for each frequency using the following equation:

Table 2
Velocity factor versus frequency based on measurements processed in the spreadsheet.

Frequency (MHz)	*Effective electrical length (λ)*	*Actual electrical length (λ)*	*Velocity factor*
1.0	0.1880	0.1880	0.6564
3.0	0.0637	0.5637	0.6568
5.0	0.4352	0.9352	0.6598
7.0	0.3078	1.3078	0.6605
9.0	0.1808	1.6808	0.6608
11.0	0.0516	2.0516	0.6617
13.0	0.4191	2.4191	0.6632
15.0	0.2880	2.7880	0.6640

$$vf \quad \frac{L_A F}{c L_E} \qquad \text{(Eq 6)}$$

where:

vf = velocity factor
L_A = actual length of line (37.0 meters)
F = frequency in MHz
c = speed of light in free space (299.8 Mm/sec)
L_E = electrical length of line in λ.

The results are listed in Table 2.

This variation of velocity factor with frequency was not expected as all that I had read on the subject had indicated that for any particular line it had a fixed value. My initial thoughts were that the results must be suspect; but if that were the case, I would have expected them to be erratic rather than changing progressively with frequency. Furthermore, the results appeared to be consistent with

Table 3
Velocity factor versus frequency based on measurements of resonances.

Resonance	*Frequency (MHz)*	*Velocity factor*
1/4 λ	1.325	0.6541
3/4 λ	4.016	0.6608
1 1/4 λ	6.710	0.6625
1 3/4 λ	9.405	0.6633
2 1/4 λ	12.099	0.6636
2 3/4 λ	14.811	0.6647

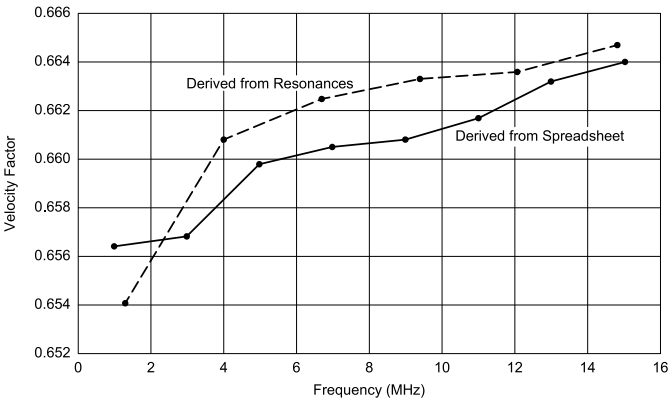

Figure 6—Velocity factor against frequency measured on RG-213.

Table 4
Comparison of the various measurements of impedance of the dummy antenna as described in the text.

	Frequency	1.0	3.0	5.0	7.0	9.0	11.0	13.0	15.0	MHz
A	Calculated impedance of dummy antenna.	99.1-j9.3	92.6-j26.2	81.8-j38.6	69.7-j46.0	58.2-j49.3	48.2-j50.0	40.0-j49.0	33.3-j47.1	ohms
B	Impedance of dummy antenna measured at the impedance bridge terminal.	99.7-j10.8	92.0-j27.2	80.5-j38.9	68.6-j44.8	56.3-j48.4	47.1-j49.1	39.8-j50.5	30.8-j48.4	ohms
C	Measured remotely using measured line length and TLD* programme.	100.3-j0.9 (0.23)	93.8-j28.3 (0.41)	80.9-j38.8 (0.53)	70.5-j43.8 (0.63)	58.4-j47.5 (0.72)	51.9-j52.3 (0.79)	42.9-j55.0 (0.87)	39.7-j53.0 (0.93)	ohms (dB)
D	Measured remotely using original spreadsheet with 20 ohm known termination.	100.4+j12.3 (0.196)	97.1-j26.3 (0.064)	80.5-j38.0 (0.435)	72.0-j42.1 (0.311)	58.7-j47.0 (0.182)	50.0-j51.5 (0.054)	35.8-j48.4 (0.417)	36.2-j48.5 (0.297)	ohms (λ)
E	Measured remotely using original spreadsheet with 120 ohm known termination.	102.1-j5.0 (0.179)	96.5-j26.9 (0.063)	80.4-j38.1 (0.435)	67.6-j42.5 (0.305)	56.8-j46.5 (0.179)	47.2-j49.9 (0.049)	37.6-j50.1 (0.421)	29.5-j48.7 (0.278)	ohms (λ)
F	Measured remotely using new spreadsheet with 20 and 120 ohm known terminations.	102.8-j7.0 (0.188)	93.5-j26.0 (0.064)	82.6-j40.0 (0.435)	69.7-j46.8 (0.308)	58.4-j48.5 (0.181)	46.6-j52.1 (0.052)	38.9-j50.7 (0.419)	29.2-j48.3 (0.288)	ohms (λ)
G	As row C but using velocity factor values derived from new spreadsheet.(refer fig. 3)	100.3-j0.1 (0.6564)	95.6-j26.3 (0.6568)	81.1-j38.7 (0.6598)	69.7-j43.8 (0.6605)	57.0-j47.1 (0.6608)	48.4-j50.6 (0.6617)	36.8-j49.6 (0.6632)	32.2-j45.3 (0.6640)	ohms (v.f)

Row C. The figures in brackets are the "book" values of matched line loss sourced from the TLD* programme. The same values were also used in the original spreadsheet derivations (Rows D and E). The "book" value for velocity factor, also sourced from the TLD* programme was 0.66.

Rows D,E and F. The figures in brackets are the effective electrical lengths derived using the spreadsheet.

Row G. The figures in brackets are the velocity factor values derived from the new spreadsheet (refer to text).

* AC6LA's Transmission Line Details programme (see text).

previous observations on other lines that when the quarter-wave resonant frequency of an open terminated line is measured using a noise bridge the odd number harmonic resonances are not exact multiples of the fundamental. I therefore decided to conduct that experiment on the same piece of line and to use the results to calculate velocity factors, again using Eq 6. The results are listed in Table 3.

The results in Tables 2 and 3 are presented graphically in Fig 6.

TLD provides for the line parameters to be changed if required. Accordingly, the remote impedance derivations using measured line length and TLD were reworked using the velocity factor values listed in Table 2 above. The results appear in Row G of Table 4.

Comment

The published values of characteristic impedance of RG-213 as given in the TLD software are 50 - *j*1.44 ohms at 1 MHz changing progressively to 50 - *j*0.34 ohms at 15.0 MHz. The results that I obtained (Fig 3, row 15) showed a degree of scatter which I attributed to the limitations imposed by the accuracy of my impedance bridge. The measured values of matched feeder loss were generally in pretty good agreement with the published values (row 16 in Fig 3 and row C in Table 4).

The impedance measurements made with the dummy antenna connected directly to the impedance bridge terminal were generally in good agreement with the calculated values (rows A and B in Table 4). The remote measurements processed using TLD were in remarkably good agreement with the calculated and directly measured values from 3.0 to 9.0 MHz but there was a progressive loss of agreement with increasing frequency above that range (row C in Table 4).

In some cases, there were significant differences between the effective electrical lengths derived from the 20- and 120-ohm terminations using the original spreadsheet; but in every instance where this occurred, the same readings processed in the new spreadsheet gave a value equal to the average (rows D,E and F in Table 4). Overall, the remote impedance results derived with the new spreadsheet were significantly better than with the original spreadsheet and at the higher frequencies were better than those based on measured line length and processed using TLD. However, as we saw earlier, the results presented here suggest that velocity factor is frequency dependent and when the results were reworked in TLD using the velocity factor values derived from the new spreadsheet the remote impedance results improved significantly at the higher frequencies (row G in Table 4).

While the observed variations in velocity factor may appear to be small, they are far from negligible in the context of remote impedance measurement. Take as an example the case of a 10-m antenna at the end of 150 feet of RG-213. The difference in electrical length between the specified velocity factor of 0.660 and 0.665 at 28.5 MHz would be 17 electrical degrees. Reference to a Smith chart will show just how much error such a discrepancy could introduce. Similarly, Table 3 illustrates the potential for error in using the quarter-wave resonance as a means of determining the electrical length of a line that is several λ long. For the example shown the quarter-wave resonance of 1.325 MHz equates to an electrical length of 2.830 λ at 15 MHz; yet when measured with the method described here, it was shown to be 2.788 λ, a difference equivalent to 15 electrical degrees.

Conclusions

A method of remote impedance measurement has been presented that is independent of specified transmission line parameters, all of which are determined together with the effective electrical length from two impedance measurements with known terminations. A further measurement with the antenna connected enables its impedance to be derived. The method is based on math which would be prohibitively time-consuming without the use of a computer but which is straightforward with the complex algebra facility in *MS Excel*.

The method was evaluated using a dummy antenna of known impedance and the results showed a significant improvement over the method described in the earlier article, which was dependent on published values of the line's characteristic impedance and loss and had no provision for taking account of any reactive component in the characteristic impedance. At the higher frequencies, it also gave better results than those based on an accurate physical measurement of line length and the published values of line parameters. The evidence suggests that this was due to a variation of velocity factor with frequency of which I was unaware, and about which I am still hesitant to be categorical. I would be pleased to hear of the experience of others on this point. I would also be very interested to see the work reported in Fig 3 repeated using a professional-grade network analyzer. Are there are any readers of *QEX* who have access to the necessary equipment and who are sufficiently interested in the subject to spare the time to do it?

Acknowledgments

I would like to express my appreciation to Dr. Steven Best, VE9SRB, for his series of articles on transmission line theory in *QEX* in 2001 which considerably advanced my understanding of this fascinating aspect of radio communication.

I would also like to thank Dan Maguire, AC6LA, for very kindly authorizing me to make use of his *TLDetails* software in the evaluation of the spreadsheet.

Last but not least I would like to thank Morrison Hoyle, VK3BCY, for useful discussion and for testing the spreadsheet using alternative software to *MS Excel*.

Notes

[1]R. Barker, G4JNH, "A Spreadsheet for Remote Antenna Impedance Measurement, "*QEX*, Sept/Oct 2001, pp 3-11.

[2]R. D. Straw, N6BV, Editor, *The ARRL Antenna Book*, 17th edition, pp 27-28.

[3]S. R. Best, VE9SRB, "Wave Mechanics of transmission Lines Part 1: Equivalence of Wave Reflection Analysis and the Transmission Line Equation," *QEX* Jan/Feb 2001 pp 3-8.

[4]*The ARRL Antenna Book*, 17th edition, Chap. 27, pp 23-26.

[5]W. N. Caron, "A Simple and Accurate Admittance Bridge," *Communications Quarterly*, Summer 1992, pp 44-50.

[6]W. N. Caron, "The Hybrid Junction Admittance Bridge," *The ARRL Antenna Compendium*, Volume 3, 1993, pp 223-230.

[7]I. White, G3SEK, "MFJ -269 HF/VHF/UHF SWR Analyser," *RadCom*, May 2000, pp 34-36.

[8]*Transmission Line Details* by Dan Maguire, AC6LA, available for free download at **www.qsl.net/ac6la/tldetails.html**.

[9]P. H. Smith, *Electronic Applications of the Smith Chart,* Second Edition, 1995, Noble Publishing Corporation, Atlanta, GA. ISBN 1-884932-39-8.

Appendix 1. The Smith Chart as a Modified Argand Diagram

As stated in the text, the Smith chart is a reflection-coefficient Argand diagram with modified coordinates. Instead of being scaled in the rectangular coordinates of the real and imaginary components of the complex reflection coefficient, it is scaled in the circular coordinates of resistance and reactance to which they are related by Eq 4. Effectively, when resistance and reactance values are entered on to a Smith chart, the chart solves Eq 4. This is demonstrated in Fig 7 in which a reflection coefficient Argand diagram has been superimposed onto a Smith chart. Note that the chart is orientated with the resistance line horizontal which was the preference of its originator. The example shown is for an impedance of 25+*j*25 ohms on 50-ohm line which normalizes to the 0.5 +*j*0.5 ohms Ω entered on the chart. Putting these values into Eq 4 gives a reflection coefficient of -0.2+*j*0.4, which corresponds to the Argand co-ordinates shown in Fig 7. Smith chart impedance transformations are actually conducted as reflection coefficient transformations and when the transformed impedance is read off, the chart effectively solves Eq 4 in its transposed form which is:

$$Z \quad Z_0 \frac{1+\rho}{1-\rho} \qquad \text{(Eq 7)}$$

In the introduction to his book *Electronic Applications of the Smith Chart*, the inventor of the chart, Phillip H. Smith, describes how it was derived from a rectangular transmission line chart he developed in 1931 based on earlier work by J. A.Fleming in 1911.[9] It differed from the Smith chart in having linear rectangular scales for both resistance and reactance but the SWR circles were not concentric and the line length radials were curved and non-linear. Details of how the Smith chart was derived from its rectangular progenitor are given in Appendix B of the book and it does not involve the Argand diagram. However, in Chapter 8 which describes the graphical representation of the transmission and reflection coefficients, his Fig 8.3 which is captioned "Vol. refl. coeff. – rect. coord." is quite definitely an Argand diagram. It is presented again in Fig 8.5 as an overlay for the Smith chart. The only reference that I could find to the Argand diagram is the following sentence on p 4 which to me implies recognition of its relationship to the Smith chart:

"It became apparent shortly after publication of Fig I.3, (the now familiar chart) as thus oriented, that a horizontal representation of the resistance axis was preferable since this conformed to the accepted convention represented by the Argand diagram in which complex numbers (x ± *iy*) are graphically represented with the real (x) component horizontal and the imaginary (y) component vertical."

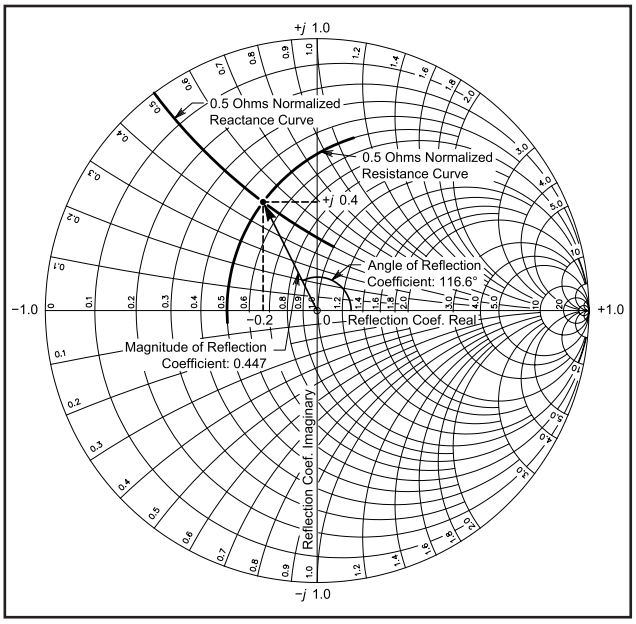

Figure 7—Argand diagram overlaying a Smith chart.

Appendix 2. Complex Algebra Calculations using *MS Excel*

2.1. Enabling the Complex Algebra Facility

For *Excel* to perform complex algebra calculations, the engineering functions facility has to be enabled. Should the simple test described in the text show that this function is not enabled click on Tools and then on Add-ins. A panel will appear headed Add-ins available. Tick the box marked Analysis Toolpak to enable the engineering functions. If Analysis Toolpak does not appear in the Add-ins panel it will be necessary to insert the *Excel* CD ROM and run *Setup* to install it. It will then be necessary to enable the facility as just described.

2.2. Complex Algebra Facilities Available in *Excel*

To display a list of the complex algebra facilities available in *Excel*, click on Help and then on Contents and Index. The Help Topics panel will appear. Click on the tab marked Index, type ENG in the box and click on display. A panel will appear which lists all of the engineering functions available. The ones relevant to complex algebra are COMPLEX and all of those which start IM. Click on each of these in turn for a description of what they do and how to use them.

□□

A Tutorial Dispelling Certain Misconceptions Concerning Wave Interference in Impedance Matching

Walt Maxwell responds to Steven Best's description of how reflected waves act at mismatched boundaries.

By Walter Maxwell, W2DU, ARRL Technical Advisor

In a three-part article appearing in *QEX*,[1] Dr. Steven R. Best, VE9SRB, wrote about the wave mechanics involved in impedance matching. In that article, he disputes the treatment of wave mechanics appearing in the writings of Slater[2] and Alford,[3] in all editions of "*Reflections,*" [4, 5, 7] and my article in *QEX*.[6]

The errors in Steve's article follow from an invalid premise. This detailed tutorial is presented to describe and correct that. The invalid premise is revealed in his Eqs 6, 7, and 8 of his Part 1.

All three of these equations are invalid because Steve misinterpreted the universally known equations for determining the amplitude of voltage, E, of the standing wave as the equations for determining forward voltage V_{FWD}. The two separate voltage values, voltage E of the standing wave, and forward voltage V_{FWD}, resulting from these two equations differ significantly. As we know, the amplitude of the voltage standing wave is the phasor sum of the forward and reflected voltages, which varies alternately between maximum and minimum with varying distance along the line. However, on lossless lines, the amplitude of forward voltage V_{FWD} is constant throughout the entire length of the line. The forward voltage can be determined using the correct expression

$$V_{FWD} = \sqrt{P_{FWD} \times Z_0} \qquad \text{(Eq 1)}$$

where P_{FWD} is the total forward power, and Z_0 is the characteristic impedance of the line. That expression is proven correct through the following mathematical exercise: Forward current

$$I_{FWD} = \sqrt{\frac{P_{FWD}}{Z_0}} \qquad \text{(Eq 2)}$$

and $V_{FWD} \times I_{FWD} = P_{FWD}$. A numerical example presented later verifies it. In addition, contrary to Steve's assertion, P_{FWD} equals the sum of the source and reflected powers,

[1]Notes appear on page 50.

243 Cranor Ave,
DeLand, FL 32720-3914
w2du@arrl.net

not the voltages, which will also be proved later. The derivation of the familiar equations for determining standing-wave voltages, *E,* along the line that Steve misinterpreted to obtain his Eqs 6, 7, and 8 can be found in Johnson,[8] Sec 4.3, pp 98 and 99.

In Steve's Eq 6 in Part 1, the expression shown below for forward voltage V_{FWD}, is invalid because the left-hand term of the equation V_{FWD} does not equal the sum of the terms on the right-hand side of the equation.

$$V_{FWD} \quad V1 + V1\left(\rho_S \rho_A e^{-2\gamma L}\right) + V1\left(\rho_S{}^2 \rho^2{}_A e^{-4\gamma L}\right) + V1\left(\rho_S{}^3 \rho^3{}_A e^{-6\gamma L}\right) + \ldots \quad \text{(Eq 3)}$$

(Steve's Eq 6)

The terms on the right-hand side of his Eq 6 yield the voltage E of the standing wave, not the forward voltage V_{FWD}. His Eqs 7 and 8 are also invalid for the same reason. So, let's demonstrate that his Eq 8 is invalid, which will also prove his Eqs 6 and 7 invalid.

$$V_{FWD} = V1\left(\frac{1}{1 - \rho_S \rho_A e^{-2\gamma L}}\right) \quad \text{(Eq 4)}$$

(Steve's Eq 8)

V1 = source voltage,

ρ_S = reflection coefficient looking back into the source, and

ρ_A = voltage reflection coefficient of the load (antenna) mismatch.

First, using a lossless line, we let $\rho_S = 1$, and $\rho_A = 1$. In this case the denominator is zero, thus $V_{FWD} = \infty$, which is an impossibility. Second, we change ρ_A to 0.5 resulting from a 3:1 mimatch at the antenna. In this case the denominator is 0.5 and $V_{FWD} = V1 \times 2$—also impossible. We will show later that under the conditions just stated, the forward voltage increase factor caused by the integrated reflections added to the source voltage is 1.1547. Therefore, the forward voltage in this case is $V_{FWD} = V1 \times 1.1547$. Consequently, we have shown that Steve's Eqs 6, 7, and 8 do not yield the correct forward voltage V_{FWD}, as he claims. They only yield the standing wave voltage E, where L in the exponent of Eq 8 specifies the position on the line.

As we'll also prove later, forward current I_{FWD} equals source current $I1 \times 1.1547$. Thus, since forward power $P_{FWD} = V_{FWD} \times I_{FWD}$, the power increase factor is $1.1547^2 = 1.3333$ when $\rho_A = 0.5$, which is a well-known result. The derivations of the voltage, current and power increase factors, which prove this treatment to be true, will also be presented.

VE9SRB's Fallacy

At the opening of his Part 3, Steve calls total re-reflection a fallacy. He states: "*…it is a misconception that total re-reflection of reflected power occurs at a match point as the result of an impedance match being established there.*"

Then, after attempting to prove total re-reflection doesn't exist, he concludes, "*…the concept of total re-reflection is inconsistent with generally accepted transmission-line theory, basic circuit theory, and network theory.*" Then from his summary, *"It was demonstrated that the concept of total power re-reflection is inconsistent with both transmission-line and circuit theories."*

On the contrary, his mathematical treatment did not demonstrate any inconsistency in the concept of total re-reflection. And an additional claim in his conclusion is also untrue: *"A total re-reflection of power at the match point is not necessary for the impedance match to occur."* His conclusion is untrue because, as we will show, without total re-reflection the impedance match would not be accomplished. Furthermore, Steve has it backward: the impedance match *results* from total re-reflection, not the other way around.

To show that total re-reflection is not a fallacy, let's first examine the implications of his Eq 2, Part 3,

$$P_{FWD} = P_{DEL} = \frac{1}{1 - k^2 |\rho A|^2} \quad \text{(Eq 5)}$$

that he states, "*… develops the relationship between delivered and forward power.*" He continues, writing: *"Eq 2 is independent of whether an impedance match occurs at the T-network input.… Eq 2 does not support the concept of total re-reflection of power when an impedance match is established at the T-network input."*

Of course it doesn't, because a vital term is missing in his Eq 2: the reflection term ρ_S, which determines the reflective condition seen by the reflected waves on return to the network input, and thus determines the amount of energy in the reflected waves will be re-reflected. Consequently, with term ρ_S missing, both the amount of re-reflection and the increase in forward power are undeterminable using his Eq 2. However, the complete *correct* equation,

$$P_{FWD} = \frac{1}{1 - k^2 |\rho_S \rho_A|^2} \quad \text{(Eq 6)}$$

derives the forward-power increase factor based on the reflection coefficients at *both* ends of a transmission system, not just at the load end. The term k^2 represents the decimal value of power lost to line attenuation, the term ρ_A represents the reflectivity of the load, or antenna mismatch, and the term ρ_S represents the reflectivity to the power in the reflected waves on their return to either the network input or the source. When $\rho_S = 0$, the reflected power is totally absorbed in the source, thus *no* re-reflection and *no* increase in forward power, as in the classical generator. On the other hand, when $\rho_S = 1$, which is the prevalent condition at both the network input and at the source when adjusted to deliver all the available power, there is *total* re-reflection and maximum increase in forward power, indicating an impedance match at the input. *Without total re-reflection there would be no match.* This issue appears to be the crux of the problem concerning total re-reflection: the wave activity that occurs at the network input, the matching point in the network. How the reflective condition $\rho_S = 1$ to reflected waves is established at the network input will be explained later while discussing the establishment of open and short circuits by wave interference.

Steve created another misconception: that the forward traveling source and re-reflected voltage waves are vectorial in nature. He asserts, **"***The forward traveling voltage in the transmission line is a complex phasor that can be written in the general form of a vector* $\mathbf{V} = x + jy = V\angle\theta$*."* Thus, citing his Eq 9, Part 3,

$$P_F = \frac{|V_1 + V_2|^2}{Z_0} \quad \text{(Eq 7)}$$

he asserts incorrectly that phasors V_1 and V_2, are added vectorially to obtain the forward power in a mismatched transmission line, where P_F = forward power, and V_1 and

V_2 are the phasors of the source and re-reflected voltages, respectively.

His Eq. 9 is an invalid expression for use on a line with re-reflections, because in a lossless line, the relative phase angles for both V_1 and V_2 are $\theta = 0°$ everywhere along the line. Keep in mind that on a lossless line, voltage and current in the forward wave are always *in phase*, while voltage and current in the reflected wave are always 180° *out of phase*. Consequently, reflected power is real, not reactive power. To be reactive, the phase relation between voltage and current would need to be other than 0° or 180°. As will be explained in the section discussing open and short circuits established by wave interference, the wave action on re-reflection brings *all* re-reflected voltages and currents into zero phase relative to the source waves, regardless of their phase relationship prior to re-reflection. Consequently, Steve's lengthy dissertation on the different values of forward power that could result from various θ angles of V_1 and V_2, and Eq 9 itself, are irrelevant. *Voltages V_1 and V_2 are never at other than 0° phase relative to the source phase at any time on lossless lines.* Although V_2 is the resultant of two reflected waves whose magnitudes are equal, with equal but opposite phase angles, phase angle θ of the *re-reflected* resultant voltage V_2 following re-reflection is always zero on lossless lines.

An additional point that Steve failed to recognize is that the addition of the source and reflected voltages establishes the standing wave, not the forward voltage, which has a constant value with zero phase everywhere along the line. So let's examine what happens when we use his Eq 9 to perform this addition.

Steve's Fig 1, Part 3 shows a 100 W, 50-ohm source feeding a T-network connected to an antenna of impedance Z_A = 150 ohms through a lossless 50-ohm, 1 wavelength transmission line. In his example, source voltage V_1 = 70.71; forward power incident on the antenna, P_{FWD} = 133.33 W; and power reflected P_{REF} = 33.33 W. For P_{FWD} = 133.33 W, the total forward voltage V_{FWD} must be 81.65 V, and with reflection coefficient ρ_A = 0.5, reflected voltage V_2 = 40.825 V. In addition, the source current is I_1 = 1.414 A, total forward current I_{FWD} = 1.633 A, and reflected current I_{REF} = 0.8165 A. Each of these values is correct; the article also states correctly that the re-reflected voltage must equal the reflected voltage.

However, Eq 9 is invalid because it states *incorrectly* that re-reflected voltage V_2 adds directly to source voltage V_1 to establish forward power—*it does not*. Steve does state correctly that the in-phase 40.825 V re-reflected voltage V_2 and 70.71 V source voltage V_1 cannot be added together such that the total voltage will be 81.65 V. Whoa! This should have been a clue that source and reflected voltages add only to establish the voltage *standing wave*, *not forward voltage* V_{FWD}, because $V_{FWD} \times I_{FWD}$ = 133.33 W. We prove his Eq 9 for forward power, P_{FWD} erroneous by showing that

$$P_{FWD} = \frac{|V_1 + V_2|^2}{Z_0} = \frac{|70.71 + 40.825|^2}{50} \quad 248.8 \text{ W} \quad \text{(Eq 8)}$$

not the correct 133.33 W. However, it must be said that Eq 9 is valid when there are *two separate and independent sources*, such as two generators. But it must also be kept in mind that the power in the reflected waves is delivered by only *one* source, the transceiver. Apparently, this anomaly, and knowing that the relationship between forward and reflected voltages is vectorial, are what led to the erroneous concept of a vectorial relationship between the forward and re-reflected voltages.

We'll now reveal the correct mathematical expression for obtaining forward power from V_1 and V_2 that proves source and reflected powers do indeed add to establish the total forward power. The universally known reciprocally related equations for determining either forward power P_{FWD} or delivered power P_{DEL} in a mismatched transmission line are:

$$P_{FWD} = \frac{|V_1|^2 + |V_2|^2}{Z_0} \quad \frac{|70.71|^2 + |40.825|^2}{50} \quad 133.3 \quad \text{(Eq 9)}$$

and

$$P_{DEL} = \frac{|V_{FWD}|^2 - |V_2|^2}{Z_0} \quad \frac{|81.65|^2 - |40.825|^2}{50} \quad 100 \quad \text{(Eq 10)}$$

where V_1 = source voltage, V_2 = reflected voltage, and V_{FWD} = forward voltage. The terms in the numerators are *power terms*, thus either of the two equations above indicates that forward power equals source power plus reflected power. Steve disagrees that forward power equals source power *plus* reflected power, so it's ironic that he somehow agrees that power delivered to the load is equal to the forward power *minus* the reflected power. See *Reflections*, Chapter 3, Eq 3-9, and Johnson,[8] p 150, Eqs 6.14 thru 6.17 for the derivation of those equations. To verify that the correct forward power is 133.33 W, we'll now use an alternate method to determine that value. Using the standard equation for calculating the forward-power increase factor from the earlier example,

$$\frac{1}{1 - |\rho_S \rho_A|^2} = 1.333 \quad \text{(Eq 11)}$$

where ρ_S = 1 and ρ_A = 0.5, with source power 100 W, we have shown that the total forward power is 133.33 W on a lossless line.

So let's carry the math in this exercise a little further to provide additional proof that the exercise has been performed correctly. From Ohm's Law, we know that when forward power on a 50-ohm line is 133.33 W, the forward voltage must be 81.65 V and the forward current must be 1.633 A. Also from Ohm's Law, when resistance is constant in a circuit, voltage equals the square root of power. So we'll now take the square root of the P_{FWD} equation to establish both the forward voltage and current increase factor,

$$V_{IF} = I_{IF} = \sqrt{\frac{1}{1 - |\rho_S \rho_A|^2}} = \sqrt{1.333} = 1.1547 \quad \text{(Eq 12)}$$

where, as above, ρ_S = 1.0 and ρ_A = 0.5. As before, source voltage V_1 = 70.71 V, and source current I_1 = 1.414 A. Thus $V_1 \times V_{IF}$ = 70.71 V × 1.1547 = 81.65 V = V_{FWD}, the forward voltage determined earlier, and $I_1 \times I_{IF}$ = 1.414 × 1.1547 = 1.633 A, I_{FWD}, the forward current. Now, V × I = P, 81.65 V × 1.633 A = 133.33 W, thus proving our case.

Note that the forward voltage V_{FWD}, 81.65 V, is an increase of only 10.94 V from the 70.71 source voltage V_1, and the forward current 1.633 A is an increase of only 0.219 A from the 1.414 A source current. However, these small increases in voltage and current represent the correspond-

ing increase in forward power from 100 W to 133.33 W, proving that it is the reflected power adding to source power that establishes the forward power, *not the addition of the reflected voltage to source voltage.*

We can now show that the steady-state forward voltage V_{FWD} *plus* the reflected voltage V_2 establishes the maximum of the voltage standing wave, (81.65 V + 40.82 V = 122.47 V), and V_F *minus* V_2 establishes the minimum of the voltage standing wave (81.65 V – 40.82 V = 40.82 V). Note also that the ratio of the max and min voltages of the standing wave is 122.47 ÷ 40.82 = 3.0, verifying that the values above are correct. We have thus disproved the assertion that adding source and reflected powers to establish the forward power is a fallacy.

Open and Short Circuits Established by Wave Interference

In another quote from Part 3 of Steve's article he asserts that open and short circuits to reflected waves *cannot* be established by the wave interference involved in impedance matching. He writes, *"For a total re-reflection of voltage, current, or power to occur at a T-network, transmission line theory requires that the physical or measurable impedance seen looking rearward into the matching network be a short circuit, open circuit or purely reactive. Since this generally would not be the case with a practical T-network impedance matching circuit, the concept of total power re-reflection contradicts this fundamental aspect of transmission-line theory."*

That is fundamentally incorrect and also disputes Slater[2] and Alford.[3] Those authors have shown that a physical short or open circuit is not what accomplishes total re-reflection of the reflected waves. Wave interference between two sets of reflected waves traveling in the same direction within a transmission line or network that are conjugately related at the matching point establish either a one-way *short* circuit or a one-way *open* circuit to the rearward-traveling reflected waves. We'll now show how two sets of reflected waves traveling in the same direction are established in the impedance-matching process, and how they also establish the one-way short or open circuit that prohibits any further rearward travel of the reflected waves, in other words, total re-reflection at the match point.

In general, the impedance-matching process involves three harmonically related traveling waves arriving at the match point: a forward wave delivered by the source (Wave 1), and two conjugately related rearward-traveling reflected waves (Waves 2 and 3) developed by two conjugately related physical discontinuities. Wave 2 is the wave reflected from a mismatched line termination that requires cancellation, and Wave 3 is the canceling wave reflected by the matching device at the match point, its input connection to the source line. Because of their conjugate relationship, Waves 2 and 3 are mirror images of each other.

First, with waves traveling in opposite directions on a transmission line, we know that reflected waves pass through forward waves unimpeded, and the interference between them establishes only a standing wave—no open or short circuits are established. However, when two sets of voltage and current reflected waves are traveling in the *same* direction and are conjugately related at the matching point in an impedance matching device, the interference between these two sets of reflected waves establishes either an open or short circuit at the matching point. Whether an open or short circuit is established depends on the boundary conditions of the mismatched load and the distance from the load to the matching point. When the match point at the normalized unity-resistance point using a *series* stub on the line occurs within the first quarter-wavelength from the load, an open circuit to reflected waves occurs at the match point when the resistive component R of load $Z_L > Z_0$. A short circuit to reflected waves occurs when the resistive component R of load $Z_L < Z_0$. The reasons for these phenomena will become clear as we proceed.

In learning how one-way open and short circuits are established through wave interference, it is helpful to first understand what happens to an electromagnetic field on encountering a physical open or short circuit. It is universally known that when an electromagnetic field encounters an open circuit, the electric field (or voltage wave) is totally reflected with 0° change of phase, and the magnetic field (or current wave) is totally reflected with a 180° change of phase. Conversely, when an electromagnetic field encounters a short circuit, the electric field (or voltage wave) is totally reflected with 180° change of phase, and the magnetic field (or current wave) is totally reflected with a 0° change of phase. *It is of vital importance to the issue of total re-reflection to understand that these relationships are reciprocally related.* Consequently, when the resultant voltage and current angles established by wave interference are 0° and 180°, respectively, an open circuit to the reflected waves is established. Conversely, when the resultant voltage and current angles are established at 180° and 0°, respectively, a short circuit to the reflected waves is established. Thus, when either an open or a short circuit is established at the matching point by wave interference between the two sets of conjugately related reflected waves traveling rearward, the direction of the voltages, currents, and energies in both sets of reflected waves is reversed. That results in total re-reflection of the reflected waves.

Let us now determine why open or short circuits are developed by wave interference. From King,[9] we know that voltage and current traveling along the line can be represented by individual generators placed at any point along the line. Those generators are called "point generators." For the purpose of analysis, a point generator is an impedance-less EMF that can represent or replace the voltage and current on the line equal to the voltage and current actually appearing at that point on the line, without disturbing the wave action on the line.

To simulate and analyze interference between two waves of equal magnitude and opposite phase traveling in the same direction, such as the two sets of reflected waves generated by the load mismatch and the stub mismatch, we can connect two point generators together in either of two different configurations. Each generator replaces the voltage and current of each individual wave at the point of interference, the match point. In the first configuration, the two generators are connected *in phase*. Because their voltages are equal and in phase, the differential voltage is zero, resulting in no current flow. This connection is equivalent to an *open* circuit between the generators. In the second configuration, the generators are connected with their terminals reversed. Their voltages are now *in opposite phase* at the interference point and the resulting voltage is the *sum* of the voltages delivered by each generator; i.e., twice the voltage of each generator. This connection results in a *short* circuit between the two generators.

Identical wave-interference phenomena establishing a short circuit also occur in free space in the same manner

as in guided-wave propagation along transmission lines. For example, when the fields emanating from two radiators in an array of antennas are of equal magnitude and 180° out of phase at a point in space, a virtual short circuit is established by destructive wave interference, resulting in a null in the radiation pattern at that point. Following Poynting's Theorem, the energy in the combined fields propagating is reversed in direction at that point; and with the constructive interference that follows, that energy adds to that in the fields propagating in the opposite direction, thus achieving gain in the that direction.

Stub matching on a mismatched transmission line provides an elegant model to illustrate the mechanism in wave interference that establishes one-way open or short circuits to reflected waves on transmission lines.[10] When placed at the matching point on the transmission line, the stub is designed to introduce a mismatch. That produces a canceling reflection having the same magnitude as the reflection from the mismatched load terminating the line, but with the opposite phase angle. The following example illustrates this condition.

Assume a lossless line of Z_0 = 50 ohms terminated in a pure 150-ohm resistance, Z_L, yielding a 3:1 mismatch for a voltage reflection coefficient ρ = 0.5. An appropriate point to place a series stub on the line is at a normalized point of unity resistance. When ρ = 0.5, the first point of unity resistance appears at 30° rearward from the load toward the generator. The line impedance at this point is 50 – *j*57.7 ohms. Traditionally, a + *j*57.7-ohm inductive reactance inserted in series with the line at this point cancels the – *j*57.7-ohm capacitive line reactance, achieving a Z_0 impedance match at this point, leaving a 1:1 flat line between the inductance and the source, and 3:1 mismatch on line between the inductance and the load. However, it makes no difference whether a series lumped inductor or a series stub, each presenting + *j*57.7 ohms, supplies the inductive canceling reactance. Either one establishes the impedance match.

But there is more occurring here than a simple cancellation of reactances. The matching process is actually performed by the mechanics of wave interference at the matching point that generates either an open or short circuit to the reflected waves, preventing them from traveling rearward past the stub point. To examine the wave action, we focus mainly on the reflection coefficients of the reflected voltage and current waves that appear at the stub point, and to a lesser extent of those at the load, as shown below, where voltage and current coefficients are indicated by V and I, respectively. The remaining nomenclature is self-explanatory.

ρ_{VLoad} = 0.5, θ = 0°
ρ_{ILoad} = 0.5, θ = 180°
$\rho_{Vline\ at30°}$ = 0.5, θ = –60°
ρ_{Vstub} = 0.5, θ = + 60° Resultant $\angle\theta_{RV}$ = 0°
$\rho_{Iline\ at30°}$ = 0.5, θ = + 120°
ρ_{Istub} = 0.5, θ = – 120° Resultant $\angle\theta_{RI}$ = 180°

Note that the magnitudes of all reflections are equal at ρ = 0.5. Note also that the voltage angles for the line and stub equal but of opposite sign, as are the corresponding current angles. In addition, note that the resultant angles of the voltage and current are θ_{RV} = 0°, and θ_{RI} = 180°, respectively. We learned from the earlier detailed discussion above, that when the magnitudes of the reflections are equal, and the resultant voltage and current angles established by wave interference are 0° and 180°, respectively, as they are in this case, an open circuit to the reflected waves is established. Consequently, the open circuit prevents any further rearward wave travel beyond the matching point—*total re-reflection*—resulting in a Z_0 match at the stub point.

An Analysis of Steve's T-Network Tuner

Refer to Steve's section, *"The T-Network Tuner,"*[1] in Part 3, where he analyzes the wave actions in a system comprising a 50-ohm, 100 W source; a lossless tuner feeding a 1.20 λ, transmission line; and a 50-ohm lossless line terminated in a 150-ohm load (the antenna). As stated earlier, the load mismatch at the antenna establishes reflection coefficient ρ = 0.5, SWR = 3:1. The line then transforms the 150-ohm load impedance to impedance Z_L = 18.213 – *j*14.237 ohms, ρ = 0.5 at the main line input connected to the output of the source. The object is to match Z_L to the 50-ohm source. However, in examining the analysis, we find errors, such as:

1) the mathematical model is inconsistent with realistic wave activity in the steady state,

2) the setup is treated using mostly initial-state conditions, not the steady state,

3) reflected voltages are added incorrectly, as described earlier, to determine forward power,

4) forward and reflected powers determined from his Eqs 5 and 6 are using either incorrect voltages or incorrect values of Z_0.

The mathematical model used in Steve's analysis begins correctly, showing 133.33 W of incident or forward power arriving at the antenna and 33.333 W reflected because of the 3:1 mismatch at the antenna. Using that model, however, his analysis shows *incorrectly* that useful re-reflection occurs at the output of the network and none at the input, while in fact, *all useful* re-reflections occur at the input, the matching point, as we will prove.

Steve's article states that on encountering reflection coefficient ρ = 0.5 at the tuner output, 25 percent (8.33 W) of the 33.333 W reflected at the antenna is re-reflected back to the antenna and 75 percent (25 W) "…[is] the level of rearward power delivered back into the T network." He further states: "… the rearward-traveling voltage delivered back into the main transmission line, V_{BACK} is –32.940 + *j*12.843 V." It is significant to note that after traveling rearward through the network, the 25 W of the 33.33 W reflected from the antenna mismatch–which *must* arrive at the network input–is totally ignored. However, Steve then writes: *"This rearward-traveling voltage is the exact negative of the reflected voltage created at the input of the T network* (+32.940 – *j*12.843 V). *Therefore the total steady-state rearward-traveling voltages within the main transmission line is 0 v. This cancellation of all rearward-traveling waves is the mechanism that causes the effective steady-state input impedance to be 50 ohms at the input to the T network."*

Cancellation of *all* rearward traveling waves? This is a huge stretch from simply canceling the reflected *voltages*. Our earlier explanation of the matching process proves that it is not that simple. Does canceling the rearward-traveling waves also cancel the energy carried in those waves? In addition to not accounting for the 25 W of reflected power, he also neglected the rearward-traveling *current*, which is a component of the 25 W that returned from the tuner output mismatch to the tuner input. Consequently, he did not incorporate the resultants of the reflection coefficients of both voltage *and current* at the network input to determine their necessary participation in the wave interference process that

accomplishes total re-reflection. Failure to consider the currents involved, and believing that re-reflection does not occur at the network input, led to an inappropriate development of the equations with erroneous results.

Now let's analyze the T network from Steve's article, using the same network parameters as shown below, but with a different mathematical model that will show that *all* re-reflections pertinent to impedance matching occur at the network input. C_1 and C_2 are the input and output capacitors, respectively.

Beginning at the input of the network, recall that the input impedance Zin = 117.810 – *j*57.061 when load impedance Z_{LOAD} = 50 ohms, verified by the equations below.

$$X_{C1} = -j269.496,\ X_L = j104.216,\ X_{C2} = -j150.146,\ Z_0 = 50$$

$$Zin \quad \frac{1}{\frac{1}{Zload + X_{C2}} + \frac{1}{X_L}} + X_{C1} \qquad Zin \quad 117.809 - j57.061$$

(Eq 13)

Initially the source delivers 100 W into impedance Z = 50 + *j*0 at the input of the main line connecting the source to the network. Source voltage V_S = 70.71 V. On encountering the initial impedance Zin = 117.809 – *j*57.06 ohms at the network input, where, ρ_{IN} = 0.466 – *j*0.182 ($|\rho|$ = 0.5, SWR = 3:1), 75 W enter the network and 25 W are reflected toward the source. The initial reflected voltage equals $V_S \times \rho_{IN}$ =32.94 – *j*12.843 V. On reaching the source, the 25 W reflected rearward from the network input creates an initial 3:1 mismatch between the source and the line input, thus reducing the initial source delivery to 75 W. On reaching the steady state the impedance at the network input changes to Z_{IN} = 50 + *j*0, thus the source returns to delivering 100 W, and the 25 W initially reflected toward the source is now transmitted through the network in the forward direction, along with the original 75 W. However, on reaching the steady state, the reflected voltage increases to 38.036 – *j*14.830 V. As explained in the earlier math example, we showed that in the steady state the forward voltage increased by the forward-increase factor 1.1547 from 70.71 V to 81.65 V. However, Steve states incorrectly that "*…the total voltage at the network input is equal to the sum of the source and reflected voltages, 103.651 – j12.843 V.*" These voltages *cannot* be added directly, as we proved earlier. However, we will also see that in the steady state the voltage reflected at the input will have increased to 38.036 – *j*14.830 V, only to be canceled later by its conjugate returning from the load mismatch as the reflected power becomes re-reflected.

Steve's account of the wave actions described in his analysis is incorrect for the same reasons that the steady-state voltage created at the network input is not +32.940 – *j*12.843, but is really +38.036 – *j*14.830. Consequently, it is evident that the voltage returning from the antenna is *not* the exact negative of what he believes is reflected at the network input. Instead, it is its *conjugate*. This same oversight also resulted in using an incorrect mathematical model of the system.

As explained earlier and in references,[2,4,6,7,9] undesired reflections from a load mismatch are canceled by the conjugately related mirror-image reflections generated by the mismatch established by the matching device; in this case, the T network. We'll now show how the conditions described above have set the stage for total re-reflection at the input of the network.

Using terminology set forth earlier, Wave 1 is the source wave, Wave 2 is the wave reflected from the load mismatch (the antenna), and Wave 3 is the canceling wave established by reflection of Wave 1 at the network input. The voltage and current of Wave 1 initially see impedance Z = 117.810 – *j*57.060 ohms at the network input, establishing reflection coefficients of Wave 3: ρ_{Vin} = 0.466 – *j*0.182 = 0.5, θ_{Vin} = –21.333°, and ρ_{Iin} = 0.5, θ_{Iin} = +158.666°, respectively. Also, on arrival rearward at the network input, Wave 2 "sees" impedance Z = 117.810 + *j*57.060 ohms, the conjugate of the impedance seen by Wave 1. Wave 2 thus establishes reflection coefficients ρ_{Vref} = 0.466 + *j*0.182 = 0.5, θ_{Vref} = +21.333°, and ρ_{Iref} = 0.5, θ_{Iref} = –158.666°. Note that coefficients of Wave 2 are mirror images, or conjugates of those of Wave 3, because the impedances appearing at the network input from opposite directions are conjugates of each other. Consequently, steady-state voltages and currents at the network input are:

Wave 2 = 38.036 + *j*14.83 V = 40.825 V, θ_{V2} = +21.3°,

Wave 3 = 38.036 – *j*14.83 V = 40.825 V, θ_{V3} =–21.3°

...resultant $\angle\theta_{RV}$ = 0°

Wave 2 = 0.7607 – *j*0.2966 A = 0.8165 A, θ_{I2} = –158.666°,

Wave 3 = 0.7607 + *j*0.2966 A = 0.8165 A, θ_{I3} = +158.666°, resultant $\angle\theta_{RI}$ = 180°.

Note that the voltage magnitudes are equal and their resultant phase θ_{VR} = 0°, while the corresponding current reflection coefficients are 180° out of phase with the voltage coefficients. The magnitudes of current are equal and their resultant phase θ_{IR} = 180°. Thus, in accordance with the principles described earlier, when resultant voltage and current phases are θ_{VR} = 0° and θ_{IR} = 180°, an open circuit to rearward traveling reflected waves is established and total re-reflection is achieved.

In general, when the equal but opposite phase angles of the two reflected voltages are between 0° and ± 90°, the resultant phases of voltage and current are θ = 0° and 180°, respectively, establishing an open circuit. Conversely, when the equal but opposite voltage phase angles θ are between ± 90° and 180°, the resultant phases of voltage and current are 180° and 0°, respectively, establishing a short circuit.

We'll now examine the reason the phases of the reflected waves change to zero for both voltage and current relative to the source waves after re-reflection. Because the resultant voltage phase at the open circuit is already at 0° prior to re-reflection, there is no change in phase of voltage on re-reflection. Thus the resultant voltage component of the powers re-reflected from both the network output and the antenna mismatch is now traveling forward in phase with the source voltage wave as part of the total forward-traveling voltage wave. Because the resultant current phase is 180° prior to re-reflection but encounters a 180° change in-phase on re-reflection at the open circuit, the resultant current component of the re-reflected powers is now also traveling in phase with the source current wave as part of the total forward-traveling current wave. Consequently, the ultimate result is that all of the power reflected at the load mismatch and transmitted rearward through the network output is totally re-reflected at the network input.

Power Loss Through Use of Steve's Eq 13

Let's now examine Steve's Eq 13, Part 3:

$$P_F \quad (\sqrt{P_1} + \sqrt{P_2})^2 \qquad \text{(Eq14)}$$

derived from his Eq 9. He used Eq 13 in the section "The T Network Tuner," with the manipulation 75 W + 8.33 W = 133.33 W, with P_1 = 75 W of source power and P_2 = 8.33 W of reflected power. Using this equation led him to overlook 50 W in his power budget, necessary to correct the error in the power equation above. Substituting P_1 and P_2 in Eq 13 does indeed yield 133.33 W, but this answer itself proves the equation invalid. The reason for this error is in incorrectly adding V_1 and V_2 as vectors with phases other than zero. So, why would such an error be made? On discovering that the sum of the in-phase re-reflected and source voltage waves did not yield the correct forward voltage, 81.65 V, he evidently assumed that the two voltage waves must then be added vectorially to obtain the correct 81.65 V. Had he considered that forward voltage and current travel in phase on a lossless line, thus making both V_1 and V_2 travel at zero phase, the analysis likely would have come right.

Continuing the discussion concerning the missing 50 W mentioned above, we'll now examine what happened to the 25 W that reached the network input (at –32.940 + *j*12.843 V, Steve asserts) after traveling rearward from the network output. This brings us directly to the cause of the

It's a Real Rat Race!

Here is a specific circuit example that may surprise some of you. It proves that a physical discontinuity is not necessary to achieve open and short circuits in transmission lines.

One of the gems of all transmission-line circuitry is the ring diplexer, also known as a hybrid ring or "rat race." See Fig 1. Its apparent magic is traditionally used to isolate two signal sources closely related in frequency that deliver power into dual loads. It uses only wave interference to obtain isolation between the sources. It seems like magic because wave interference is established in the diplexer with no physical discontinuities anywhere. It is an elegant way to drive crossed dipoles to obtain circular polarization (CP) by simply adding baluns at the terminals of the dipoles, plus an additional λ/4 line section in one of the two lines. Right-hand CP is developed from one transmitter and left-hand CP from the other.

Observe that the diplexer comprises nothing more than a continuous loop of transmission line having four terminal ports: two inputs (A and C) and two outputs (B and D). Note that both lines AB and BC on the left-hand side are λ/4 in length, for a total of 180°; on the right-hand side, line AD is l/4 and line DC is 3λ/4, for a total length of 360°. The differential line length between the two sides is therefore 180°, which is the desired number to obtain isolation between the two sources. Here is how it works.

Current induced by voltage applied at A splits at A and travels to C along both sides of the diplexer, through B and D. Because of the 180° difference in length between the two sides, equal voltages arrive at C 180° out of phase, establishing a short circuit at C. The reverse is true also: Current induced by voltage applied at C travels to A in a similar manner, where two equal voltages from C arrive at A 180° out of phase, thus establishing a short circuit at A. Consequently, the short circuit at C prevents current from A from entering the source at C; similarly, the short circuit at A prevents current from C from entering the source at A.

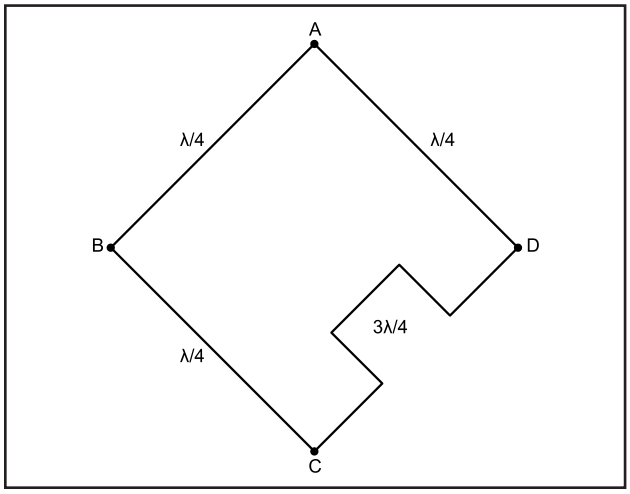

Figure 1—Ring diplexer configuration.

With Z_0 loads placed at B and D, current applied at A will enter both loads, but will not enter lines BC and DC (except in the amount required to overcome resistive loss to maintain the short circuit at C). Similarly, current applied at C will enter both loads but will not enter lines BA and DA (except enough to maintain the short circuit at A). Why? Here's where the apparent magic continues.

Observe that the lengths of all the lines are odd multiples of a quarter wavelength, λ/4 and 3λ/4. Short circuits have been established at both A and C. Terminated in a short, lines whose lengths are odd multiples of λ/4 see an open circuit at their input terminals. Consequently, in traveling to loads at B and D, current from A sees an open circuit looking into lines BC and DC because of the short circuit at C. Similarly, in traveling to loads B and D, current from C sees an open circuit looking into lines BC and DC because of the short circuit at A. Consequently, there are two open circuits looking in opposite directions from both B and D. With the open circuits at B and D between A and C, in tandem with the short circuits at A and C, we have two frequency-dependent sections providing mutual isolation between A and C.

In practice, the degree of isolation depends on the exactness of line lengths and the uniformity of the dielectric constant of the insulating material. By measurements of diplexer circuits I've fabricated in stripline printed-circuit boards, with Teflon/Fibreglass as the insulating material, I've obtained 40 dB of isolation between A and C at high-band VHF.

In systems where the source and load impedances both equal Z_0, the characteristic impedance Z_{0DL} of the diplexer lines must account for the parallel circuitry at the source ports. Therefore,

$$Z_{0DL} \quad \sqrt{2Z_0^2} \qquad \text{(Eq 15)}$$

Thus, where Z_0 = 50 ohms, Z_{0DL} = 70.7 ohms, which allows two parallel 100-ohm line inputs at both A and C to present a 50-ohm load to the sources.

So it's not really magic but just simple wave mechanics that establish open and short circuits without any physical discontinuities. Neat, eh? *W2DU*

error concerning the missing 50 W. In Steve's example, the power source initially delivers 100 W into impedance Z = 50 + *j*0 at the input of the line connecting the network to the source. Repeating earlier statements for convenience, on encountering the initial impedance Z = 117.81 – *j*57.06 ohms at the network input, where, ρ = 0.5, there are 75 W transmitted through the network and 25 W reflected toward the source. Note that the voltage reflected at the network input is 32.94 – *j*12.843 V, the negative of the voltage he claims arrived rearward from the network output. On reaching the source, the 25 W reflected rearward from the network input creates an initial 3:1 mismatch between the source and the network input, thus reducing the initial source delivery to 75 W. However, on reaching the steady state, the network input impedance has changed to $Z_{IN} = 50 + j0$; thus the source again delivers 100 W, and the 25 W initially reflected toward the source is now re-reflected in the forward direction at the network input. This is the first 25 W of the missing 50 W that Steve overlooked.

Further, observe that although the values are incorrect, the voltage initially reflected rearward from the network input appears to be the exact negative of the voltage at the input in his model because of the rearward-traveling 25 W returning through the network. Seeing this relationship, he reached the incorrect conclusion because these voltages appeared to cancel and there could be no further rearward travel of voltage into the source line. In the steady state, the 25 W initially reflected rearward from the network input toward the source actually becomes re-reflected forward at the input, and the 25 W that traveled rearward through the network is also re-reflected forward at the input. Those two 25-watt packets of power comprise the 50 W of power overlooked. That is why he considered the source was delivering only 75 W, where he states, *"The fact that the forward source power is 75 W, rather than 100 W, is significant in correctly interpreting the steady-state conditions and the relationship between the total steady-state forward and re-reflected powers."* We earlier proved the above statement to be untrue, and that Steve's Eq 13 is invalid when there is only a single source. We have also proven that in the steady state, the source is delivering 100 W; and we have also found the missing 50 W.

Conclusion and Acknowledgements

To conclude, we have exposed, analyzed, and corrected certain misconceptions, proving that claims that material appearing in *Reflections* is incorrect are unfounded. I want to thank George Baker, W5YR, and James Reid, KH7M for their support on this article.

Notes

[1]S. R. Best, VE9SRB, "Wave Mechanics of Transmission Lines, *QEX,* Part 1, Jan/Feb 2001, Part 2, July/Aug 2001, Part 3, Nov/Dec 2001.

[2]J. C. Slater, *Microwave Transmission,* McGraw-Hill, New York, pp 58-60, 1943, (Chairman, Dept of EE, MIT.)

[3]A. Alford, "Broad-Band Antennas", *Very High-Frequency Techniques*, Radio Research Laboratory, Harvard University, McGraw-Hill, New York, pp 10-15, 1947.

[4]W. Maxwell, W2DU, *Reflections*, Chapter 3, Sec 3.1, 1990.

[5]W. Maxwell, W2DU, *Reflections II*, Chapter 3, Sec 3.1, and Chapter 23, 2001.

[6]W. Maxwell, W2DU, "Examining the Mechanics of Wave Interference in Impedance Matching, *QEX*, Mar/Apr 1998, and Chapter 23, Reflections II.

[7]W. Maxwell, W2DU, "Another Look at Reflections," Part 4, *QST*, October 1973.

[8]W. C. Johnson, *Transmission Lines and Networks,* McGraw-Hill, 1950, Pages 98, 99 and 150, Eq 6.17.

[9]R. W.P. King, Professor of Physics, Harvard University, *Theory of Transmission Lines,* McGraw-Hill, 1955, and Dover Publications, 1965, pp 244 and 464.

Walt's first membership in the ARRL was in 1928, and he has been a Life Member of both the ARRL and QCWA since 1968. He is a Fellow in the Radio Club of America. Licensed as W8KHK in 1933, and continuously licensed since then for 71 years, he held the Advanced Class from 1939 to 1967, when he earned the Extra Class license. Later call signs, W8VJR, W2FCY, and then W2DU in 1968. He was also trustee of the original Boy Scout station, K2BSA. He entered Central Michigan University in 1935 and earned a BS degree in math and physics.

After obtaining 1st Class Radio Telephone and 2nd Class Radio Telegraph licenses, and while baby-sitting BC station WMFJ, Daytona Beach, FL in 1940, with no teletype yet available he copied the news for broadcast from Press Wireless WCX/WJS at 38 wpm.

He engineered antennas at secondary FCC monitoring stations and was a Navy instructor of aviation radio technicians during WW2. Following the war, and a few years as an AM broadcast engineering consultant, he joined the RCA Laboratories, Princeton, NJ, as an engineer in its antenna laboratory. He was a charter engineer at RCA's newly created Laboratories' spinoff, the Astro-Electronic Division, designer and manufacturer of government sponsored spacecraft, also at Princeton.

Walt designed and directed, hands-on, the five VHF ground stations spanning from Cape Canaveral to California, supporting the orbiting Atlas rocket of Project SCORE, carrying the World's first repeater in space. He also designed all antenna systems that flew on the World's first weather satellite, TIROS I, and continued through the VHF antennas on TIROS M (9). Walt invented a 56 dB VHF helical resonator notch filter weighing 7.8 oz, used in TIROS and other satellites. He also designed the antennas that flew on ECHO 1 and 2.

Walt was chief engineer of RCA-Astro's antenna lab until his retirement to Florida in 1980. His 1970's R&D research into more than 1,000 configurations of the quadrifilar helix antenna led to the use of VHF and UHF quadrifilars on all TIROS-N and all now flying as NOAA polar-orbiting weather satellites. His R&D report on the quadrifilar helix antenna research can be viewed in his book, Reflections—Transmission Lines and Antennas II, and can also be downloaded from his web page at **http://home.iag.net/~w2du**.

Walt's hobbies include experimenting in his own well-equipped RF lab, technical writing, photography, performing on string bass in big bands and small jazz groups, Florida boating, and global cruising with his wife, Jean. □□

Resistance—The Real *Story*

A brief discussion of resistance in electronics

By Doug Smith, KF6DX

Background

One of the first things neophytes learn in electronics is Ohm's Law, $R=V/I$, where V is voltage, I is current and R is resistance. What they typically do not learn until later is that Ohm's Law is not a perfect description under all conditions. Further, resistance can be defined in at least two ways—1) a thing that opposes current flows in a conductor and 2) the characteristic impedance of a transmission line or that of free space.

I shall try to show that those two definitions are in perfect harmony and that they are just different ways of expressing the same concept. I begin with a third, rather unusual definition at which we arrive by examining other electrical units.[1]

Postulate 1: Resistance is Time Divided by Distance

You may be thinking, "How is he going to prove that?" Well, it is reasonably straightforward given an understanding of how conduction currents work. In Reference 1, E. M. Purcell explains it quite well. Here is my try at it.

Model

Current in a circuit is a measure of how many charged particles pass the measurement point per unit time. For instance, one coulomb of charge passing in one second is one ampere. Charged particles like free electrons within a conductor move when electromotive force (EMF or voltage) is applied to the circuit. That is because the presence of voltage implies the presence of an electric field, E; and each charge q experiences force qE.

An electron has mass and by Newton's Law, $F=mA$, it should experience a constant acceleration $A=qE/m$ under the influence of a constant force qE. Why then does a constant EMF produce a net electron flow having constant velocity instead of constant acceleration?

Ohmic resistance can be traced to elastic collisions and encounters among electrons and other particles found in a conductor. Electrons repel each other because of their identical charges. It is not strictly right to say the particles collide in the sense of coming in actual contact, but particle physicists tend to use that term. Constant force qE does indeed accelerate electrons, and for an unchanging EMF or dc applied voltage, the force is always in one direction.

Conduction electrons usually cannot travel far before encountering other electrons and particles in a conductor. Free electrons in a room-temperature conductor are bopping around quite rapidly because of thermal effects. At 293° C above absolute zero (room temperature, or 293 K), an electron's thermal velocity is many orders of magnitude higher than that of ordinary current flows. In a good conductor, collisions caused by thermal motion are vastly more frequent than those caused by applied EMF.

Since the direction of recoil after an elastic collision is random, collisions tend to interfere with the desired net current flow. It is just a kind of friction. Some of the momentum acquired by charge carriers from the applied field is essentially transformed to heat—just more random bopping around of electrons and ions in the conductor.

In other words, because it takes almost no energy to mobilize electrons in a good conductor, they do zip around at incredible speeds because of their thermal (kinetic) energy; but under the influence of an applied EMF, they do not get far before being influenced by other charged particles that, in effect, make them *forget* where they were going. When I set up a current in a wire, forgetful electrons tend to oppose that current. A description of mobile electrons bopping around inside a conductor is in fact based on the ideal gas laws.

It follows that we can find an average distance, d, for electron travel between collisions in a conductor and thus an average travel time between collisions, t, based on temperature. Thus resistance is related to both time and distance.

To look at this another way, consider that resistivity can be expressed as the ratio of field strength to current density. The practical unit of resistivity is the ohm × cm, because electric field strength is in volts/cm and current density is in amperes/cm^2. The ratio is (volts/cm)/(amperes/cm^2) = (volts/amperes)(cm)=ohm × cm.

Field strength can also be expressed as charge/cm^2. Since current is charge/s, surface current density is (charge/s)/cm^2. Now the expression for resistivity becomes (charge/cm^2)/(charge/cm^2–s) = s! The impractical unit for resistivity is the second and therefore the units for resistance are s/cm. It turns out that 1 ohm≈1.14×10^{-12} s/cm.

To take a real example, Cu at room temperature exhibits a resistivity of about 1.9×10^{-18} s in those impractical units; in practical units, that is about 1.7×10^{-6} ohm-cm. Knowing the density of Cu and assuming each atom yields one conduction electron, we can compute average time t between collisions. Knowing the mass of an electron, its charge, and estimating its thermal

[1]Notes appear on page 53.

225 Main St
Newington, CT 06111-1494
kf6dx@arrl.org

velocity from ideal-gas theory allows calculation of the distance, d between collisions.

Eq 1 (from References 1 and 3), which follows from the foregoing discussion, yields average time t between collisions:

$$t \quad \frac{m_e}{\rho N e^2} \qquad \text{(Eq 1)}$$

where m_e is electron mass in grams, ρ is resistivity in seconds, N is the density in cm^{-3} and e is the charge of an electron in esu. Crank in room temperature numbers for Cu from the ITT book[2] and get $t \approx 2.4\times10^{-14}$ s—not much time! To see why Eq 1 produces a result in seconds from such a hodgepodge of other units, see the Sidebar.

Kinetic theory tells us that electron thermal velocity at room temperature is around $v=10^7$ cm/s. Compare that with a 0000 AWG Cu wire carrying 1000 A dc, in which the net current flow amounts only to several cm/s—little more than a snail's pace—and you get an idea why thermal motion is so important in resistance. Distance d between collisions is $vt \approx 2.4\times10^{-7}$ cm or 24 Å. That is perhaps eight or nine atomic spaces in the Cu crystal lattice. It is interesting that an electron can go even that far before a collision, since Cu is rather dense as metals go and the atoms are in rather close proximity in the lattice. Note that not all those collisions we are talking about are head-on. They occur at every possible angle.

This sort of billiard ball theory of resistance is fine as far as it goes, but really quite a bit more is involved in conduction models for metals. Still, it allows one to see how charge carriers, having acquired momentum from an applied field, lose their way because of collisions or near encounters and some of the momentum goes to heat. Higher conduction currents do begin to increase the number of collisions and the quantity of heat produced, of course.

The theory also predicts a relaxation time: the average time taken for current to cease once the E field has been removed. Physicists have shown that the relaxation time is within a factor of two of the mean time between collisions, t.

Materials continuously absorb and radiate energy. It is the movement of atomic particles that makes it happen because that is the measure of heat. The reason for the known correlation between that part of the spectrum in which maximum radiation transfer occurs and temperature can also be traced directly to t. Were you to heat a fireplace poker in a kiln, it would glow—dull red at first. As it got hotter, the glow would shift from red to orange to yellow, indicating ever shorter wavelengths of emission. (The term color temperature, expressed in kelvins, is related to that.) Particle velocity would be increasing, and both t and d decreasing; but not necessarily at the rate that holds resistance t/d constant. Particle velocity approaches a limiting value because, among other effects, the increasing frequency of collisions tends to damp their motion. Almost all known metals and alloys exhibit increasing resistivity with increasing temperature, but materials such as graphite go the other way! So clearly something is missing from the billiard ball theory. I will not go into it further here, though, because it gets rather complex as you bring in quantum mechanics and I do not understand it all yet.[3]

Ohm's Law holds as long as thermal velocity is large with respect to velocities attained through applied EMF. We expect it to break down when the applied force is enough to accelerate electrons to velocities approaching the thermal velocities. As shown, however, that would involve millions of amperes in a reasonably small wire and I do not believe that has ever been tried in a successful (read flameproof) experiment. We can state that Ohm's Law is really just a special case wherein V/I just happens to be very nearly equal to R.

Postulate 2: Measured Resistance Always Implies Conversion of Energy

For the impedances of electrical circuits, the conventional notation is $R+jX$, where R is the real or resistive part and X is the imaginary or reactive part. I say that any measured electrical circuit impedance having a positive, nonzero, finite real part R implies the existence of a real resistance somewhere that converts energy from one form to another. More specifically, that conversion implies the transformation of energy from the momentum of charge carriers to another domain. In the case of ohmic resistors, the conversion is to heat; for antennas and light emitting devices, the conversion is to electromagnetic radiation.

Model

As explained above, ohmic resistance involves elastic collisions among particles. Energy put into an ohmic system as EMF is transformed to thermal energy because of the random nature of the angles of particle collisions.

In the case of antennas, a transformation between kinetic energy and radiation energy occurs. Acceleration of electrons in a conductor produces changing electromagnetic fields that escape before they have a chance to oppose the changing currents that created them. Resistive conversion of energy in radiative systems is known as radiation resistance. In light-emitting diodes and certain other devices, energy conversion may involve phenomena that are not treated here. Conservation of energy requires a resistive explanation for all those effects, though.

A resistance defined as the ratio V/I is an absolute implication of a real resistance somewhere. From Ohm's Law, the presence of voltage V cannot produce real current I without a resistance R. Therefore, any resistance measured in a circuit not involving radiative effects must be associated with an ohmic resistance, which converts electrical energy to heat.

Special cases occur in the propagation of radio waves along a transmission line and in free space. A transmission line exhibits a characteristic resistance that fixes the ratio V/I of ac waves traveling in it. In the steady state, one end of a finite, lossless transmission line would not present an impedance having a finite, nonzero resistive part unless its other end were terminated in a load impedance having a resistive part. In the transient state, before waves reflect from the distant end of a long, lossless transmission line, the line would present a resistance equal to the line's characteristic resistance.

An electromagnetic wave propagating in a vacuum may be said to experience a characteristic resistance like that of a transmission line. The resistance is the ratio of the electric field strength in V/m to the magnetic field strength in A/m. Theory and measurement reveal the characteristic resistance of free space to be $120\,\pi$ or about 377 Ω. Where is the implication of a real resistance that converts forms of energy?

In each case, the kinetic energy of moving charged particles has been converted to energy stored in electromagnetic fields. A transmission line propagates waves because of the continual transfer of energy between electromagnetic fields in and around its conductors and the mobile charge carriers in the conductors. In a vacuum, continuous energy transfer takes place between electric and magnetic fields. *Displacement current* in a vacuum gives rise to magnetic fields in the same way moving charges do. Displacement current in a vacuum is not the movement of actual charge, but

Mass of an Electron and the Mean Time Between Collisions in a Conductor

Perhaps the most famous equation ever, $E=mc^2$, tells us the exact relation between mass and energy. Given that an electron has charge and charge gives rise to an electric field, it follows that part or all of an electron's observable mass is contained in its electric field. To find the mass equivalent of the energy in an electron's field, we have to integrate the energy over all space where the field exists—to infinity. We want to use variable E to represent the electric field, so let us use variable U to represent energy.

At a point some distance r from an electron with charge e, the magnitude of the electric field is:

$$E \quad \frac{e}{r^2} \tag{A1}$$

It has been shown that the energy in an electric field is directly proportional to the square of the field strength. Further, the energy in any volume element dv at some non-zero distance from an electron with charge e is:

$$dU \quad \frac{E^2}{8\pi=}dv \quad \frac{e^2}{8\pi\mp^4}dv \tag{A2}$$

For a sphere of radius r, volume is:

$$v \quad \frac{4\pi\mp^3}{3} \tag{A3}$$

It is convenient to use r as the variable of integration, so we express dv in terms of dr

$$\frac{dv}{dr} \quad 4\pi r^2 \tag{A4}$$

$$dv \quad 4\pi\mp^2 dr$$

and we are ready for our integration. We shall integrate from an arbitrarily small radius r_0 to infinity:

$$U \quad mc^2 \quad \frac{1}{8\pi\mp}\int_0^{\infty}\left(\frac{e^2}{\mp^4}\right)\left(4\pi r^2\right)dr$$

$$\frac{e^2}{2}\int_{r_0}^{\infty=} r^{-2}dr \tag{A5}$$

$$\frac{e^2}{2r_0}$$

Solving for m yields:

$$m \quad \frac{e^2}{2r_0c^2} \tag{A6}$$

Note that were $r_0=0$, mass would be infinite. Since no one knows how to measure the radius of an electron unambiguously, we can only take its measured mass and compute a radius r_0. That would be the so-called classical electron radius, which turns out to be about 2.8×10^{-13} cm or 2.8×10^{-5} Å. But Eq A6 yields only half that radius. What gives? The answer is that an electron also has a magnetic field because of its spin and that is where the other half of the energy (mass) resides.

At any rate, we were interested in how all that jibes with Eq 1's result in units of seconds. Substitute the modified Eq A6 for mass into Eq 1 and get:

$$t \quad \frac{\left(\frac{e^2}{r_0c^2}\right)=}{\rho\mp Ne^2} \quad \frac{1}{r_0c^2\rho\mp N} \tag{A7}$$

Taking the units of each variable does indeed make a result in seconds:

$$s \quad \frac{1}{(cm)\mp\left(\frac{cm}{s}\right)^2=(s)\left(cm^{-3}\right)} \tag{A8}$$

its effects are virtually identical.

What is this displacement current? In a vacuum, it is just the rate of change of the electric field, or dE/dt. Although its magnetic-field equivalent dB/dt does not have a special name, it gives rise to electric fields just as the displacement current gives rise to magnetic fields.

Superposition Holds in Linear Systems Everywhere

Again, the real part of the ratio V/I is an implication of an actual resistance R somewhere. The establishment of that ratio at a signal source does not necessarily mean the source resistance is R or any function of R. It certainly indicates some conditions about the load.

In linear systems such as radio-frequency transmission lines, voltages and currents combine linearly as waves travel along them. No individual wave can affect another except to add or subtract linearly. The same is obviously true for electromagnetic waves traveling in free space.

Notes

[1]E. M. Purcell, *Electricity and Magnetism*, McGraw-Hill, New York, 1965.

[2]*Reference Data for Radio Engineers*, 5th Ed, Howard W. Sams & Co, Indianapolis, 1975.

[3]*Encyclopaedia Britannica*, "Electricity and Magnetism," pp 231-242, 15th Ed, Chicago, 1989. □□

Book Reviews

The Radioman's Manual of RF Devices

by Harold Kinley, WA4GIB, Noble, Atlanta, 2004, ISBN 1-884932-45-2; 315 pp, hardcover, list price $94.00

This book concentrates not on discrete RF devices such as diodes and transistors, as you might infer from the title, but on test equipment and other RF accessories. It begins with definitions of basic units of measure such as those used for voltage and power ratios (the decibel), electric field strength and power density. A discussion of impedance and impedance transformations follows, accompanied by a step-by-step explanation of how to use a Smith chart to design passive networks, both with and without *winSmith* software. The software is not included with the book.

The majority of the book covers RF measurement tools and accessories. The author aptly uses plentiful examples and equipment screen prints to make clear how to use a spectrum analyzer, RF millivoltmeter, SINAD meter, directional wattmeter and so forth. He shows the need for such accessories as attenuators, combiners, splitters, directional couplers and the like; he illustrates how they are constructed and what makes them tick.

In the last portion, the author covers certain practical issues that are in play in many radio installations, such as site noise and receiver "desense." He brings in devices such as cavity filters, isolators and circulators, focusing in large part on what happens when many transmitters and receivers are co-located. The book's final chapter deals with transmission lines and antennas. Readers would do well to read the segment on transmission lines before the chapter on Smith charts, rather than waiting until the last.

The Radioman's Manual of RF Devices is perfect for the technician who has a good background in electronics but wants to learn the fundamentals of RF instrumentation and measurement. It will not show him or her how to solder a coax connector; but it will demonstrate why an average-reading wattmeter indicates about 40% of the peak envelope power in a two-tone, how to calculate path loss, and how to find the electrical length of a transmission line. The book uses a minimum of mathematics. It is an excellent practical guide for the journeyman hobbyist or professional who requires a quick start into the world of RF measurement and analysis. We recommend it highly for that purpose.

Harold Kinley has over 30 years of experience in two-way radio systems. He is the author of at least two other books as well as articles in *Popular Electronics* and *Mobile Radio Technology*, among other magazines. He holds an Amateur Extra Class license and is an ARRL member—*Doug Smith, KF6DX, QEX Editor.*

Newnes Guide to Radio and Communications Technology

by Ian Poole, Elsevier Limited, Oxford, 2003, ISBN 0-75065-612-3; list price $24.99

In this brand new volume, Ian Poole begins with a fine introduction to radio, suitable for almost all readers. He explains about the history and development of the art from the work of Gilbert and Faraday onward. He attributes Maxwell with the prediction of radio waves that travel at the speed of light and the first proven radio transmission to Hertz. He puts Marconi's role in its proper perspective—as a developer.

Marconi's alleged transatlantic reception of three dits—the letter S—late in 1901 is not questioned. It seems to us that any scientifically minded individual should question it. Edouard Branly, who invented the coherer used in the experiment to detect the signals, is not mentioned. Also unmentioned are Lord Kelvin, Lord Rayleigh, Einstein, Hall, Schockley, Bardeen or Brattain, among others along the timeline of developmental events throughout the years.

Despite those omissions, the book is an excellent way for neophytes to step into radio and learn something about it. It begins with the basics and gradually brings in more advanced concepts. Propagation modes, modulation (including spread spectrum), antenna systems and the basis of superheterodyne receivers are all covered in quite some detail, along with circuit specifics. Transmitters are also covered, with analysis of standard FM, SSB and AM methods. No DSP-centric information is included.

The remainder of the book discusses broadcasting, including digital audio broadcasting, cellular, satellite and short-range wireless communications. We recommend it as an addition to the technical libraries of intermediate-level technical readers. It is an interesting read, even for the advanced engineer—*Doug Smith, KF6DX, QEX Editor.* □□

Antenna Options: A Yagi Case Study Part 1—Design Options

By L. B. Cebik, W4RNL

Introduction

"This antenna is the best thing since sliced bread." Such is too often the claim made for antennas by individual builders and commercial makers alike. I'll bet those who make this and similar claims have not stopped to consider that for many meals, sliced bread is exactly the wrong bread to serve. I know a nice little restaurant that serves excellent soups in freshly baked bread bowls. I would not eat there if they tried to serve the soup in sliced bread.

So it is, too, with antennas. For any general application, we have options. Only when we evaluate those options against our specific requirements and our situational limitations can we decide on the best antenna for the circumstances. Notice that the result is not simply "the best antenna." It is the best antenna for the given job and the conditions under which it will have to do that job.

Since I cannot know every circumstance in which amateurs set up antennas, I cannot say what the best antenna is for any amateur activity. I can, however, use the space that *QEX* has allotted to me to discuss some options and alternatives for specific tasks. In small spaces, I cannot cover every possible option and certainly not all of the details that attach to each option. However, I can (hope to) begin a thinking process that may ultimately let you make the best final decisions for yourself. The options that I have in mind are not brand A vs brand B commercial offerings. I do not have the appropriately rated test range for this kind of discussion. Instead, I shall look at options among antenna types, antenna construction, matching systems and so forth that one might face in deciding what to build.

In virtually all areas of antennas, there are facets of design and performance that we easily overlook, and many of them have an important place in our decision-making processes. To make the process even more concrete, let's look at the myriad of options that attach to a seemingly simple case study that I call *A Tale of Three Yagis*.

Yagi arrays require the antenna-builder to make three major decisions on the way from idea to reality:

1. What design is best?
2. What material is best for the elements?
3. What assembly method is best?

These three questions ultimately rest on another: What are the uses, purposes, or goals for the antenna? How all of these questions interrelate is part of the motivation for this set of notes.

To keep our work confined within a space that we can control, I shall examine only 2 m Yagis. Within that space, I shall further assume that the user will take the antenna into the field for one or more of a variety of portable operations. To make matters even simpler, I shall restrict the discussion to 3-element Yagis with 30-inch boom lengths or less.

Even with these restrictions, we still have design choices. We may select a narrow-band, high-gain design to maximize potential for point-to-point com-

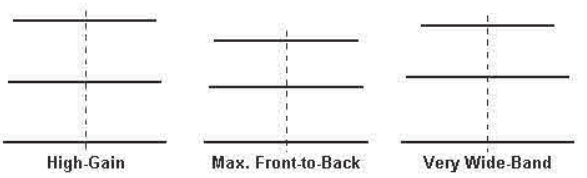

Fig 1—Relative proportions of the three 3-element Yagi designs based on 3/8 inch diameter elements.

Table 1
High-Gain Yagi Dimensions for Round Elements

Dimensions: L = Element half-length—double the L-value to obtain the full element length. Dimensions in inches—multiply by 25.4 to obtain dimensions in millimeters.

El. Dia.	*Ref L*	*Dri L*	*Dir L*	*R-Dr Sp*	*R-Dir Sp*
0.125	20.24	19.33	18.25	13.24	27.50
0.1875	20.18	19.23	18.08	13.34	27.51
0.25	20.00	19.15	17.90	13.95	28.10
0.375	19.95	18.97	17.66	14.30	28.25
0.50	19.88	18.85	17.43	14.40	28.35

1434 High Mesa Dr
Knoxville, TN 37938-4443
cebik@cebik.com

munications. Alternatively, we may select a design with a very high 180° front-to-back ratio (F/B) for direction-finding uses. Finally, we may select a design that covers the entire 2-m band with an exceptionally low 50-ohm SWR. For each design, there are trade-offs that we shall examine along the way.

Once we select a design, we need to select the material for the elements. If we choose to use rod or tubing for the elements, we may simply optimize the design for the element diameter we wish to use. In fact, the design information provided in the tables will cover most common 2-m rod and tubing sizes. However, my e-mail regularly poses questions about the use of non-standard materials, such as flat stock, L-stock, whips, and tape. Therefore, we shall spend a bit of time looking at a technique for determining what adjustments we might have to make for some of these materials. I shall provide some data that emerged from my own use of these techniques, but the techniques themselves will be your better guide to handling materials that I have not imagined.

Finally, we shall look at a few methods of overall assembly that are suitable for the element material, the overall size of the antenna, and the intended use. For such a short boom, there is no reason to avoid a non-conductive boom. In most cases, the choice will be between PVC and Fiberglass, with PVC being easier to find and somewhat more versatile.

In the end, these notes are just a sample of a thought process you can and should extend to other bands, other designs, and other operating purposes.

Part 1: The Three Yagi Designs

The first step in our *Tale of Three Yagis* is to describe the Yagis themselves. There is a high-gain, narrow-band version, a maximum F/B version, and a very wide-band version. A papa bear, mama bear, and chubby baby bear analogy in these characterizations is likely not accidental.

For each antenna design, the tables will provide detailed dimensions for a variety of element diameters from 1/8 up to 1/2 inch, in readily available rod and tube sizes. The material may be aluminum (recommended for its light weight and strength), brass, or copper. The performance figures are based upon aluminum, although changing the material will not alter the performance in any detectable way.

The tables also provide performance data from *NEC-4* models at the design frequency. All designs attempt to achieve a minimum of 20 dB F/B across the listed passband. The particular design, however, will reveal variations of where within the operating passband the maximum F/B occurs. All 3-element Yagi designs show a gradual increase in gain across the operating passband.

Fig 1 shows the relative proportions of the three Yagi designs, using the 3/8 inch diameter element versions as the basis for the sketch. The high-gain version has nearly equal spacing between elements and an almost uniform taper

Table 2
High-Gain Modeled Performance at the Design Frequency

Performance at 144.5 MHz

El. Dia. (Inches)	*Free-Space Gain(dBi)*	*Front-to-Back Ratio(dB)*	*Feed Impedance (R±jX ohms)*	*25-ohm (SWR)*
0.125	8.23	24.61	24.73–*j*0.77	1.033
0.1875	8.27	24.63	24.15–*j*0.57	1.042
0.25	8.31	24.64	24.65+ *j*0.30	1.019
0.375	8.31	24.71	24.77–*j*0.65	1.028
0.50	8.31	24.67	25.06–*j*0.04	1.003

Table 3
High-Gain Modeled Performance at the 1-MHz Operating Passband Edges

Passband Edge Performance: Values are free-space gain (dBi) / 180-degree F/B (dB).

El. Dia.	*144*	*145*
0.125	8.17 / 26.32	8.30 / 22.04
0.1875	8.21 / 26.40	8.34 / 22.17
0.25	8.24 / 24.48	8.37 / 23.29
0.375	8.25 / 25.23	8.38 / 23.10
0.50	8.25 / 25.06	8.38 / 23.30

Table 4
25-ohm SWR Performance

El. Dia.	*144*	*145*	*146*
0.125	1.19	1.14	1.61
0.1875	1.17	1.15	1.59
0.25	1.12	1.17	1.58
0.375	1.15	1.11	1.47
0.50	1.12	1.12	1.45

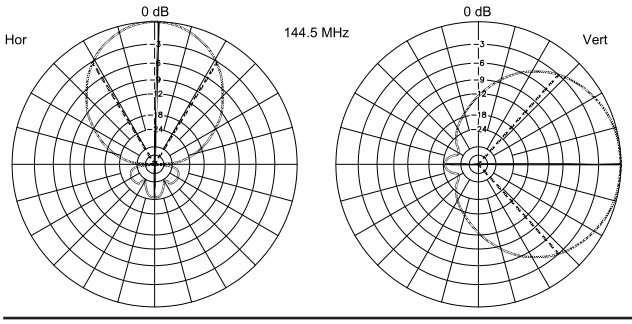

Fig 2—High-gain 3-element Yagi—typical horizontal and vertical patterns. Dashed lines are at –3 dB.

Table 5
Maximum F/B Yagi Dimensions for Round Elements

Dimensions: L = Element half-length—double the L-value to obtain the full element length. Dimensions in inches—multiply by 25.4 to obtain dimensions in millimeters.

El. Dia.	*Ref L*	*Dri L*	*Dir L*	*R-Dr Sp*	*R-Dir Sp*
0.125	20.21	18.78	18.02	11.79	23.85
0.1875	20.20	18.64	17.82	12.09	24.10
0.25	20.18	18.51	17.64	12.49	24.50
0.375	20.11	18.32	17.42	13.09	24.90
0.50	20.06	18.16	17.21	13.39	25.10

of the elements. The departure of the spacing and taper from uniformity is essential to achieving the performance. The maximum 180° F/B design preserves a similar driver-reflector structure, but shortens the length and spacing of the director to achieve the deep rear null. Both antennas have a feed-point impedance near 25 ohms. The very wide-band version requires a 50 ohm feed-point and therefore widens the reflector to driver spacing. Note also the relatively short director.

144.5 MHz High-Gain 3-Element Yagi

The high-gain Yagi is designed for maximum gain with a reasonable boom length and modest bandwidth. It will cover about 2 MHz of the 2-m band if the design frequency is moved from 144.5 MHz to 145 MHz. However, its present design recognizes that most point-to-point activity is in the first MHz of the band. So the design frequency is set at 144.5 MHz. Within the first MHz, the SWR is less than 1.2:1 for any listed element diameter. Although horizontal operation is the norm for the low part of 2-m, the antenna is equally operable horizontally or vertically.

The feed-point impedance is resonant at about 25 ohms. This arrangement is intentional to avoid the need for excessive mechanical connections at the antenna proper. A ¼ λ section of RG-83 (35-ohm) or a parallel section of RG-59 (or similar 75-ohm) coax will provide a match to the 50-ohm main cable. Cut the section for 144.5 MHz, allowing for the cable's specific velocity factor. Alternatively, one may modify the design to shorten the driver so that it shows about 25 ohms of capacitive reactance. Then, a hairpin or gamma match becomes applicable.

It is not possible to let the maximum F/B of the high-gain, narrow-band design coincide with the design frequency for all element diameters. The smaller the element diameter, the more likely the maximum F/B is to fall below the design frequency. However, the F/B exceeds 22 dB from 144 to 145 MHz for all versions of the design.

Table 1 provides dimensions for the design using round elements from ⅛ inch up to ½ inch in diameter. Table 2 shows the modeled free-space performance at the design frequency, 144.5 MHz, for each size material. Simplified values for the edges of the 1 MHz operating passband appear in Table 3, while Table 4 suggests the usable operating bandwidth with 25-ohm SWR values at 144, 145, and 146 MHz. If the builder uses a ¼ λ matching section for a 50-ohm coaxial

Table 6
Maximum F/B Yagi Modeled Performance Across 2-m

0.125 inch Diameter Elements.

Freq. (MHz)	*Free-Space Gain (dBi)*	*Front-to-Back Ratio (dB)*	*Feed-point Z R±jX (ohms)*	*50-ohm (SWR)*
144	7.60	20.23	72.49+*j*11.74	1.519
145	7.66	26.36	62.15+*j*4.33	1.260
146	7.74	50.67	50.92–*j*0.30	1.019
147	7.84	26.42	39.62–*j*1.78	1.266
148	7.97	20.14	29.34–*j*0.38	1.704

0.1875 inch Diameter Elements.

Freq. (MHz)	*Free-Space Gain (dBi)*	*Front-to-Back Ratio (dB)*	*Feed-point Z R±jX (ohms)*	*50-ohm (SWR)*
144	7.61	21.34	69.70+*j*10.70	1.459
145	7.67	27.61	60.42+*j*4.18	1.226
146	7.75	54.07	50.28–*j*0.01	1.006
147	7.85	26.89	39.98–*j*1.48	1.254
148	7.98	20.80	30.44–*j*0.46	1.643

0.25 inch Diameter Elements.

Freq. (MHz)	*Free-Space Gain (dBi)*	*Front-to-Back Ratio (dB)*	*Feed-point Z R±jX (ohms)*	*50-ohm (SWR)*
144	7.62	22.01	68.20+*j*10.91	1.435
145	7.68	28.25	59.77+*j*4.83	1.220
146	7.76	52.26	50.47+*j*0.79	1.018
147	7.86	27.61	40.92–*j*0.90	1.223
148	7.98	21.51	31.91–*j*0.30	1.567

0.375 inch Diameter Elements.

Freq. (MHz)	*Free-Space Gain (dBi)*	*Front-to-Back Ratio (dB)*	*Feed-point Z R±jX (ohms)*	*50-ohm (SWR)*
144	7.65	22.96	67.13+*j*9.41	1.399
145	7.72	29.33	59.22+*j*3.58	1.199
146	7.80	51.05	50.35–*j*0.29	1.009
147	7.90	27.90	41.19–*j*1.91	1.219
148	8.02	21.97	32.52–*j*1.37	1.540

0.5 inch Diameter Elements.

Freq. (MHz)	*Free-Space Gain (dBi)*	*Front-to-Back Ratio (dB)*	*Feed-point Z R±jX (ohms)*	*50-ohm (SWR)*
144	7.66	23.34	65.90+*j*8.24	1.364
145	7.72	29.42	58.47+*j*2.95	1.180
146	7.81	56.80	50.17–*j*0.60	1.012
147	7.90	28.96	41.60–*j*2.14	1.209
148	8.02	22.82	33.41–*j*1.76	1.500

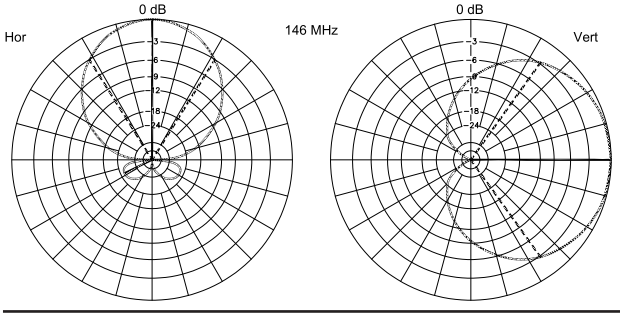

Fig 3—Maximum F/B 3-element Yagi—typical horizontal and vertical patterns. Dashed lines are at –3 dB.

feed line, the 50-ohm SWR at the junction of the matching section and the main feed line will be similar. Fig 2 shows free-space E-plane and H-plane patterns for the array at the design frequency. These patterns replicate the pattern shapes when the antenna is used over ground in the horizontal and vertical positions, respectively.

The charts show clearly that the bandwidth for any particular characteristic tends to increase with an increase in element diameter. However, note that each increase in element diameter requires a change in element spacing as well as element length to sustain the performance curves over the 144-145 MHz passband. Most of the change in element spacing occurs with respect to the driver and reflector, since this spacing, relative to a given element diameter, largely determines the feed-point impedance of the array, once we have set the performance values with the spacing and length of the director.

To change the design frequency, scale both element lengths and element spacing. Take the ratio of the old (144.5 MHz) frequency to the new frequency and multiply or divide all dimensions in the tables by the result. If the scaling is within the 2-m band, no element diameter adjustment is necessary. If the frequency ratio is greater than about 1.2:1 or less than 0.8:1, then element diameter scaling is necessary to retain the performance characteristics.

146 MHz Maximum F/B 3-Element Yagi

The applications for a high-gain design are obvious. A maximum F/B design has more limited application, for example, in the field of Amateur Radio direction finding. The antenna should have sufficient gain to locate the desired signal and a sufficiently sharp and deep rear null to provide a reliable bearing toward the target transmitter. Although the horizontal pattern for any parasitic beam will include rear quartering lobes, the vertical pattern will show a clear single null. Most direction-finding activities use vertical polarization.

I have set the design frequency for the maximum F/B at 146 MHz, because there is no absolute standard for direction-finding frequencies. However, for operation within the 2-m band, one may scale the dimensions according to previously given principles without concern for scaling the element diameter. However, for scaling outside the limits of the 2-m band, one should also scale the element diameter.

Table 7
Very Wide-Band Yagi Dimensions for Round Elements

Dimensions: L = Element half-length—double the L-value to obtain the full element length. Dimensions in inches—multiply by 25.4 to obtain dimensions in millimeters.

El. Dia.	*Ref L*	*Dri L*	*Dir L*	*R-Dr Sp*	*R-Dir Sp*
0.125	20.80	19.23	17.25	13.79	26.00
0.1875	20.45	19.17	17.15	14.80	26.50
0.25	20.44	19.16	17.05	15.60	27.00
0.375	20.42	19.15	16.90	17.10	28.05
0.50	20.46	19.15	16.80	18.10	28.60

Table 8
Very Wide-Band Yagi Modeled Performance Across 2-m

0.125 inch Diameter Elements.

Freq. (MHz)	*Free-Space Gain (dBi)*	*Front-to-Back Ratio (dB)*	*Feed-point Z R±jX (ohms)*	*50-ohm (SWR)*
144	6.93	18.84	49.77–*j*9.65	1.213
145	6.93	19.51	50.09–*j*5.01	1.105
146	6.96	19.96	49.97–*j*0.25	1.005
147	7.00	20.16	49.43+*j*4.69	1.100
148	7.06	20.07	48.49+*j*9.87	1.224

0.1875 inch Diameter Elements.

Freq. (MHz)	*Free-Space Gain (dBi)*	*Front-to-Back Ratio (dB)*	*Feed-point Z R±jX (ohms)*	*50-ohm (SWR)*
144	7.10	18.16	49.78–*j*8.88	1.195
145	7.11	19.73	49.92–*j*4.88	1.103
146	7.13	21.26	49.58–*j*0.72	1.017
147	7.17	22.61	48.80+*j*3.67	1.081
148	7.23	23.48	47.61+*j*8.35	1.195

0.25 inch Diameter Elements.

Freq. (MHz)	*Free-Space Gain (dBi)*	*Front-to-Back Ratio (dB)*	*Feed-point Z R±jX (ohms)*	*50-ohm (SWR)*
144	7.09	18.49	51.18–*j*7.89	1.171
145	7.11	20.05	50.93–*j*4.17	1.088
146	7.14	21.64	50.26–*j*0.24	1.007
147	7.19	23.16	49.20+*j*3.95	1.085
148	7.25	24.21	47.77+*j*8.45	1.196

0.375 inch Diameter Elements.

Freq. (MHz)	*Free-Space Gain (dBi)*	*Front-to-Back Ratio (dB)*	*Feed-point Z R±jX (ohms)*	*50-ohm (SWR)*
144	7.08	19.10	52.56–*j*7.34	1.163
145	7.11	20.67	51.75–*j*3.87	1.087
146	7.15	22.36	50.61–*j*0.13	1.012
147	7.22	24.07	49.15+*j*3.92	1.084
148	7.29	25.29	47.41+*j*8.31	1.195

0.5 inch Diameter Elements.

Freq. (MHz)	*Free-Space Gain (dBi)*	*Front-to-Back Ratio (dB)*	*Feed-point Z R±jX (ohms)*	*50-ohm (SWR)*
144	7.04	19.78	52.58–*j*7.78	1.173
145	7.09	21.40	51.40–*j*4.92	1.096
146	7.14	23.20	49.95–*j*0.76	1.015
147	7.22	25.10	48.24+*j*3.23	1.078
148	7.30	26.42	46.30+*j*7.58	1.191

Although not radically finicky, the maximum F/B frequency for a Yagi design is a narrow-band phenomenon. Hence, one should construct the antenna for the frequency of intended use. As the performance tables will show, the F/B decreases steadily off frequency until the design shows no distinct null. However, the design has sufficient gain and F/B to make it a useful performer for other purposes.

The feed-point impedance for this design is set for about 25 – *j*25 ohms. The models all use an identical shorted transmission line stub across the feed-point to simulate a hairpin match. Hence, the SWR curves are for 50 ohms. The modeled feed-point resistance is actually close to 27 ohms, and the required inductive reactance of the hairpin is 54 ohms. You may construct a U-shaped hairpin for the antenna by calculating the characteristic impedance for the spacing and wire diameter used. Then the length follows standard shorted-transmission line equations found in *The ARRL Antenna Book*, Chapter 24. A normally good construction method for the hairpin is to choose a distance between the parallel lines that is equal to the spacing between the driver terminals.

As an example, AWG #14 wire (0.0641 inch diameter) has a 400-ohm characteristic impedance at a center-to-center line spacing of 0.901 inch. A shorted stub or hairpin made from this line would need to be 1.73 inch long to achieve 54 ohms inductive reactance at 146 MHz. The final adjustment requires care, since the terminal structure at the feed-point normally introduces some reactance that may add to or subtract from the amount provided by the hairpin. Lower characteristic impedances yield longer stubs for the same reactance. Narrowing the line spacing or fattening the conductor will lower the characteristic impedance. The goal is a hairpin that is short enough to be sturdy in field use but not so short as to make the final feed-point adjustment too finicky.

If you build this design for its intended purpose, general field adjustment also requires care. Contrary to most received wisdom, the reflector is not chief source of the F/B in the design. The reflector is relatively insensitive and serves primarily to establish the feed-point impedance by virtue of its length and spacing from the driver. The most sensitive element relative to establishing the ideal F/B will be the director. The director length will be more sensitive than its spacing from the driver, although both dimensions deserve the label "sensitive."

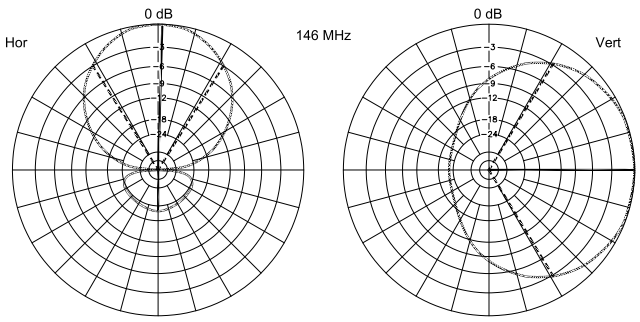

Fig 4—Very-wide-band 3-element Yagi—typical horizontal and vertical patterns. Dashed lines are at –3 dB.

Table 5 provides dimensions and Table 6 supplies performance values based on *NEC-4* models for element sizes ranging from $^1/_8$ inch to $^1/_2$ inch. In all of the designs in these notes, the dimension values presume a non-conductive boom or the use of mountings that insulate and isolate the elements from the influences of a conductive boom. See "Scaling and Adjusting VHF/UHF Yagis" at my Web site for notes on adjusting element lengths for insulated through-boom construction (**www.cebik.com/scales.html**). However, for boom lengths under 30 inches or so, and for direct-feed drivers, there is little reason to use a conductive boom.

The performance values show the increasing performance—although very gradually increasing—as we increase the element diameter and also adjust both element length and spacing to optimize performance for each new element size. This clear picture emerges largely because the design aligns the design feed-point impedance and the maximum F/B at the same frequency. The only performance figure for which variations make no difference is the 146 MHz F/B—I ceased optimizing when this value exceeded 50 dB.

Fig 3 shows free-space E-plane and H-plane patterns, which replicate the patterns you will obtain when using the antenna in a horizontal or vertical orientation, respectively. Over ground, expect the vertical pattern to have less gain but a wider beamwidth than the horizontal pattern. However, when used vertically, the rear quadrants will show a single deep, sharp null.

146 MHz Very Wide-Band 3-Element Yagi

The third design stresses smooth performance over the entire 2-m band with a 50-ohm SWR of less than 1.2:1. The design achieves this goal by using a variation of a W6SAI design from the 1980s, modified for 2-m and for the full range of rod and tube diameters. Although the gain is about a full dB less than the high-gain model, the wide-band Yagi will provide roughly equal performance anywhere in the band. Thus, it is fit for flipping from horizontal to vertical and back again as we change to and from point-to-point and FM repeater operations.

The Yagi uses a direct 50-ohm feed-point with no matching network required—although common mode current suppression measures are advisable. The need to establish the SWR curve as the primary design goal has consequences as we increase the element diameter. The F/B shows improvement with each larger element, but the low end of the band does not quite make the 20 dB level. Very quickly in the sequence, the gain ceases to increase with increasing element diameters. Although not clearly apparent in the performance figures, both the peak gain and the peak F/B occur at ever higher frequencies. Above the smallest element size, the peak F/B occurs above the upper end of 2-m.

Nevertheless, the very wide-band 3-element Yagi is a true general utility antenna for use anywhere in the band. Table 7 provides the dimensions for elements ranging from $^1/_8$ inch to $^1/_2$ inch in diameter. Table 8 supplies the modeled performance figures. Fig 4 gives the shape of patterns when we use the antenna horizontally and vertically. All previous notes about scaling this antenna to other frequency bands are applicable with the very wide-band Yagi.

The very wide-band version of the 3-element Yagi completes the family of designs that we shall consider. Other variations may be possible, but these three cover the major performance parameters with which amateurs are most concerned: gain, F/B, and operating or SWR bandwidth. One might further optimize the designs, but the level of optimizing used here gets the most out of each design that we can for each size element. The next step—assuming that one of these designs will meet an operating need—is deciding upon the element material. We shall explore those options next time. □□

Tech Notes

A "LIGHTHOUSE" PROTOCOL FOR RANDOM MICROWAVE CONTACTS

By Nickolaus E. Leggett, N3NL
1432 Northgate Square, Apt 2A
Reston, VA 20190-3748
n3nl@arrl.net

In routine HF and VHF operations, operators set up a contact by sending out a general call and listening for a response. This process of random calling and responses is part of the basic appeal of Amateur Radio communication. You never know for sure whom you will be talking to and there are always a variety of stations to be worked.

This approach of random contacts works because at these frequencies, antennas have fairly low gain, and so a general call covers a large area and a variety of active stations who can respond.

This situation does not hold in the Amateur Radio microwave bands. In these bands, the antennas have very high gains and the transmitted beams are very narrow. The radio waves transmitted are like light from a searchlight or flashlight. This makes it very difficult to establish random contacts like those enjoyed in the rest of Amateur Radio. The operators do not know where to point the beam to call CQ.

In conventional microwave communications, additional VHF radios are used to coordinate the microwave communication allowing the operators to schedule and plan microwave calls. This article proposes a protocol for microwave operation that will allow the microwave station to do the calling.

Lighthouse Operation

This protocol is based on a rotating antenna system operating like a low-RPM version of a radar antenna. In the call setup phase of a contact, the antenna rotates while the amateur station sends out CQ calls and listens for responses. When another microwave station responds and is heard, the rotation stops and a contact is carried out. Aviators will recognize a similarity to a radar station interrogating a remote transponder. This lighthouse protocol can be carried out manually or it can be completely automatic, using digital microwave stations.

Manual Lighthouse Operation

In manual operation, the antenna is rotated slowly as the operator sends short CQ calls with listening periods for replies between them. The rotation rate selected is a function of the beamwidth of the antenna and the length of the calls. Wide beamwidth antennas can be rotated relatively rapidly and still be able to pick up replies. Narrow beamwidth antennas must be rotated very slowly because the narrow beam quickly turns away from areas where prospective ham stations are located.

If your antenna has a beamwidth of one degree, it takes 360 slices to make up a full circle around the horizon. If it takes 20 seconds to call CQ and listen for a reply, then it would take 7200 seconds to call CQ in every direction around the horizon. This is a period of 120 minutes or 2 hours. Such a slow rate of searching for contacts is why microwave operators use VHF coordinating stations.

However, if you use an antenna beam width of 10°, it takes only 36 slices to make a full circle around the horizon. If it still takes 20 seconds to call CQ and listen for a reply, it would take 720 seconds to call CQ in every direction. This period is only 12 minutes. We are moving toward a more practical process that is closer to that on the lower Amateur Radio bands. Indeed, a diligent operator could use this lighthouse approach to search for other ham stations. If fast contest-style calls were used, even more time could be shaved off the process. For example, five-second periods of calling and response result in 180 seconds (3 minutes) to call in every direction. Using a tape device to send your call once each five seconds and to time the listening periods would facilitate this process.

Automatic Digital Lighthouse Operation

We can shorten the calling period by using automatic digital call-request packets and responses. Each packet is a short sequence of bits containing the calling station's call sign and a sequence indicating that a contact is requested. This call packet can be quite short. For example at 8 bits per character, only about 50 to 100 bits would be required to form the call request packet. A similar length packet could be used to reply to a call.

Using a slow transmission rate of 300 bits per second, one of these packets could be sent in a third of a second. At a rate of 1 Mbits per second, one packet could be sent in about 100 microseconds. This rapid transmission rate would allow one or more call request packets to be sent in each directional slice with long periods of listening between them. A microwave station calling CQ could use an antenna revolving at a fairly rapid rotational rate.

Responding Stations

The responding microwave station could also be using a rotating antenna of its own. In this case, contact would be established when the two rotating antennas are looking at each other. The lighthouse protocol would include a requirement that each station would always start its antenna rotation at a random azimuth bearing. This requirement would prevent the antennas from revolving synchronously with them never pointed at each other.

After Contact is Established

When a call request packet is received, the receiving station stops its antenna rotation. It sends a reply packet at that azimuth bearing. Upon receiving the reply packet, the sending station stops its antenna rotation and the contact is carried out along a fixed microwave path for point-to-point communication.

Refinements of the Protocol

This type of protocol can be applied to an arc pattern instead of a full circle. This alternative can be applied in mountain valleys where a full-circle rotation wastes time and call request packets.

If only a few microwave stations are active in an area, the calling station can be programmed so that it calls only on the bearings pointing at the known licensed stations.

Suggestions for Further Development

Extensive use of the Amateur Radio microwave frequencies depends on a protocol that supports traditional random contacts established using the microwave station itself. This protocol can be developed to allow our microwave bands to become fully populated.

Advanced amateurs may wish to design, build and use an electronically controlled phased-array system instead of a physically rotating antenna. □□

Letters to the Editor

A 200-W Power Amplifier (Jan/Feb 2004)

Doug,

Carl, K9LA, has noted that 0.15 nH is awfully small for the input inductors L3 and L4 in the Taniguchi 40-m amplifier. He suspected, rightly, that they should be 0.15 µH coils. The marked part number is TKENS T1045 00429, which allowing for a slight nomenclature change, is a 0.15 microhenry part from TOKO, as shown by Digikey.—*73, Kent Potter, KC6OKH, California Institute of Technology, 1200 E. California Blvd., Pasadena, CA, 91125;* **potter@caltech.edu**

Various (Jan/Feb 2004)

Dear Editor,

I was pleased that [this] issue of your excellent magazine included articles concerning simple items of test equipment and also a long overdue treatise on the pitfalls encountered in the intermodulation testing of HF receivers. With reference to inductance testing, I would like to extol the virtues of having a well-calibrated variable capacitor on hand. That, together with the procedure for the measurement of Q outlined in *Experimental Methods in RF Design*, p 7.36, will reveal both the Q and the inductance of the tuned circuit using a spectrum analyzer (preferably with tracking generator). Should a spectrum analyzer not be available, a signal generator and counter together with an AD8307-based power meter could be used. The necessary calculations can be simplified using a programmable pocket calculator.

For too long now, amateur technicians and engineers have given us this idea of "rogue" mixers to explain the anomalous behavior exhibited by some mixers under IMD test conditions. I too have been concerned with my inability to get good, consistent, IP3 results at lower two-tone testing powers. Klaus Eichel's article has given me a fresh impetus to have another go at the problem. I need only concern myself with IP3s in the region of +27 dBm. I am using oscillator output stages with a 2N5109/2N5160 complementary pair, each of which yields +23 dBm output power. Properly terminated low-pass filters (LPFs) precede a 40-dB [isolation] combiner. Another terminated LPF in the combined output brings the power to –2 dBm for each tone. My test set will be completed with a receiver using a +23 -dBm mixer and three low-cost crystal filters in the IF. If that doesn't do the trick, I'll give up!—*73, Colin Brock, G3ISB/DJØOK, Keusgasse 21, 52159 Roetgen, Germany*

RF (May/June 2004)

Dear Doug,

The following comments were suggested by Zack Lau's article in the May/June 2004 *QEX*. They do not criticize anything in the article, but rather comment on the efficiency of stacking where the lower antenna is a less effective single radiator than the upper.

Consider two similar horizontal Yagis stacked on a tower h ft. high and separated by s ft. If the upper Yagi excites 1 unit of voltage in a distant antenna, the lower Yagi might be expected to excite a lesser voltage, say c ($\leq$1) units. In free space c=1 and both Yagis should be equally driven. But if c is small what should be done? There are three possibilities: 1) drive only the upper Yagi, 2) drive both Yagis equally (the usual stacked array) or 3) drive the two Yagis with unequal powers. The third option includes the other two as special cases. The problem is then to determine the optimum division of power between the two Yagis. Assume both are matched, and that their respective currents are 1 and x (powers 1 and x^2). The stacking gain, i.e. the amount by which the pair's signal exceeds the lower's, is then:

$Gx=(1+cx)^2 / (1+x^2)$

It is easy to show that Gx is maximized by $x=c$, and that this optimum is:

$Go=1+c^2$

The stacking gain for equally driven Yagis is (x=1) :

$Ge=(1+c)^2 / 2$

A comparison of the three options for various values of c is shown in the following table, all values being in decibels:

c(db)	Go(db)	Ge(db)
0	3.01	3.01
-1.16	2.47	2.45
-2.50	1.94	1.85
-3.01	1.76	1.63
-6.02	0.97	0.51
-7.66	0.69	0
-12.04	0.51	-1.07
-inf	0	-3.01

The first line corresponds to free space, the last to the case where there is no signal in the distant antenna from the lower Yagi. Note that if c<0.414 the usual stacking design actually results in a loss, not a gain.The above calculations seem to show that the most important factor in increasing the stacking gain is increasing c. What does c depend on, and how close to 1 can it be made?

In the simple propagation model of the stacked Yagis and the distant receiving antenna above a flat earth:

$c=1-s/h$

To get a more physical picture of the amounts involved, the following table relates the stacking gains to the height of the upper Yagi instead of c. These are all for s=10 ft and correspond to the 2nd, 3rd and 5th lines of the first table (all values again in dB):

h	Go	Ge
80 ft	2.47	2.45
40 ft	1.94	1.85
20 ft	0.97	0.51

Why not raise the lower Yagi, making s smaller (c larger)? A common answer is that making s less than a certain value causes the capture areas of the two Yagis to overlap too much. This is intuitively satisfying and it gives a simple estimate of the minimum spacing in terms of wavelength and Yagi gain:

$0.358wg^{-0.5} \geq s$

where w is the wavelength in the same units as s and h, and g is the power gain of each Yagi.

A more accurate way to calculate s is to choose a spacing that minimizes the mutual radiation resistance of the two Yagis. This could conceivably result in more than 3 dB stacking gain. The formulas given above assume zero mutual radiation resistance, but a more general theory is known and not too complicated. Still more efficiency would be gained if the two stacked Yagis are designed as a pair at an optimum spacing distance.

If anyone is at all interested I'd be glad to supply more details and references.

73 de Art Laemmel, W2MIV, 4 Oak Lane, Northport, NY, 11768, **ael@rama.poly.edu**

Doug,

On page 59, left column, 3rd line from bottom you reference Table 3. The context is: "You use the same brass and

aluminum tubing sizes, just longer lengths. The measured return loss is shown in Table 3." But going to Table 3 on page 57, that is titled "Power Divider made from RG-11 and UHF Connectors". I believe it should have referred to Table 4 on page 58. There is no other text reference to Table 4 in the article that I can find.

Again on page 59, center column on the 13th line, you reference Table 2. The context is: "For instance, according to Table 2 the optimum frequency is 151 MHz." Looking at Table 2, it appears to me that the optimum frequency should be around 145 MHz. or so. Am I looking for the wrong "optimum" thing in the table?

If you ever have need to republish the drawings (and by the way, the whole article is quite valuable!), may I suggest you position the top array (array 1) of 3A and 3B the same. You can get same appearance by taking 3B and doing a 180 degree rotation on it, relabeling the new top one of 3B as array 1. It would then not introduce an additional visual reversal of phase. Only array 2 in both the A and B parts would be different from each other and show your intended point much better.—*73, Don Jackson, AE5K, PO Box 859, Yellville, AR, 72687;* **don1103@azark.com**

Don,

One of my intended points was to show how tricky it is to get the phasing right—that it is far too easy to put something that looks okay but is 180 degrees out of phase. You are right that the first reference should be to Table 4 instead of Table 3. The second reference should be to Table 3 or Table 4 instead of Table 2.—*73, Zack Lau, W1VT,* QEX *Contributing Editor* □□

Next Issue in QEX/Communications Quarterly

In the Sep/Oct issue, Jim Hall, W7TVI, and Tony Barrett, N7MTZ, bring us their design for a pocket APRS transmitter. It weighs only a few ounces, runs from a small, inexpensive battery and opens a world of possibilities for experimenters. The unit should be attractive to those who can't justify the cost of a separate transceiver to do APRS-based position tracking for hiking, biking, snowmobiling, ballooning and other activities. It mitigates much of the complexity of interfacing an APRS encoder to external transceivers. Check it out! □□

Electronics Officers
Needed for U.S. Flag Commercial Ships Worldwide

Skills required: Computer, networking, instrumentation and analog electronics systems maintenance and operation.
Will assist in obtaining all licenses.

Outstanding pay and benefits.

Call, Fax or e-mail for more information.

ARA-MEBA, AFL-CIO
Phone: 504-831-9612
Fax: 775-828-6994
arawest@earthlink.net

NATIONAL RF, INC.

VECTOR-FINDER
Handheld VHF direction finder. Uses any FM xcvr. Audible & LED display.
VF-142Q, 130-300 MHz $239.95
VF-142QM, 130-500 MHz $289.95

ATTENUATOR
Switchable, T-Pad Attenuator, 100 dB max - 10 dB min BNC connectors
AT-100, $89.95

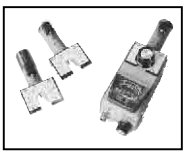

DIP METER
Find the resonant frequency of tuned circuits or resonant networks—ie antennas.
NRM-2, with 1 coil set, $219.95
NRM-2D, with 3 coil sets (1.5-40 MHz), and Pelican case, $299.95
Additional coils (ranges between 400 kHz and 70 MHz avail.), $39.95 each

DIAL SCALES
The perfect finishing touch for your homebrew projects. 1/4-inch shaft couplings.
NPD-1, 3 3/4 × 2 3/4 inches 7:1 drive, $34.95
NPD-2, 5 1/8 × 3 5/8 inches 8:1 drive, $44.95
NPD-3, 5 1/8 × 3 5/8 inches 6:1 drive, $49.95

S/H Extra, CA add tax

NATIONAL RF, INC
7969 ENGINEER ROAD, #102
SAN DIEGO, CA 92111

858.565.1319 FAX 858.571.5909
www.NationalRF.com

ATOMIC TIME

1010 Jorie Blvd. #332
Oak Brook, Il 60523
1-800-985-8463
www.atomictime.com

Office School Clock #1
WT-3121A $39.95>
This wall clock is great for an office, school, or home. It has a professional look, along with professional reliability. Features a manual set option, daylight saving time disable option, and a safe plastic lens and case.

Atomic Digital Wristwatch
<H15U $34.95
A high tech digital wristwatch with a sophisticated look. Features a metal link band, 12/24 hr time formats, backlight, date, and day of week.
Use coupon code: H15U34

Arcron Atomic Watch
<56G24-4 $249.99
This elegant watch features a shock-resistant titanium case with hardened mineral lens. Silver dial with arabic numerals, and high quality replaceable leather band. Watch can change to any world time zone. Case diameter 40mm. Made in Germany.

1-800-985-8463
www.atomictime.com

^LaCrosse Digital Wall Clock $34.95
This digital wall / desk clock comes with a beautiful cherry wood frame. It shows time, date, day of week, temperature and moon phase. 12/24 format.

Tell time by the U.S. Atomic Clock -The official U.S. time that governs ship movements, radio stations, space flights, and warplanes. With small radio receivers hidden inside our timepieces, they automatically syncronize to the U.S. Atomic Clock (which measures each second of time as 9,192,631,770 vibrations of a cesium 133 atom in a vacuum) and give time which is accurate to approx. 1 second every million years. Our timepieces even account automatically for daylight saving time, leap years, and leap seconds. $7.95 Shipping & Handling via UPS. (Rush available at additional cost) Call M-F 9-5 CST for our free catalog.

EZNEC 3.0

All New *Windows* Antenna Software by W7EL

EZNEC 3.0 is an all-new antenna analysis program for Windows 95/98/NT/2000. It incorporates all the features that have made ***EZNEC*** the standard program for antenna modeling, plus the power and convenience of a full Windows interface.

EZNEC 3.0 can analyze most types of antennas in a realistic operating environment. You describe the antenna to the program, and with the click of the mouse, ***ENZEC 3.0*** shows you the antenna pattern, front/back ratio, input impedance, SWR, and much more. Use ***EZNEC 3.0*** to analyze antenna interactions as well as any changes you want to try. ***EZNEC 3.0*** also includes near field analysis for FCC RF exposure analysis.

See for yourself

The ***EZNEC 3.0*** demo is the complete program, with on-line manual and all features, just limited in antenna complexity. It's free, and there's no time limit. Download it from the web site below.

Prices – Web site download only: $89. CD-ROM $99 (+ $3 outside U.S./Canada). VISA, MasterCard, and American Express accepted.

Roy Lewallen, W7EL *Phone:* ***503-646-2885***
P.O. Box 6658 *fax:* ***503-671-9046***
Beaverton, OR 97007 *e-mail* ***w7el@eznec.com***

http://eznec.com

ARRL CCEP
Certification and Continuing Education Program

where hams learn more…Online!

Register Online! www.arrl.org/cce

There's no better time to improve your skills.

Online Classes are Available Now through the ARRL Certification and Continuing Education Program. Complete 100% of your training via the Internet:

- **Self-paced (asynchronous) format**—you attend class when and where you want.
- **High quality web experience** enhanced with graphics, audio, video, hyper-linking and interactive modules.
- **Online Mentoring**. Individually assigned instructors help advance each student toward successfully completing the course material.
- **Pre-register Now!** Classes open regularly.

Available Courses

Antenna Modeling...EC-004


Author: L B Cebik, W4RNL (left)
Editor: Dean Straw, N6BV (right)

In the last decade the science of modeling antennas using computer software has advanced by huge leaps and bounds. While some absolutely unique, brand-new antenna designs have resulted from computer studies, the real progress has been in our understanding of how even common, ordinary antennas work. Consider how our understanding about even a garden-variety antenna like a dipole has significantly been enhanced with modern modeling programs—especially over wide frequency ranges.

Computer modeling has allowed us to optimize a number of types of antennas more exotic than a simple dipole. A modern Yagi is an especially shining example of how computer modeling can be used to optimize coverage over previously unheard of bandwidths. The science of "stacking" Yagis vertically to enhance desirable performance characteristics is another area of great interest to modelers, particularly contesters and DXers. The influence of nearby structures, including other antennas, on the patterns of our antenna systems is another exciting area of study.

Despite the large of amount of science used to model antennas, a certain amount of "art" is still needed. It is, in fact, not difficult to construct computer models that don't even come close to resembling reality! There are subtle things to avoid, as well as straightforward things you should do every time to make sure your model is adequate.

ARRL's on-line **Antenna Modeling Course** is an excellent way to learn the ins and outs and the nitty-gritty details of modeling antennas. The course was written by the well-known author and historian L B Cebik, W4RNL, and edited by ARRL Senior Assistant Technical Editor—and antenna guru—Dean Straw, N6BV. Cebik, a computer-modeling expert, has combined the expertise of his long career as a college professor with his love of antennas and antenna modeling to offer a comprehensive, yet practical, course of study. **Member: $85 / Non-member: $115**

Antenna Design and Construction…EC-009

Students become familiar with antenna design theory and experience hands-on construction techniques. The course includes several optional antenna construction projects for HF, VHF, and UHF. Authored by *QST* Contributing Editor, H. Ward Silver, NØAX.
Member: $65 / Non-member: $95

HF Digital Communications…EC-005

Understanding HF digital Amateur Radio communications and developing awareness and stronger skills for many HF digital modes. **Member: $65 / Non-member: $95**

Level 1 Amateur Radio Emergency Communications…EC-001

Introduction to Amateur Radio Emergency Communications. A basic course to raise awareness and provide additional knowledge and tools for any emergency communications volunteer.
Member: $45 / Non-member: $75

Level 2 Amateur Radio Emergency Communications…EC-002

Intermediate Amateur Radio Emergency Communications. A more in-depth study into amateur radio emergency communications to enhance the skills and knowledge received from previous experience. Requires prior completion of EC-001.
Member: $45 / Non-member: $75

Level 3 Amateur Radio Emergency Communications…EC-003

Advanced Amateur Radio Emergency Communications. Bridging the gap between basic participation and leadership. Requires prior completion of EC-001 and EC-002.
Member: $45 / Non-member: $75

Radio Frequency Interference…EC-006

Learn to identify sources and victims of interference. Tips and suggestions for solutions and for handling those ticklish problems that crop up with difficult neighbors and other aggrieved parties. Tools to help foster ingenuity, intuition, and determination for solving interference problems.
Member: $65 / Non-member: $95

VHF/UHF—Life Beyond the Repeater…EC-008

An introduction to Internet linking, amateur satellites, direction finding, APRS, weak signals, VHF contesting, microwaves, amateur television, and high speed multimedia radio. Great for both the newly licensed and more experienced hams.
Member: $65 / Non-member: $95

Technician License Course…EC-010

The course prepares students to earn their first Amateur Radio license. There are no prerequisites. Individually assigned online mentors assist students as they advance toward successfully completing the course. Registration includes the ARRL book, *Now You're Talking!* and online graduate support.
Member: $99 / Non-member: $139

Online courses are produced by American Radio Relay League, Inc. and are available through ARRL's partnership with the Connecticut Distance Learning Consortium (CTDLC), a nonprofit organization that specializes in developing on-line courses for Connecticut colleges and universities. Continuing Education Units (CEUs) are available for all ARRL Certification and Continuing Education courses. The ARRL Certification and Continuing Education Program is funded in part by course fees from interested hams who support public service and quality continuing education. For further information, e-mail your questions to **cce@arrl.org**, or write to **ARRL C-CE**, **225 Main Street**, **Newington**, **CT 06111**.

ONLY $19.95

ARRL's Vintage Radio

QST articles about the lure of vintage Amateur Radio gear

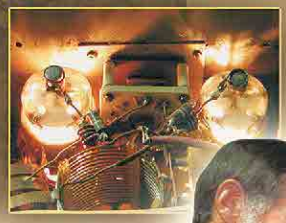

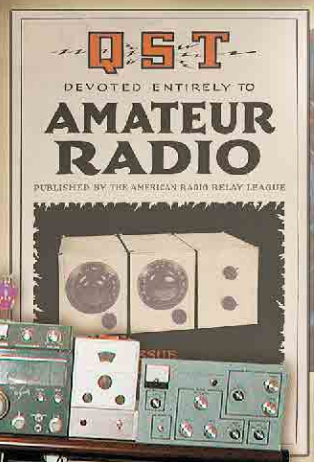

- Equipment
- Techniques
- Personal Experiences
- Restoration
- Classic Ads

...and more!

Published by:

ARRL *The national association for AMATEUR RADIO*

Order Toll-Free 1-888-277-5289 ▪ www.arrl.org
or visit your local ARRL dealer